On Transverse Momentum Event-by-Event Fluctuations in Nuclear Collisions at CERN SPS

Katarzyna Grebieszkow
Ph.D. Dissertation

Warsaw University
Institute of Experimental Physics

February 2005

Abstract

Results on event-by-event fluctuations in transverse momentum of forward-rapidity charged particles are presented. The system size dependence of dynamical fluctuations is studied by use of p+p, C+C, Si+Si and Pb+Pb collisions at 158 AGeV. The energy dependence is performed by analyzing central Pb+Pb collisions at 20, 30, 40, 80 and 158 AGeV. All available data sets were recorded by the NA49 detector at CERN. Three different methods are applied: measuring the average transverse momentum ($M(p_T)$) of the event, evaluating the Φ_{p_T} fluctuation measure and studying two-particle transverse momentum correlations. Results are compared with predictions of models and with other experimental results.

Dynamical fluctuations (dynamical part of event-by-event fluctuations) are rather small in this kinematic region (all Φ_{p_T} values are below 16 MeV/c). However, a significant system size dependence of Φ_{p_T} is observed with a maximum value for peripheral Pb+Pb interactions. No significant energy dependence of p_T fluctuations is observed for negatively charged particles but significantly increased Φ_{p_T} values appear for positively charged particles at lower SPS energies. This effect, however, might be explained by a higher fraction of re-scattered participants (correlated by the momentum conservation law) in a sample of positively charged particles at lower energies.

This is the first analysis presenting significant system size dependence of transverse momentum fluctuations at CERN SPS. Moreover, the NA49 experiment is the only one that recorded central Pb+Pb interactions in a rather wide energy region covering both the probable phase transition region and the region where QGP is probably created in every Pb+Pb collision. These two arguments makes the analysis complex, unique and truly attractive.

Acknowledgments

At the beginning I would like to thank my supervisor prof. Ewa Skrzypczak for providing me the opportunity to work in the heavy ion group at Warsaw University and for her continuous support beginning from the fourth year of my study and throughout my Ph.D. study. I am indebted very much for her inspiring remarks to the draft of my Ph.D. thesis.

I had a pleasure to work with one of the most efficient, inspiring and enthusiastic physicist I have ever met - Marek Gaździcki, without whom this thesis probably could not be written. He was my closest adviser and instructor at the NA49 experiment and I am very grateful for his support and help at every stage of this work and for introducing me into an inspiring and prestigious environment I had a possibility to work with.

I am very glad for having an opportunity to work also with Stanislaw Mrówczyński. Together with Marek Gaździcki he suggested the method of measuring transverse momentum fluctuations which became the topic of my Ph.D. dissertation. He provided me a lot of theoretical ideas, countless suggestions and a huge dose of optimism.

I am very appreciative of work done by Robert Korus from Swietokrzyska Academy, especially by preparing the output from HIJING simulations which became the basis of my analysis included in one of the chapters of this thesis.

During the first two years of my Ph.D. study I was working together with Waldemar Retyk. We were doing complementary analysis on transverse momentum fluctuations; therefore I would like to take an opportunity to thank for his company, his help, advices and new ideas and for always having the time for interesting discussions.

I am very grateful for efforts of all members of the NA49 collaboration who were preparing and developing the experiment and without whom I would not be able to do this analysis at all. Many warm thanks especially to Christoph Blume and Marco van Leeuwen who were very helpful and patient in answering for all my questions concerning the details of the NA49 software and data analysis.

Finally, I would like to thank my family and friends for taking an interest in my work, for encouraging and supporting me throughout my study.

Author's contribution

The NA49 experiment is a large, complex international project. The building and developing of the set-up and software required many years of the efforts of all collaborators. For six years the author of this thesis has been an active member of the experiment and her main contribution to the experiment was participating in data taking periods (controlling data acquisition and experimental conditions) and preparing and developing data analysis with a special emphasis on describing and fixing the available geometrical acceptance used by collaborators for the analysis of event-by-event fluctuations.

For purpose of this study the author was using completely and fully reconstructed data sets recorded in the so-called mini-root format which is used by the majority of collaborators. However, the author prepared sets of mixed events for all five energies. These events were processed through the GEANT program, simulating the response of the NA49 detector, and were reconstructed by a standard procedure of track reconstruction. Events prepared in this way are at present available in the mini-root format and can be used by all NA49 collaborators.

All calculations and results presented in chapters 4, 5 and 7, if not mentioned differently in the text, are prepared by the author of this thesis.

The author was participating in the collaboration meetings and workshops presenting the current status of the analysis. The results were also presented on international conferences such as Quark Matter 2002 and Quark Matter 2004 as a part of the NA49 plenary talks and in the form of posters (as it has been mentioned in the abstract it is the first analysis presenting significant system size dependence of transverse momentum fluctuations at CERN SPS). A significant part of the results prepared by the author and presented in this thesis was published and became an official result of the NA49 experiment.

For Jarek -
my husband and the best friend in the world

Contents

Chapter 1

Introduction

1.1 Quark-Gluon Plasma creation

This is a well established fact [1] that hadrons (for example protons, neutrons) - the elementary particles creating the matter in the Universe - consist of more fundamental objects: quarks (valence quarks and sea quark-anti-quark pairs) and gluons. Moreover, the well known property of strong interactions called *confinement* does not allow them to move freely outside the hadrons. The energy delivered to separate a single quark from a hadron will be eventually used to create a new quark - anti-quark pair. However, it was predicted long ago that if the energy density is sufficiently high, much higher than a typical energy density inside the hadron, the matter can form a gas of subhadronic degrees of freedom. In such situation quarks and gluons could move freely in the whole volume of so-called quark-gluon plasma (QGP) [2].

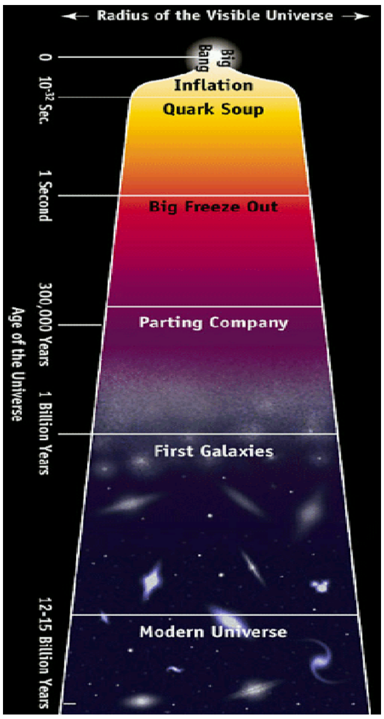

Figure 1.1: The probable scheme of the evolution of the early Universe. Figure taken from CERN Image Library.

The Big Bang model assumes that the Universe was created during an explosion of a very dense and a very small object. Fig. 1.1 illustrates the evolution of the early Universe. It is expected that at the early stage of this expansion a mixture of deconfined and thus directly interacting quarks and gluons (QGP) was filling the Universe. While the Universe was expanding and cooling down, deconfined quark and gluons were binded (merged) into color neutral particles like hadrons (for example protons and neutrons). These particles were subsequently combined into nuclei, atoms, elements up to present-day galaxies.

It has been considered repeatedly whether such a state of deconfined quarks and gluons that behave as essentially free particles can be reproduced in the laboratory. It seems that it is possible indeed. Let's imagine that very heavy nuclei (Pb, Au) collide at a very high energy. There are two possible scenarios of such reaction. One of them predicts that a very hot and dense hadron gas is created. Due to high energy and a large number of interactions between hadrons the creation of huge amount of new particles (like pions, kaons, lambdas) is possible. When the collision energy is sufficiently high the second scenario seems to be more probable - nucleons are so densely packed that their quarks and gluons do not "remember" which of the nucleons they belong to. The soup of deconfined partons is created, probably very similar to that one which existed shortly after the Big Bang. The second scenario of a heavy ion collision is presented in Fig. 1.2. The nucleons (protons, neutrons) from both nuclei that do not interact and move nearly not distorted in their original directions are called spectators (gray balls in the figure) whereas the nucleons that actively take part in the interaction are called participants. In the figure small red, blue and green balls denote quarks which are deconfined from participating nucleons.

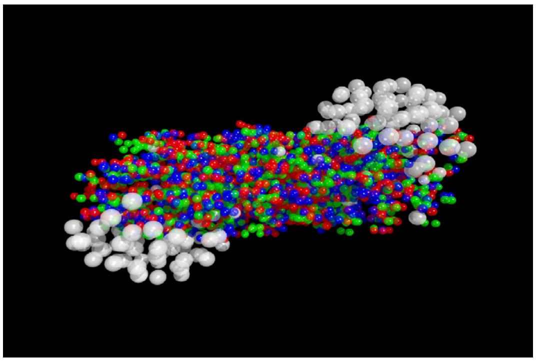

Figure 1.2: Collision of two heavy ion nuclei where QGP creation is observed. Figure taken from CERN Image Library.

The formation of QGP [2] at the early stage of the collision is expected when the system is sufficiently hot and dense. During its later evolution the system expands and cools down, partons are merged into color neutral particles (hadronization process) which finally can be registered in the detector. By studying such a final state particles, contemporary heavy ion physics tries to answer the question which scenario is realized during an interaction.

Over the last two decades heavy ion collisions have been studied in a series of experiments at different accelerators and at different beam energies. The main accelerators are: Alternating Gradient Synchrotron (AGS) in Brookhaven, Super Proton Synchrotron (SPS) at CERN in Geneva and new accelerator Relativistic Heavy Ion Collider (RHIC) in Brookhaven. In this thesis data from one of the SPS experiments (NA49) will be presented. SPS accelerator provides Pb beams at the energy of 158 GeV per nucleon which corresponds to the center-of-mass energy $\sqrt{s_{NN}} = 17.3$ GeV for a nucleon pair in Pb+Pb collisions. RHIC accelerator collides two gold beams coming from opposite directions and reaches the center-of-mass energy $\sqrt{s_{NN}} = 200$ GeV for a nucleon pair in Au+Au interactions. A new collider at CERN - Large Hadron Collider (LHC), which is presently under construction, will provide Pb+Pb collisions at $\sqrt{s_{NN}} = 5.5$ TeV per nucleon pair.

Fig. 1.3 shows schematically the space-time evolution of a heavy ion collision. The left-hand side of the diagram describes the situation where hadron gas is created while the right-hand side assumes the QGP formation during the early stage of a heavy ion collision.

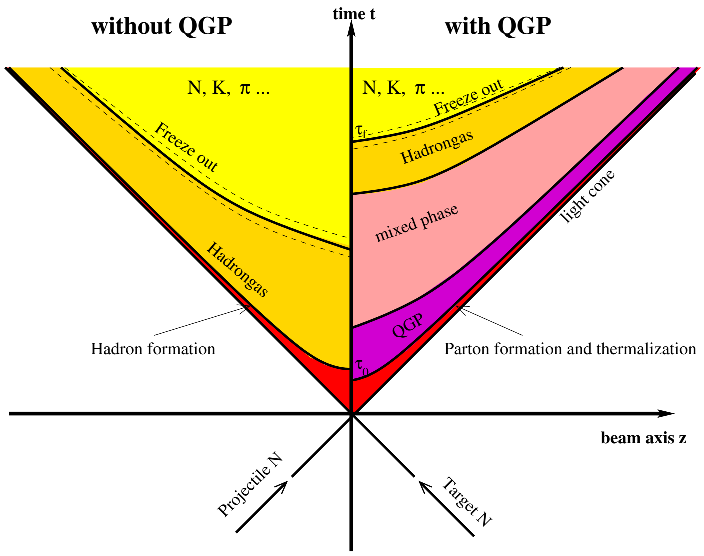

Figure 1.3: The space-time evolution of a heavy ion collision with and without QGP formation. Figure taken from [3].

Two heavy nuclei are accelerated to velocities which are very close to the speed of the light. In the case of the QGP scenario - just after the collision the number od degrees of freedom has to be rearranged and the thermal equilibration should be reached (red region in the right-hand side of Fig. 1.3). Then, after the so-called plasma formation time $\tau_0 = 1fm/c$ $(3 \cdot 10^{-24}s)$ the QGP appears. The volume occupied by matter characterized by a high energy density is called fireball. It is believed that due to a high density and a large number of interactions the system is thermally equilibrated. The typical temperature of the QGP created at the top SPS energy is about 230 MeV (more than 5 orders of magnitude hotter than the interior of the sun) and the energy density about 3 GeV/fm^3 (approximately 20 times the normal matter density). Extreme pressure gradients in the fireball lead to an explosive type of expansion. The fireball cools down and expands into longitudinal and transversal directions. The transverse expansion (not shown in figure) is slower than the longitudinal one (presented in the figure). The moment when the particles (resonances, hadrons) are already created and there are no further reactions producing or destroying new particles is called chemical freeze-out (the temperature of the chemical freeze-out T is approximately 175 MeV and the energy density ε about 1 GeV/fm^3). The typical lifetime of a fireball before reaching the chemical freeze-out is at the level of few fm/c (about $10^{-23}s$). The system, however, is still expanding and cooling down and the produced particles can interact and change their momenta. The thermal freeze-out is the moment when all particle interactions cease (non-stable particles can decay all the time) and their final momenta are established. The temperature of the thermal freeze-out is about 110 MeV and the energy density approximately 0.05 GeV/fm^3. All the above values are taken from [4]. Particles after their freeze-out can be detected in the experiment (the momenta of the emerging particles which are measured in the detector are fixed at the moment of thermal freeze-out). About 90% of all newly produced particles are pions and about 75% of total strangeness is carried by kaons. Produced particles carry information about the final state of the fireball. This information can be used to extrapolate back to the earlier stages of the evolution of the heavy ion collision. In this way experimentalists can try to answer the question whether the QGP is created or not at the very early stage of the collision.

The thermodynamical approach suggests that the energy provided to the system can be used to break the bindings (confinement) and to create a new state of the matter (like in the case of water). Such approach assumes the existence of the critical parameters like critical temperature or critical density. In the case of the nuclear matter, heating or/and squeezing (compressing) the matter leads to reaching a new phase - QGP. Thus the QGP is the nuclear matter which is an analogue of the plasma phase in an ordinary atomic matter. It is quite obvious that the thermodynamical picture can be used for macroscopic systems only whereas the nuclear collision is a microscopic one. However, in heavy ion collisions the number of participating nucleons is high and the created fireball produces thousands of particles interacting both in elastic and inelastic collisions. The exchange of the momenta is a natural expectation and therefore in calculations one can assume that the equilibration is reached. As a consequence the typical language of thermodynamics can be used. In the case of thermal equilibrium the mean kinetic energy of the particles can be described in terms of the temperature. It will be also shown later that in high energy heavy ion collisions the produced particles are emitted from a source of common temperature what can be a good argument for thermalization.

An approximate knowledge of the potential between two interacting quarks, the assumption that the thermal equilibrium has been achieved and that the baryonic chemical potential $\mu_B = 0$ enable theoretical calculations of the system evolution. Thus, in principle, the values of the critical parameters of the phase transition can be found. (Baryo-chemical potential is a thermodynamic parameter which allows to account for a non-zero baryon density of the created matter). Such numerical calculations (so-called lattice calculations [5]) are based on 4D space-time lattice. The quarks are situated on lattice sites and the gluons link them. The numerical calculations allow to simulate and follow-up their interactions. On the basis of lattice calculations it has been predicted that the temperature of the transition between QGP and hadron gas (the temperature of the chemical freeze-out) equals $T_c \approx 150 - 175$ MeV [6, 7] (depending on the number of flavors assumed in calculations). The temperature corresponds to the energy density by use of the equation of state (figure in [6]) and in principle at critical temperature T_c the critical energy density can be estimated as $\varepsilon_c \simeq (6 \pm 2) T_c^4$. Therefore for $T_c \approx 150 - 175$ MeV the energy density does not exceed the value of 1 GeV/fm^3 (for example for $T_c = 160$ MeV, $\varepsilon_c = 0.51 \pm 0.17$ GeV/fm^3).

As already mentioned the above limits of the critical temperature have been calculated at baryonic chemical potential $\mu_B = 0$ (i.e. also zero baryon density). At energies presently reached in heavy-ion experiments chemical potential is non-vanishing but has a finite value, however lattice calculations for non-zero chemical potentials are much more complicated and until recently (2001 year) were not possible at all. The recent calculations for μ_B different from zero became possible and the results will be shown later in Fig. 1.5 and Fig. 1.7.

Fig. 1.4 shows the phase diagram of a nuclear matter as a function of temperature (vertical axis) and baryon density (horizontal axis). The ordinary nuclear matter (red

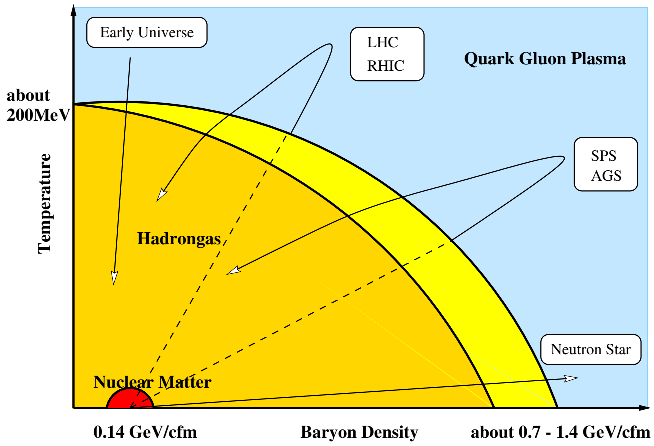

Figure 1.4: The phase diagram of the transition between nuclear matter and QGP. At high temperatures (related to high energy densities) and/or high baryon densities (matter densities) hadronic matter can undergo a phase transition. The lines correspond to different scenarios in which a QGP can be created. The critical temperature of the phase transition at zero baryon density (also zero baryon chemical potential) is put as 200 MeV, however more recent calculations indicate that it can be lower (150 - 175 MeV). Figure taken from [3].

region in the figure) has the density $\rho \approx 10^{14} g/cm^3$. It is believed that the early Universe contained low density and high temperature QGP [8] (the phase transition from QGP to hadron gas took place probably 10^{-6} - 10^{-5} s after Big Bang). The present-day cores of neutron stars probably contain so-called cold QGP - at low temperatures and high densities [9]. In present-day ultra-relativistic heavy ion experiments both high temperatures and high densities of matter seem to be reached leading to the creation of an extended volume of the matter, probably composed by deconfinement quarks and gluons. Within a QGP scenario, just after the collision, the system reaches high temperature and high baryon density crossing the phase boundary and after that hadronizes (in the hadron gas region) - the arrows at the end of the curves in Fig. 1.4 represent the freeze-out points. Within the hadron gas scenario the system does not reach the phase boundary and the whole curve is situated inside the hadron gas domain. Although in Fig. 1.4 the QGP scenario is assumed for all accelerators it is still an open question whether the collision energy at AGS and low energy SPS reactions is high enough to allow the trajectories to cross the phase boundary of the phase diagram.

The phase diagram of a nuclear matter can be also represented as a function of T and baryonic chemical potential μ_B as presented in Fig. 1.5 (baryon density corresponds to baryonic chemical potential). The shape and the position of the curve, representing the phase transition, and also the order of the transition depend on the number of quark flavors (n_f) and on their masses assumed in lattice calculations. Fig. 1.5 shows the results of lattice QCD calculations where n_f=3 is set up (2 light and 1 massive flavors). At higher μ_B the transition is of the first-order (solid line) whereas for lower μ_B and higher temperatures one can expect a crossover (dotted line). For a first-order phase transition (co-existing phases) one can expect a jump in the entropy and the baryon number density and a discontinuity (jump) of the energy density (ε) whereas in a crossover the entropy behavior is continuous and one can expect a fast but smooth change of physical variables. Therefore in the region of lower μ_B one can expect rather rapid but smooth crossover from the regime which can be described as a hadron gas to the regime of QGP. A critical point (the 'end-point' of the first-order phase transition) separates these two types of transitions. Accordingly to calculations in [10], where semi-realistic masses of quarks has been assumed (m_s has been set to be about its physical value, $m_{u,d}$ are four times heavier than in the real world), the end-point has been predicted to be located at $T^{crit} \approx 160$ MeV and $\mu_B^{crit} \approx 725$ MeV (in this work the critical temperature at $\mu_B = 0$ is reported as $T_c \approx 172$ MeV). This μ_B value at the critical point is too high to be studied both at SPS and at RHIC experiments (at RHIC top energies $\mu_B \leq 50$ MeV, whereas at top AGS energy $\mu_B \approx 550$ MeV). More recent results, calculated for realistic quark masses suggest a critical point at $T^{crit} = 162 \pm 2$ MeV and $\mu_B^{crit} = 360 \pm 40$ MeV [11]. The critical value of μ_B is still much larger than the value of baryonic chemical potential at the chemical freeze-out, estimated at top RHIC energies ($\mu_B \approx 30$ MeV). It can suggest that the transition at $\mu_B = 0$ and in almost baryon free region produced at mid-rapidity at RHIC can be rather described by a rapid crossover from a hadron gas to QGP. In [11] the critical temperature at $\mu_B = 0$ is reported as $T_c = 164 \pm 2$ MeV. The critical value of μ_B reported in [11] is close to the values of baryo-chemical potential reached in Pb+Pb interactions at SPS.

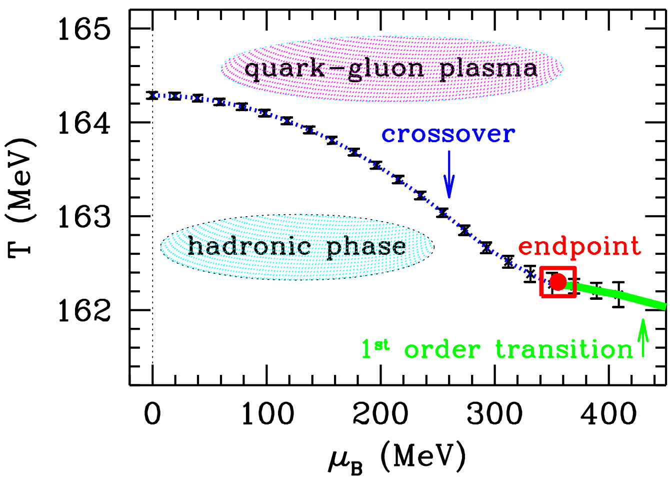

Figure 1.5: QCD phase diagram in the $\mu_B - T$ plane. Dotted line illustrates the crossover and solid line the first-order phase transition. Figure taken from [11].

The aim of present-day experiments is to find out whether the conditions for QGP creation during heavy ion collision at high energy are fulfilled. CERN SPS is nowadays one of the accelerators offering very high energies in Pb+Pb interactions (center-of-mass energy equals 17.3 GeV per nucleon pair). A very important question is how to estimate the values of T or ε parameters which can give some ideas whether the conditions achieved in heavy ion collisions are at least close to those expected for the QGP formation. Either T or ε can be determined by use of kinematic variables or/and yields of particles produced in the final state of the high energy interaction.

The first important question is how to determine the temperature of the emitting source of particles (thermal freeze-out temperature). It has been suggested by Hagedorn [12] that the transverse momenta of emitting particles carry information about the freeze-out temperature. In principle, the distribution of the transverse mass of produced particles ($m_T = \sqrt{{p_T}^2 + {m_0}^2}$, where m_0 is the rest mass of a particle) for low transverse momenta (for example $p_T < 2$ GeV/c) is quite well described by the so-called Hagedorn formula:

$$\frac{dN}{dm_T} = C m_T exp(\frac{-m_T}{\alpha}) \qquad (1.1)$$

Assuming thermal equilibration and comparing the formula with a simple Boltzmann's distribution one can immediately find that α parameter (so-called inverse slope parameter) can be identified with the temperature of the emitting source. The α parameters measured by several CERN experiments have been found to vary between 150-450 MeV and have depended linearly on the mass of the measured particle (a detailed figure for example in [13]). It has been proposed then that the value measured in the experiment ($\alpha = T_{sl}$) is the real thermal freeze-out temperature (T_{fo}) plus additional part connected with the transverse expansion of the system. Within this approach the inverse slope parameter is given by the formula:

$$T_{sl} = T_{fo} + \frac{1}{2} m_0 \beta_T^2, \tag{1.2}$$

where β_T is connected with already mentioned transverse flow (β_T is the transverse velocity of the emitting source). Taking into account the last formula (one should note that the main formula describing m_T distribution can be modified in different models and by use of different parameterizations) it has been estimated that the real thermal freeze-out temperatures calculated for different types of particles are about 117-131 MeV even for the lowest SPS energies (20 and 30 AGeV) [14] and about 115-140 MeV for higher SPS energies (40, 80 and 158 AGeV) [15]. The slopes of the m_T spectra of particles and anti-particles are very similar. Common value of T_{fo} for different particle types indicates that the thermalization is indeed reached in such collisions. Fig. 1.6 shows the transverse mass distributions of selected hadrons produced in central Pb+Pb collisions at 20 and 30 AGeV. The values of thermal freeze-out temperatures and transverse velocities result from the fit. β_T has been found to be about 0.5c for all SPS energies. Fig. 1.6 and the above mentioned results concern central Pb+Pb collisions (7-10% most central interactions), however, it has been observed experimentally that even for the same collision energy thermal freeze-out temperature decreases with increasing centrality (T_{fo} is lowest for the most central events). This difference can be significant (T_{fo} for peripheral events can be even 20% higher than that for central ones) so one has to be careful when combining different centralities.

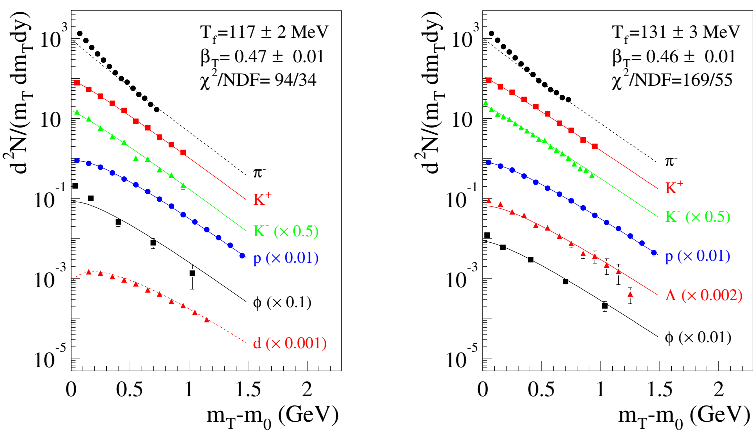

Figure 1.6: Transverse mass spectra of hadrons produced in central Pb+Pb collisions at 20 (left) and 30 (right) AGeV together with estimated thermal freeze-out temperatures. Figure taken from [14].

It has been suggested that by use of the total multiplicities and a hadron gas model

[16] (hadron gas is at least close to the chemical equilibrium) one can determine the temperatures of the chemical freeze-out, which are predicted to be larger than thermal ones. The values obtained for SPS energies vary between 145 and 160 MeV [15, 17] and are indeed a bit higher than the thermal freeze-out temperatures. In Fig. 1.7 the values of chemical freeze-out temperatures and baryon chemical potentials (chemical freeze-out points) extracted from the analysis of hadron multiplicities in central A+A collisions are compared for SIS, AGS, SPS and RHIC energies. The gray line represents the phase boundary between hadronic matter and QGP obtained from lattice calculations. The shape of the gray line and the position of the critical point (E) comes from [11] whereas the chemical freeze-out points come from [18]. Chemical freeze-out points have been found to lie on a smooth curve, and for RHIC and higher SPS energies this line is close to the expected phase boundary to QGP, indicating that the estimated temperatures of the chemical freeze-out are very close to temperatures required for the phase transition and it is very probable that at the early stage of the collision the system crossed the phase boundary creating the QGP matter. The "vertical" trajectories at different energies are sketched to pass through the chemical freeze-out points, the position of the early stage point at 30 AGeV follows from the observation of the onset of deconfinement at this energy. The position of the early stage points at top SPS and RHIC energies are strongly model dependent.

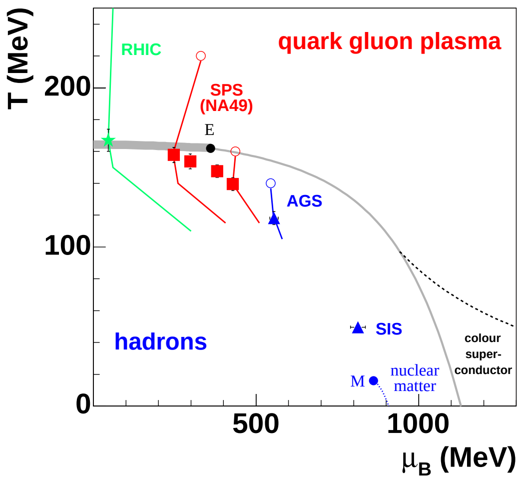

Figure 1.7: The phase diagram of strongly interacting matter. Grey line corresponds to theoretical predictions (lattice calculations) of the phase boundary. The chemical freeze-out points (closed symbols) are determined from a fit with a statistical hadron gas model [18]. The open symbols schematically indicate possible values of initial parameters of the reaction systems, which then might evolve along paths as depicted by the vertical lines. Figure taken from the NA49 Image Library. See the text for details.

In Fig. 1.7 the chemical freeze-out points are determined for central A+A interactions. It is known empirically that one can change the position of the freeze-out points by changing the collision energy. In principle, the fireballs tend to freeze out at decreasing values of the baryonic chemical potentials and increasing temperatures when the center-of-mass energy increases. It has been also observed experimentally that thermal freeze-out temperatures (extracted for example from Fig. 1.6) decrease with increasing centrality (T_{fo} is lowest for the most central events). The chemical freeze-out points also change their positions when changing the centrality of the collision. The fact that larger systems freeze out later (at lower temperature) has been established by studying the A dependence of the freeze-out temperature via analysis of flow, Coulomb effects and pion interferometry (the references given in [19]). Therefore in order to properly analyze the whole area of the phase diagram of the hadronic matter and to find the position of the predicted critical end-point the experiments should focus both on the centrality and energy scan program. Until now the heavy ion experiments have probed the region of relatively high temperatures (of the order of 100 MeV) and small to medium baryon chemical potentials (0 - 600 MeV), anyway theorists predict that exactly this region can have an interesting feature - the critical end-point of the first-order phase transition.

Accordingly to the Björken formula [20] the energy density of the central rapidity [1] region created in a heavy ion collision can be determined by use of the formula:

$$\varepsilon \approx \frac{[dE_T/d\eta]_{y^*=0}}{A\tau_0} \tag{1.3}$$

where $[dE_T/d\eta]_{y^*=0}$ is the transverse energy density in pseudo-rapidity space estimated in the central rapidity region, τ_0 is the formation time and A is the overlapping area of the colliding nuclei. E_T is the transverse energy of the collision (one can also use the relation: $[dE/dy]_{y^*=0} = [dE_T/dy]_{y^*=0} = \langle m_T \rangle [dN/dy]_{y^*=0}$). An estimation of the energy density at SPS energies has been performed using $\tau_0 = 1$ fm/c and the value of ε has been found to be about 3.2 GeV/fm^3 [21] for the most central Pb+Pb interactions at 158 AGeV. The energy density, however, seems to be also rather high ($\varepsilon = 1.3$ GeV/fm^3 [21]) even for light systems such as central S+S interactions at 200 AGeV. These estimations are correct to the factor of 2 due to the poor knowledge of τ_0 parameter. Nevertheless, the energy density reached in present experiments seems to be high enough to allow for the QGP formation. One can note, for comparison, that the energy density of the normal nuclear matter is roughly 0.15 GeV/fm^3. Recent results from Relativistic Heavy Ion Collider (RHIC) show that for central Au+Au collisions at center-of-mass energy 200 AGeV the values of ε can reach even 5 GeV/fm^3 [22, 23].

Summarizing, nowadays there are many high-energy heavy-ion experiments - some of them are situated at CERN SPS accelerator. It seems that the temperatures (and the corresponding energy densities) achieved in A+A interactions in such experiments are high enough to create QGP during the early stage of the collision. Even so, it is very important to find possible and reliable signatures of the QGP formation. It is also essential to measure a large variety of signals with different interaction energies and different sizes of the colliding systems, namely also elementary nucleon+nucleon collisions (N+N) should be analyzed carefully as the reference for A+A interactions. This might help to prove or rule out the QGP scenario.

1.2 QGP signatures and the phase transition

Nucleus+nucleus collisions at relativistic energies have been intensely studied over the last two decades; the main goal of these efforts is to understand properties of strongly interacting matter under extreme conditions, where the creation of QGP is expected. Rich experimental results indicate that that QGP indeed occurs at the collision early

[1] for each particle the rapidity in the laboratory reference system is defined as: $y = \frac{1}{2} ln \frac{E+p_L}{E-p_L}$, where E is the total energy of a given particle and p_L - its longitudinal momentum. The transformation between the center-of-mass system and the laboratory system can be determined from the formula: $y = y^* + y_{mid}$, where y^* is the rapidity of the particle in the center-of-mass reference system and y_{mid} is the rapidity of the center-of-mass in the laboratory frame.

stage when the system is sufficiently hot and dense. However, there is a non-trivial problem how to observe the QGP because the final state particles, which are registered in the detector, have returned from a plasma phase via the hadronization process. Therefore the suggested QGP signatures should survive hadronization process. The solution can be found in the analysis of the observables which are not sensitive to hadronization. Namely, analysis of the dynamical observables or studying the particles which - after having been created in the QGP can be modified in electromagnetic or weak interactions only. There are several QGP signatures suggested by theory. The most popular are:

1. Strangeness enhancement (proposed by Rafelski and Muller [24])- it is energetically easier to create strange quarks in QGP than to produce strange hadrons in the case of hadron gas. Thus the ratio of the total number of strange particles to the total number of non-strange particles is increased when QGP is created in the early stage of the collision. Such effects have been observed by experiments at top SPS energies. The example of a plot showing strange particle production (the total yield of K mesons divided by the total yield of pions) which is enhanced for A+A interactions when compared to p+p and p+A collisions can be found in [25]. An enhancement factor in $\langle K \rangle / \langle \pi \rangle$ for A+A systems is at the level of 2. It has been noticed that the enhancement becomes stronger for particles with higher strangeness content and varies between 2.7 for Λ hyperons to 3.8 for Ξ hyperons [26]. The analysis of strange particle production is also a very important part of the NA49 program.

2. Charmonium suppression (proposed by Matsui and Satz [27]) - in the presence of quarks and gluons (QGP) the color charge of a quark is screened (so-called Debye screening) and therefore, in principle, the interaction force between c and anti-c pair (J/ψ meson) becomes weaker thus leading to melting (dissociation) of newly produced J/ψ particles and finally to the suppression of J/ψ production in the case of QGP scenario. The J/ψ suppression (the strongest effect seen for the most central Pb+Pb collisions at 158 AGeV) has been observed at top SPS energies by the NA50 experiment and the results are presented for example in [28, 29]. The J/ψ meson yield is exhibited as a function of the energy density and the anomalous suppression, which cannot be explained via J/ψ absorption in normal nuclear matter, is seen only for central Pb+Pb collisions at energy density higher than 2.2 GeV/fm^3 [28]. This effect might be explained as a charmonium melting in a presence of QGP. However, one has to keep in mind that a broad set of experimental data suggests that the QGP might be created not only in central Pb+Pb collisions at SPS energies but generally in central A+A interactions (S+S, Pb+Pb) at SPS energies.

3. Electromagnetic probes - leptons and photons produced in a heavy ion collision do not participate in strong interactions (during hadronization process) and therefore carry information about the initial state of the collision, where the QGP might be created. One can expect the possibility to observe the emission of the thermal radiation of photons and leptons if the early stage is sufficiently hot and dense. The spectra of produced photons and leptons have been measured by one of the SPS experiments - CERES and such effect has been observed indeed [30].

4. Event-by-event fluctuations - which are sensitive to the dynamics of the colliding system. It is predicted, by various theoretical considerations, that significant event-by-event fluctuations in temperature, transverse momentum, multiplicity and conserved quantities such as net charge may be a signature of the phase transition.

Event-by-event fluctuations are the topic of this thesis and therefore this point will be discussed more precisely in the next sections.

Apart from the fact that QGP indeed seems to be created in heavy ion collisions at top SPS energy, it would be also very interesting to see at what energy region the phase transition may take place (there has to be an energy below which the conditions are not sufficient to create QGP - the system does not cross the phase boundary at the early stage of the collision and above which QGP is created at the early stage of the heavy ion interaction). By use of the Statistical Model of The Early Stage (SMES) M. Gaździcki and M. I. Gorenstein suggested that the onset of deconfinement (the energy region in which the deconfinement transition takes place) is located between top AGS (11.7 AGeV) and top SPS energies (158 AGeV) and that above a certain energy (30 AGeV) a QGP is formed in the collision [31]. The SMES model uses so-called 'Bag model'; the model assumes the first-order phase transition in the whole μ_B region (there is no critical end-point predicted within the Bag model). Thus the SMES model also implies that the deconfinement phase transition is of the first-order, namely there is a confined, mixed and a deconfined phase. SMES is a type of a thermodynamical model which assumes that at the early stage of the collision quarks and gluons that compose QGP are thermalized. One of the basic establishments of this model is that the number of internal degrees of freedom g increases at deconfinement, due to activation of partonic degrees of freedom. The entropy in the final state is proportional to the total number of pions (in high energy collisions the entropy is carried mainly by final state pions). Additionally, it is assumed that the total number of created strange quarks (generally heavy flavors) and the total entropy are the same before and after hadronization. This insensitivity to expansion and hadronization processes leads to the conclusion that the analysis of the particle production in the final state can bring information about the early stage of the collision. The SMES gives exact predictions of the particle yields in high energy heavy ion interactions. In the SMES model the critical temperature (chemical freeze-out, hadronization) is taken as T_c = 200 MeV (it will be seen also as a temperature of the mixed phase in Fig. 1.8).

In principle this model predicts a kink-like structure in the energy dependence of the total entropy of the created state to the number of nucleons participating in A+A collision. One has to remember that the total entropy is closely related to pion production and therefore the ratio of pion multiplicity (measure of entropy) to - for example - the number of wounded nucleons is predicted to increase linearly with Fermi's energy measure F ($F = (\sqrt{s_{NN}} - 2m_N)^{3/4}/(\sqrt{s_{NN}})^{1/4} \approx s_{NN}^{1/4}$, where $\sqrt{s_{NN}}$ is the center-of-mass energy per nucleon pair and m_N the rest mass of the nucleon). The slope of this rise is proportional to $g^{1/4}$ where g, as already mentioned, is the number of degrees of freedom at the early stage. g is higher for QGP state than for hadron state leading to the increase of the slope of this rise.

As the next signature a horn-like structure in strangeness to entropy ratio is expected with a sharp maximum for the transition region (low SPS energies). The SMES predicts that the strangeness to entropy ratio for the ideal gas of massless particles equals $1/4\frac{g_s}{g}$, where g and g_s are the total and strange numbers of degrees of freedom. The $\frac{g_s}{g}$ is expected to be about 0.5 for hadron state and 0.22 for QGP state. Therefore a phase transition from gas of massless hadrons to massless QGP should lead to a decrease of strangeness to entropy ratio by a factor of 2. This simplified prediction is significantly modified when the finite mass of the strangeness carriers is taken into account (numerical calculations have to be carried out). Due to the relatively high masses of strange particles (higher than the system temperature) the strangeness to entropy ratio increases rapidly with increasing energy for 'lower' energies. At QGP a reduction of mass of the strangeness carriers is expected ($m_{K,\Lambda}$ for hadron gas $\rightarrow m_S$ for QGP). At $T = T_c$ the predicted strangeness to entropy ratio is higher for hadron state than for the QGP state and therefore the increasing fraction of QGP (mixed phase) leads to the drop in the strangeness to entropy ratio down to the value characteristic for QGP. For higher energies (pure QGP state) due to the low mass of strange quark (lower than the system temperature) only a very weak dependence of strangeness to entropy ratio on energy is predicted.

Finally, as the last signature, a step-like structure in the energy dependence of the early stage temperature is predicted. Within a hydrodynamical approach in pure confined and deconfined phases (outside the transition regions) the temperature (inverse slope evaluated from transverse momentum or transverse mass spectra) increases with the energy density (therefore with the collision energy) whereas for mixed phase it does not depend on energy (in SMES it is assumed that inside the transition region $T = T_c = 200$ MeV). This leads to the plateau for energies close to the phase transition. The SMES predicts the transition region between F=2.23 and 2.90 GeV$^{1/2}$ (p_{lab} from 30 to 64 AGeV).

Fig. 1.8 presents the results of the numerical calculations for all three effects (predictions), described above.

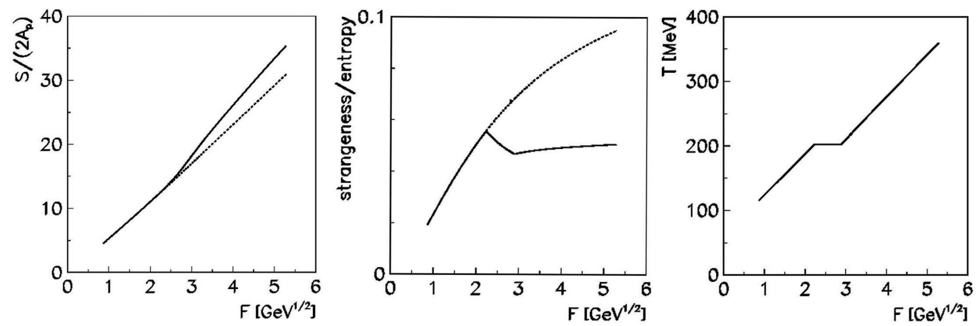

Figure 1.8: The dependence of the total entropy of the created state to the number of nucleons participating in A+A collision (A_p - number of participant nucleons from a single nucleus) on energy measure F (left), the dependence of the total number of s and $\bar{s}$ quarks to the entropy (strangeness to entropy ratio) on energy measure F (middle) and the dependence of the initial temperature of the matter (the early stage temperature) on energy measure F (right) predicted by the Statistical Model of the Early Stage. The full lines indicate the expected dependences where the phase transition to QGP is assumed while the dotted lines correspond to the hadron phase. Figure taken from [31].

The predictions of the SMES and a hope to observe the anomalies in the energy dependence of pion and kaon production in central Pb+Pb collisions became a motivation of a dedicated energy scan program of the NA49 experiment. Within this project central Pb+Pb collisions at 20, 30, 40, 80 and 158 AGeV have been recorded. The results are presented in Fig. 1.9.

The dependence of the mean multiplicity of pions per the average number of wounded nucleons on energy, represented by Fermi's energy measure F, (Fig. 1.9 - top) for central A+A collisions shows a kink-like change from pion suppression to pion enhancement, whereas for elementary interactions one can observe a linear increase. Within a statistical model $\langle K^+\rangle/\langle\pi^+\rangle$ ratio is closely related to strangeness ($s + \bar{s}$) to entropy ratio (the strangeness to entropy measure $E_s = \frac{\langle\Lambda\rangle+\langle K\rangle+\langle\bar{K}\rangle}{\langle\pi\rangle}$ is also used in the literature and its dependence on F can be directly compared to SMES predictions from Fig. 1.8 - detailed

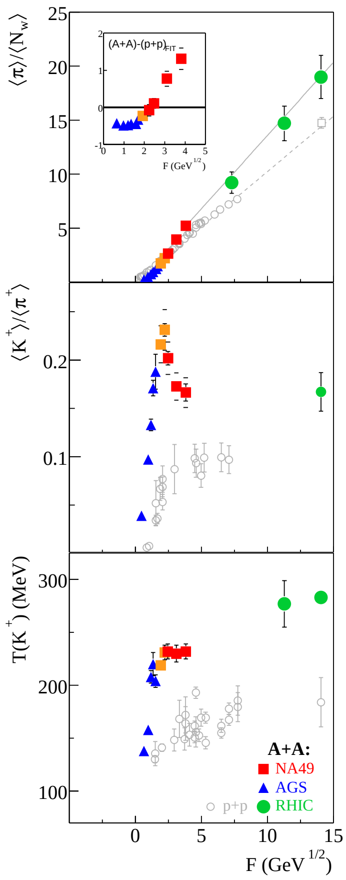

Figure 1.9: The dependence of the total pion multiplicity per wounded nucleon on Fermi's energy measure F (see the text for definition) (top), the dependence of $\langle K^+\rangle/\langle\pi^+\rangle$ ratio on F (middle) and the dependence of inverse slope parameter T, of the transverse mass spectra of K^+ on F (bottom). Figure taken from [14].

plots can be found in [15, 17]). The $\langle K^+\rangle/\langle\pi^+\rangle$ ratio dependence on energy for central A+A interactions (Fig. 1.9 - middle) exhibits a horn-like structure while for elementary interactions shows monotonic behavior. The maximum of the $\langle K^+\rangle/\langle\pi^+\rangle$ ratio can be observed for 30 AGeV. One should note that the strangeness enhancement (for A+A as compared with N+N) is observed also for low energies (AGS) and therefore probably it can not be itself a reliable signature of the QGP formation as it has been suggested previously [24]. Anyway, the existence of an enhancement confirms that the A+A collision is not a simple superposition of N+N interactions. The dependence of the temperature of positively charged kaons (inverse slope parameter) on energy (Fig. 1.9 - bottom) shows a step-like structure, namely the plateau can be observed for 30, 40, 80 and 158 AGeV central Pb+Pb interactions (SPS energies), whereas T increases with energy for AGS and RHIC data.

The energy dependence of the $\langle K^+\rangle/\langle\pi^+\rangle$ ratio (or E_s variable) has been compared to several models which do not incorporate the QGP formation such as string models (UrQMD, RQMD) and hadron gas models (detailed figures can be found in [15], [17], [32], [33]) but all of them fail to describe the observed behavior. The statistical hadron gas models provide a slightly better description of the data, however, they require an introduction of an energy dependent strangeness under-saturation factor γ_s [18] to properly reproduce the data. Instead, all the above anomalies observed both in $\langle K^+\rangle/\langle\pi^+\rangle$ ratio and in pion production and temperature (inverse slope parameter) can be naturally explained in the frame of the hypothesis that the phase transition is located at low SPS energies.

The recent results obtained by the NA49 experiment (Fig. 1.9) suggest the propriety of studying all possible experimental effects (including fluctuation measures) in a broad energy range, covering the predicted phase transition region.

1.3 Dynamical fluctuations in nucleon+nucleon and nucleus+nucleus collisions

Generally, there are two types of fluctuations in a system - statistical (due to finite multiplicity of uncorrelated particles) and dynamical ones. Dynamical (non-statistical) fluctuations are considered to be one of the important tools to study the dynamics of heavy ion collision. Dynamical fluctuations, which can appear both in kinematic characteristics and particle yields, are expected to be modified for systems approaching the phase boundary from hadron gas to QGP. Moreover, it is also predicted that for a system close to equilibration (probably at highest SPS energies) dynamical fluctuations are small. Thus, the fluctuation analysis can help to resolve a problem to what extent the strongly interacting matter, emerging from the early stage of the collision, achieves thermal [34, 35, 36] and chemical [37, 38] equilibrium. Significant transverse momentum and multiplicity fluctuations are expected to appear for systems that hadronize from QGP near the predicted second-order critical QCD end-point [19, 39] and therefore - for example - a possible non-monotonic evolution of p_T fluctuations with beam energy or centrality may be a possible probe to search for the phase transition and the QCD critical point [19]. All the above predictions became a motivation of a fluctuation program both at SPS and RHIC energies. The NA49 experiment registered data at different energies: 20, 30, 40, 80 and 158 AGeV which allow for a precise study of the dynamical fluctuations in the system close to predicted energy of the QGP transition and in nearly equilibrated systems.

There are several methods of analyzing fluctuations in order to extract the most interesting dynamical part. First of them consists of studying global characteristics of produced particles (such as transverse momentum, rapidity, azimuthal angle) and looking for non-statistical, local peaks or intermittency [40] in such distributions. The second method, so called *event-by-event analysis* is based on the comparison of a given event characteristic (e.g. mean transverse momentum per event or K/π ratio) and looking how it changes from event to event. *Event-by-event fluctuations* are usually pictured as a superposition of *statistical fluctuations* (connected with the fact that the number of particles in the system is not infinite) and *dynamical (non-statistical) fluctuations* - the subject of interest. If the studied data sample consists of very dynamically similar events then obviously event-by-event fluctuations are small (statistical part only) but if one has an opposite situation, that is there are different groups of events in the studied data sample (for example two groups - events where QGP is created and events where conditions are not sufficient for QGP formation) then these different classes of events may exhibit different global characteristics. Consequently, fluctuations of a given characteristic from one event to another (event-by-event fluctuations) are much higher. In this situation event-by-event fluctuations are affected by both statistical and dynamical fluctuations. The situation where one has two qualitatively different groups of events (the QGP is formed only in a fraction of events) is much more probable for the systems which are close to the phase transition region (at the early stage of the collision the system is approaching the phase boundary) thus one can expect enhanced dynamical fluctuations in this energy region.

Such increased dynamical fluctuations predicted for the system which is approaching the phase boundary are expected both for the first- and second-order phase transitions. In principle, the exact calculations have been carried out within the SMES model (assuming the first-order phase transition) and the expected non-monotonic dependence of the ratio of multiplicity (entropy) to energy fluctuations on the Fermi's collision energy F has been presented [41]. The 'shark fin' structure and its maximum are due to large fluctuations in the mixed phase region - the domain where the onset of deconfinement occurs.

It was shown long ago that the dynamical transverse momentum fluctuations in nucleon+nucleon collisions are determined mainly by the correlation between the average transverse momentum and multiplicity [34]. However, it appeared that other sources (for example two-particle correlations) can be a possible origin of non-zero dynamical fluctuations, either. Therefore many fluctuation measures used in the literature (for example Φ measure introduced in the next chapter) are also called *correlation measures* due to the fact that they can measure the inter-particle correlations in the system. Nevertheless, one has to remember that the inter-particle correlations, of course, are not the only source of dynamical fluctuations. Summarizing, the non-vanishing dynamical fluctuations, measured by use of the event-by-event method, can be caused by the presence of several sources, such as:

1. fluctuations which occur on an event-by-event basis, including fluctuations due to the existence of different event classes. They may be caused by dynamical fluctuations of the energy deposited for the particle production and/or creation of events with and without QGP. This kind of fluctuations should result in event-by-event dynamical fluctuations of the inverse slope parameter of the transverse mass spectra (measure of the temperature) and in a chemical composition of produced hadrons (e.g. fluctuations in the K/π ratio)

2. two-particle correlations within the same event - for example due to Bose-Einstein statistics, Coulomb effects or resonance decays (the number of resonances and the number of correlated particle pairs can fluctuate from one event to another)

3. other inter-particle correlations, where more than two (sometimes all) particles within the same event are correlated - for example effects of collective flow, jet production or finally the correlation between the average transverse momentum and multiplicity of a given event (the multiplicity and thus the average transverse momentum can fluctuate from one event to another)

From the one hand it is quite interesting to observe how dynamical fluctuations behave as a function of energy, especially for systems close to the phase transition. From the other hand one can also try to investigate how dynamical fluctuations change with the size of the colliding system. The *superposition model* assumes that nucleus+nucleus (A+A) collision is a superposition of elementary, not distorted, nucleon+nucleon (N+N) interactions and that dynamical fluctuations (due to different correlations) which are present in N+N survive in A+A collisions. In this model event-by-event fluctuations (both for A+A and N+N) are qualitatively the same and composed by both statistical and dynamical parts. The opposite model - *equilibration model* implies an important role of secondary interactions in A+A collisions thus leading to a dilution of possible correlations and finally to reduction or even disappearance (in the case when dynamical fluctuations are due to inter-particle correlations only and there are no fluctuations on even-by-event basis) of dynamical part of event-by-event fluctuations. One can expect that due to high density and secondary interactions the equilibration model better describes A+A collision. It can be therefore expected that event-by-event fluctuations for A+A collisions should be smaller when compared to N+N case and composed mainly by statistical ones. A large number of secondary interactions in A+A collision leads to the equilibration of the system. Therefore a measurement of event-by-event fluctuations is an important tool of determining the level of equilibration in A+A collision. For instance event-by-event fluctuations of multiplicity ratios of various hadrons can measure the level of chemical equilibration of the nuclear matter and event-by-event fluctuations in transverse momentum measure the level of thermal equilibration.

Event-by-event fluctuations have been already studied by the NA49 experiment by use of the transverse momentum of produced particles and the K/π ratio. The first results for central Pb+Pb interactions at top SPS energy (158 AGeV) have not shown any significant dynamical fluctuations both in p_T [42] and in the K/π ratio [43]. These results are in agreement with the equilibrium picture. Therefore, assuming that the strangeness enhancement and charmonium suppression are reliable signatures of the QGP formation at top SPS energies, one might conclude that together with negligible dynamical fluctuations it suggests that the mechanism of the reaction is very similar for each event and, in principle, the QGP might be created almost in every event at 158 AGeV. On the other hand the recent data show that event-by-event fluctuations on the K/π ratio are enlarged for lower energies (20, 30 AGeV) when compared to top SPS energy (158 AGeV) - the dynamical fluctuations of K/π ratio decrease with energy [44]. This effect cannot be reproduced within a string-hadronic model (UrQMD) indicating a presence of a new source of dynamical fluctuations. However, authors point out that further theoretical calculations are needed to interpret this observation as a possible signature of a phase transition that has been predicted at energy close to 30 AGeV. Accordingly to SMES predictions the $\langle K\rangle/\langle\pi\rangle$ ratio should be significantly different for hadron and QGP states. This would lead to an anomaly in the event-by-event fluctuations of the K/π ratio in a mixed phase (transition region) [31].

1.4 Event-by-event transverse momentum fluctuations - the subject of interest

The subject of this work is event-by-event analysis in transverse momentum, that can provide an important information about the dynamics of the A+A collisions and about the system state at the moment of freeze-out. There are two main goals of this work:

1. To observe how the fluctuations change with increasing number of nucleons participating in the collision i.e. with the system size. One can check whether the correlations present in elementary (p+p) interactions (such as the correlation between the average transverse momentum and multiplicity) survive for heavier colliding systems, as expected if A+A is a simple superposition of N+N interactions. Moreover a test will be performed of the reasonable expectation that the fluctuations become more similar to those of an equilibrated system when the number of participants increases.

2. To analyze the energy dependence of event-by-event transverse momentum fluctuations in order to find the possible anomalies connected with the region of the phase transition. In other words, if the initial conditions of the colliding system are close

to the phase boundary a QGP does not need to be created in every interaction due to the finite extent and short life-time of the system. This leads to essential differences between characteristics of "plasma events" and events where QGP is not created. As a reflection of this fact enlarged event-by-event fluctuations are expected to be observed. Studying the energy dependence of transverse momentum fluctuations might help to separate the energy region where hadron gas is created from that where QGP is created and the system crosses the phase boundary of the QCD phase diagram.

One should note that the above mentioned anomalies in the energy dependence of transverse momentum fluctuations, connected with the fact that the system is approaching the phase boundary, should appear if the phase transition is either the first-order (or the second-order) or the crossover. The important thing is the fact of crossing the phase boundary from the region of hadron gas to the region of QGP.

Additionally, qualitatively different fluctuations are predicted for the system that hadronizes close to the second-order critical end-point of the QCD phase diagram [19, 45] (the freeze-out point of the system should be located close to the predicted critical end-point). The most familiar analogy to this fluctuations is the phenomenon of critical opalescence observed in water (in the critical region matter shows anomalous properties; in the case of water large fluctuations in the size of liquid/vapor domains lead to the critical opalescence). It has been predicted that the increased dynamical fluctuations should appear both in transverse momentum and in multiplicity. As it has been already mentioned the (T, μ_B) area of the QCD phase diagram can be studied by varying both the energy and the size of the colliding system and therefore a possible non-monotonic dependence of p_T fluctuations on control parameters such as energy, centrality, ion size can help to locate the freeze-out point being a second-order critical end-point. From the one hand the non-monotonic appearance and then disappearance of the signatures of critical fluctuations can be a strong evidence of a second-order critical end-point. From the other hand when looking at a possible non-monotonic energy dependence of p_T fluctuations, a non-trivial question emerges: how to distinguish between fluctuations at the critical point from those connected with the fact that the system approaches the phase boundary in a region that can be located far from the critical end-point? So far there is no simple answer for this question. However, the observation of a non-monotonic variation in several observables predicted as the signatures of the critical point (such as p_T and multiplicity fluctuations), with the maxima at the same (or very close) values of control parameters, together with the lack of a non-monotonic variation of the observables *not* predicted as the signatures of the critical point can increase the probability that one is measuring rather the fluctuations connected with the critical end-point, than the fluctuations due to approaching the phase boundary.

All data sets used in the analysis are taken from the NA49 experiment and contain a broad range of energies: 20, 30, 40, 80, 158 AGeV central Pb+Pb data to study the energy dependence of transverse momentum fluctuations and p+p, C+C, Si+Si and 6 centralities of Pb+Pb interactions at 158 AGeV to analyze the system size dependence of transverse momentum fluctuations.

In the analysis of event-by-event fluctuations it is important to make a suitable choice of proper statistical tools to measure the fluctuations of interest namely, the dynamical part of event-by-event fluctuations. In this thesis the Φ_{p_T} measure, proposed in [34] will be used. In principle, the Φ_{p_T} can measure the expected effect of a QGP transition on temperature fluctuations. Φ_{p_T} has the property that it is insensitive to fluctuations in the impact parameter (event geometry) and the charged particle multiplicity. For alternative, but related, measures e.g. $\sigma_{p_T,dyn}$, $\Delta\sigma_{p_T}$, Σ_{p_T}, F_{p_T} and Σ_{p_T} (%) one can see the references [46], [47], [48], [49] and [50], respectively. This work extends the previous study of the NA49 experiment where the Φ measure has been used to study the p_T fluctuations [42]. Φ_{p_T} has been also calculated for a variety of nuclear models [51, 52, 53, 54, 55, 56]. These model predictions cannot, however, be directly compared to the data since the Φ measure is very sensitive to the detector acceptance which usually has not been taken into account in the model calculations.

Although the Φ measure is capable of detecting fluctuations of interest it does not say anything about the possible source of these. To gain more insight on this a study of two-particle transverse momentum correlations, as proposed in [47] (see [57] for a preliminary analysis), will be presented in addition.

Finally, as the third method of event-by-event analysis, the distribution of the average transverse momentum of the event will be studied and compared with the corresponding distribution for artificially produced events in which the particles are independent from each other (no inter-particle correlations, statistical fluctuations only).

The NA49 detector is able to register charged particles produced in heavy ion collisions. Therefore it is natural that the fluctuation analysis will be performed by use of all charged particles registered by the detector. Additionally, the fluctuation measure Φ_{p_T} will be calculated for negatively and positively charged particles, separately. The track-by-track identification is not possible in the NA49 experiment, however, one has to keep on mind that the sample of negatively charged particles produced in a high-energy heavy ion collision is composed by negative pions mainly, whereas the sample of positively charged particles is dominated by positive pions and protons (participants from the projectile). Due to these different particle contents it is expected that the transverse momentum dynamical fluctuations can be different for different charges. Moreover, the sample of all charged particles can include additional sources of dynamical fluctuations which are not present when looking at positively or negatively charged particles, separately. Therefore one should *not* expect that the Φ_{p_T} measure calculated by use of all charged particles will be directly a sum of Φ_{p_T} for positively and Φ_{p_T} for negatively charged particles.

The analysis will be performed by use of forward-rapidity [2] particles only. Due to the fact that track-by-track identification is not possible in the NA49 experiment the pion mass will be assumed for all particles.

[2] mid-rapidity region (central rapidity region) includes particles with $|y^*|$ close to zero, whereas forward-rapidity region is composed by particles with $y^* > 0$.

Chapter 2

Measures of fluctuations

2.1 Mean p_T (per event) distribution

There are a lot of observables which can be used to measure p_T fluctuations in high energy collisions. The observables presented in this chapter are based on the event-by-event method and their aim is to extract the dynamical part of event-by-event fluctuations.

A first and a very natural observable is the distribution of the average transverse momentum of the event defined as

$$M(p_T) = \frac{1}{N}\sum_{i=1}^{N} p_{Ti}, \tag{2.1}$$

where N is the multiplicity of accepted particles in a given event and p_{Ti} is the transverse momentum of the i-th particle. The distribution of $M(p_T)$ is usually compared to the corresponding distribution obtained for artificially produced 'mixed events' in which the particles are independent from each other (each particle in a mixed event is taken from a different real event) and follow the experimental inclusive distributions. The multiplicity distribution for mixed events is the same as for data (detailed description of the procedure of producing mixed events will be explained in the next chapter). A sample of mixed events is an important reference for the data because only statistical fluctuations are present in mixed events, therefore any difference between $M(p_T)$ distributions for data and mixed events can be a signature of the presence of dynamical fluctuations. In order to estimate the measured effect quantitatively a difference between the dispersions of these two distributions is calculated and the strength of non-statistical (dynamical) fluctuations can be expressed as

$$\sigma_{non-stat} = sgn(\sigma_{data} - \sigma_{mixed}) \cdot \sqrt{|\sigma^2_{data} - \sigma^2_{mixed}|}, \tag{2.2}$$

however, the method based on the use of equation 2.2 will not be used in this analysis. Usually, and as it has been observed by several experiments, the Gaussian shaped $M(p_T)$ distribution might be a slightly wider for data than for mixed events confirming the presence of dynamical p_T fluctuations. (In the case of large event-by-event fluctuations a group of any "special" events can form tails of the histogram thus increasing the total width of the $M(p_T)$ distribution.) Generally, many effects such as two-particle correlations due to quantum statistics, effects of thermalization, jet production, transverse expansion and finally effects of non-statistical fluctuations from event to event (for example temperature fluctuations) can modify the shape of inclusive p_T distribution of produced particles thus influencing the shape of $M(p_T)$.

Since the $M(p_T)$ distribution strongly depends on the particle multiplicity, the method described above cannot be used to compare systems of significantly different multiplicities.

2.2 Φ_{p_T} correlation measure

For many studied characteristics superposition models do not properly describe results on A+A collisions. For example there is no way to reproduce the strangeness enhancement using such models. It would be very instructive to check whether superposition models can be used to describe fluctuations in A+A collisions.

It has been observed that the average transverse momentum and particle multiplicity are correlated in N+N high-energy collisions [34]. This correlation should be observed for A+A as well, if the A+A is a superposition of independent N+N interactions. However there is no simple way to observe such correlation for A+A collision because A+A is composed by a large number of N+N interactions ("sources") and the correlation can be observed for particles which come from the same "source" only. In the case of an A+A collision, final state particles come from different "sources" (N+N) and there is no way to extract individual "source" from A+A interaction. Therefore the method of measuring correlations independently of the number of "sources" and multiplicity has been required. The quantity Φ, proposed in [34] is a measure which is insensitive to the system size and the effect of source superposition.

In this thesis the Φ measure is used for the analysis of p_T fluctuations (Φ_{p_T}). Following the authors of [34] one can define a single-particle variable $z_{p_T} = p_T - \overline{p_T}$ with the over-bar denoting averaging over a single particle inclusive distribution. One can easily see that $\overline{z_{p_T}} = 0$. Further, one introduces the event variable Z_{p_T}, which is a multi-particle analog of z_{p_T}, defined as

$$Z_{p_T} = \sum_{i=1}^{N} (p_{Ti} - \overline{p_T}), \tag{2.3}$$

where the summation runs over particles in a given event. Note, that $\langle Z_{p_T} \rangle = 0$, where $\langle ... \rangle$ represents averaging over events. Finally, the Φ_{p_T} measure is defined as

$$\Phi_{p_T} = \sqrt{\frac{\langle Z_{p_T}^2 \rangle}{\langle N \rangle}} - \sqrt{\overline{z_{p_T}^2}}. \tag{2.4}$$

While measuring event-by-event fluctuations in A+A collisions one should remember about the influence of two trivial sources of fluctuations. The first one is caused by event-by-event fluctuations of the collision geometry (impact parameter variation) and the second one by the finite number of particles (statistical fluctuations). Φ_{p_T} is a quantity which eliminates both these trivial sources and measures only the dynamical part of event-by-event fluctuations.

There are two most important properties of the Φ_{p_T} measure. It can be easily shown that if the large system (A+A) consist of particles that are emitted independently (no inter-particle correlations) Φ_{p_T} assumes a value of zero (detailed calculations are presented in [34] and [58]). For example in the equilibration model independent particle production is realized by a huge number of secondary interactions. On the other hand, if A+A is an incoherent superposition of many independent N+N interactions (superposition model), than Φ_{p_T} has a constant value, the same for A+A and N+N collisions. More precisely, Φ_{p_T} is *independent* of the distribution of the number of particle sources if the sources are identical and independent from each other [34, 36] and in particular, Φ_{p_T} does not depend on the impact parameter (centrality) if the A+A collision is a simple superposition of N+N interactions. If secondary interactions start to play an important role and the "sources" which compose A+A collision can interact the Φ_{p_T} value is reduced when compared to N+N and in the limiting case, when final state particles are produced independently, Φ_{p_T} equals zero.

There is a never-ending and very important question how the fluctuation measures such as $\sigma_{p_T,dyn}$, $\Delta\sigma_{p_T}$, Σ_{p_T} and Φ_{p_T} depend on the observed multiplicity. The answer, however, depends on the kind of the studied variable and - what is even more important - on the way the multiplicity is varied. If one changes the multiplicity by changing centrality (what can be treated approximately as changing the number of identical "sources") then Φ, as it has been already mentioned, remains constant (the other variables do not necessarily have such a property, for example Σ_{p_T} changes significantly with centrality). One can also change the multiplicity by changing the acceptance or detector efficiency. In this situation the behavior of Φ depends on the kind of correlations present in the system (scale of correlations). The value of Φ should not be changed if the only source of correlations are short-range correlations and the length of the correlations is smaller than the acceptance (the remaining multiplicity is still reasonable to maintain short-range correlations). But not complete acceptance or the detector inefficiency can reduce significantly long range correlations (the detector often looses one particle from a correlated pair). Summarizing, different contributions to fluctuations have different multiplicity dependences. In the superposition model Φ does not depend on centrality but its dependence on acceptance and detector efficiency is determined by the correlation nature. Therefore, it should be stressed that it is rather difficult to directly compare Φ_{p_T} values between experiments with different kinematic and geometrical acceptance. It seems to be more reasonable to make a coherent comparison of Φ_{p_T} values within the same experiment (the same detector acceptance) for several colliding systems and for different energies.

A large amount of secondary interactions leads a system to thermodynamical equilibration (on the parton or hadron level). Thus a reduction of Φ_{p_T} value, which can be connected with secondary interactions, can measure the level of equilibration in high-energy collision. However, one has to keep in mind that vanishing Φ_{p_T} does not indicate the QGP formation.

As it has been already mentioned the Φ_{p_T} has been studied by a variety of models (unfortunately most of them do not include the limited acceptance of the detector). In principle, Φ_{p_T} has been calculated for the equilibrium ideal gas [35, 36] and it has been shown that - as expected - Φ_{p_T} value vanishes for particles obeying Boltzmann statistics whereas some rudimentary correlations can be observed for quantum particles even in the case of thermodynamical equilibrium. These correlations which are of the short range in momentum space are responsible for non-zero Φ_{p_T} value - positive for bosons and negative for fermions. One has to remember that the short range correlations are significant for A+A collisions only (due to high particle density in momentum space), whereas their contribution for elementary interactions is negligible.

Φ_{p_T} has been also studied in a classical thermodynamical model assuming temperature (inverse slope parameter of p_T distribution) fluctuations from event to event [56]. The Φ_{p_T} measure has been found to be very sensitive to the temperature fluctuations. This model takes into account the possible acceptance limitations and therefore its predictions will be compared to the data in the next chapters.

2.3 Transverse momentum two-particle correlations

In spite of the above mentioned advantages, there is an important disadvantage of using Φ_{p_T} in the fluctuation analysis. While Φ_{p_T} is sensitive to the presence of dynamical fluctuations (particle correlations) in a system, it does not tell what is the correlation nature. The point is that correlations (fluctuations) of very different character contribute to Φ_{p_T}. For better understanding the fluctuation structure one can also apply a more differential method [47]. Since Φ_{p_T} is defined through the second moments of the event and inclusive p_T distributions, the event-by-event fluctuations quantified by Φ_{p_T} are related to the two-particle correlations. The correlations can be studied by plotting a cumulative variable of particle pairs. Namely, instead of p_T one introduces the variable x defined for a particle i as [59]

$$x(i) = \int_0^{p_{Ti}} \rho(p_T) dp_T, \tag{2.5}$$

where $\rho(p_T)$ is the inclusive p_T distribution, normalized to unity, which is obtained from all particles used in the analysis (all accepted particles). By its construction, the x variable varies between 0 and 1 with a *flat* probability distribution. The two-particle correlation plots, as presented in this thesis, are obtained by plotting (x_1, x_2) points for all possible particle pairs within the same event. The number of pairs in each (x_1, x_2) bin (point in figure) is divided by the mean number of pairs in a bin (averaged over all (x_1, x_2) bins). This two-dimensional plot is *uniformly* populated when no correlations are present in the system. The possible non-uniform structure can signal the presence of dynamical fluctuations for example: the inter-particle correlations due to the Bose statistics produce a ridge along the diagonal of the (x_1, x_2) plot, which starts at $(0, 0)$ and ends at $(1, 1)$, whereas the event-by-event temperature fluctuations exhibit a saddle shaped structure [47].

As will be seen in the figures, the distribution of x_1 or x_2 obtained from the two-dimensional (x_1, x_2) plots by projecting on the x_1 or x_2 axis is *not* flat although the definition (2.5) may suggest flatness. This is the result of the method by which the plots are constructed. Namely, each pair of particles is represented by a point on the plot. Therefore, the events with larger multiplicities are represented by a larger number of pairs than those with smaller multiplicities. Since the shape of p_T distribution depends on multiplicity of the event the projection of the two-dimensional plot on x_1 or x_2 is no longer flat. However, it should be pointed out that in the absence of *any* correlation the (x_1, x_2) plot is *uniformly* populated and the x_1 and x_2 projections are *flat*.

Chapter 3

NA49 experiment

The NA49 is one of the fixed target experiments carried out at CERN laboratory in Geneva. The NA49 detector is a large acceptance hadron spectrometer for the study of hadronic final states produced by p+p, p+A and A+A collisions at the CERN-SPS energies. The detectors of the NA49 experiment registered collisions at 20, 30, 40, 80 and 158 GeV/nucleon of the projectile energy. The last one corresponds to 33 TeV total beam energy and about 17 GeV center-of-mass energy per nucleon pair ($\sqrt{s_{NN}}$).

In the case of central Pb+Pb collisions at 158 AGeV the lead nuclei are accelerated to the velocity of 99.4% of the speeed of the light and are collided with thin lead foil. The NA49 is able to detect 80% of about 1500 particles produced in such collisions. The main components of the detector are four large volume Time Projector Chambers (TPC), two of them placed in the magnetic filed, for tracking and particle identification, Time of Flight (TOF) scintillator arrays for particle identification at mid-rapidity and set of calorimeters which allow for triggering and transverse energy determination. The set-up of the NA49 detector is shown in Fig. 3.1.

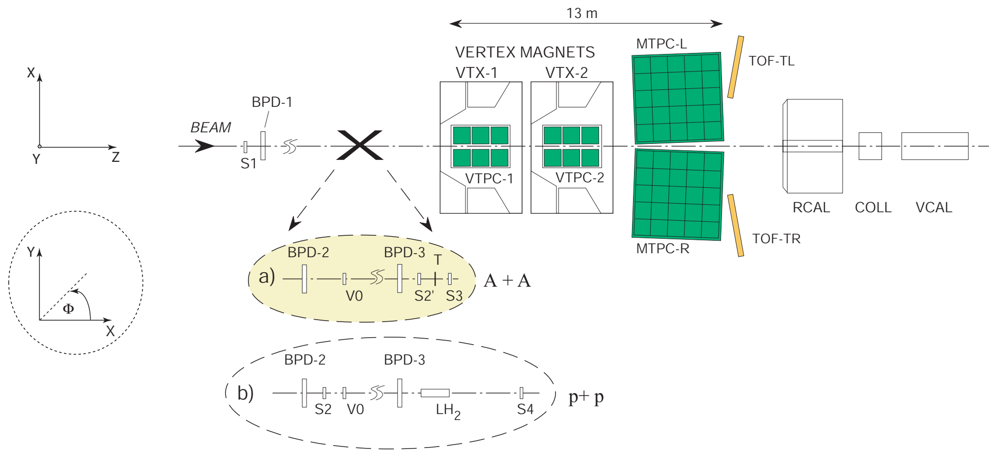

Figure 3.1: The set-up of the NA49 experiment with different beam definitions and target arrangements. Figure taken from [60].

3.1 Beam detectors and triggering

The NA49 detector is located in the H2 beam line of the North experimental hall of the SPS accelerator. The schematic drawing of present and future accelerators at CERN is shown in Fig. 3.2. The primary protons and lead ion beams, used by the NA49 experiment are produced by linear accelerator. Then they are injected into the Proton Synchrotron Booster which can accelerate the beam particles up to 95 AMeV/c and as the next step beam particles pass through the Proton Synchrotron (PS) (acceleration to 4.5 AGeV/c) and finally the beam passes into the Super Proton Synchrotron (SPS) accelerator where the maximal reachable laboratory momenta are about 450 GeV/c for protons, about 200 GeV/c per nucleon for lighter ions (Sulfur) and 158 GeV/c per nucleon for Pb ions. The particles are injected into the detector in short and separate spills. The typical intensity of Pb ions is about 10^8 per SPS pulse. The intensity extracted to the NA49 detector is of the order of 10^5 Pb ions per pulse. The H2 beam line transports beam particles (p, Pb from SPS and C, Si from the fragmentation beam) to the detector set-up where collisions with a variety of fixed targets take place. A set of beam position detectors (BPD) provides a precise measurement of the charge and the position of incoming beam particles. A set of trigger counters and calorimeters allow for triggering on different final state topologies.

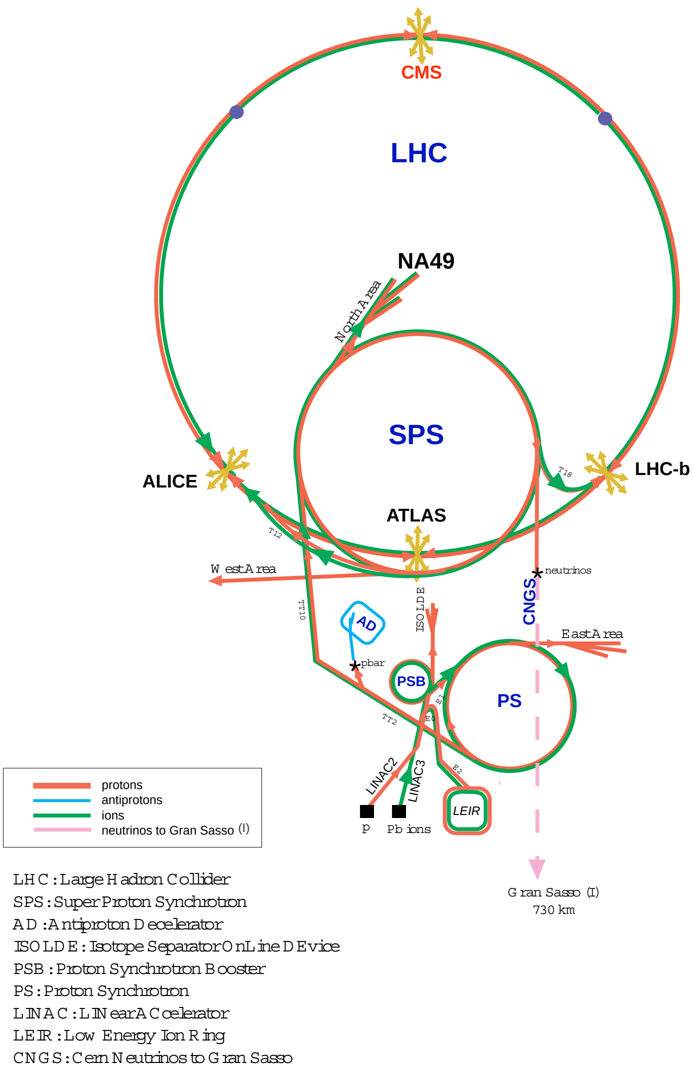

Figure 3.2: Schematic drawing of the complex of the CERN accelerators. Figure taken from CERN Image Library.

Pb beam particles are identified by their charge in a thin Helium Gas-Cerenkov counter (S2') and p beam particles by 2 mm scintillator (S2) - Fig. 3.1. They are both placed in front of the target. The study of C+C and Si+Si reactions is possible through the generation of a secondary fragmentation beam which is produced by a primary target (1 cm carbon) in the extracted Pb-beam (the fragmentation target is placed about 30 m before the experimental target). An example of Pb-beam fragmentation spectrum is shown in Fig 3.3. With the proper setting of the beam line magnets a large fraction of all $Z/A = 1/2$ fragments at ≈ 158 AGeV are transported to the NA49 experiment. On-line selection based on a pulse height measurement in a scintillator beam counter (S2) is used to select particles with $Z = 6$ (Carbon) and $Z = 13, 14, 15$ (Al, Si, P). (Using a Cerenkov trigger for such small Z nuclei is not possible - there would be no signal visible). Off-line clean-up is achieved by using in addition the energy loss measured in 6 MWPCs (BPDs) used also for the beam position determination. BPD counters (BPD-1/2/3) are small proportional chambers, along the beam line, used to measure the transverse positions of the incoming beam particles.

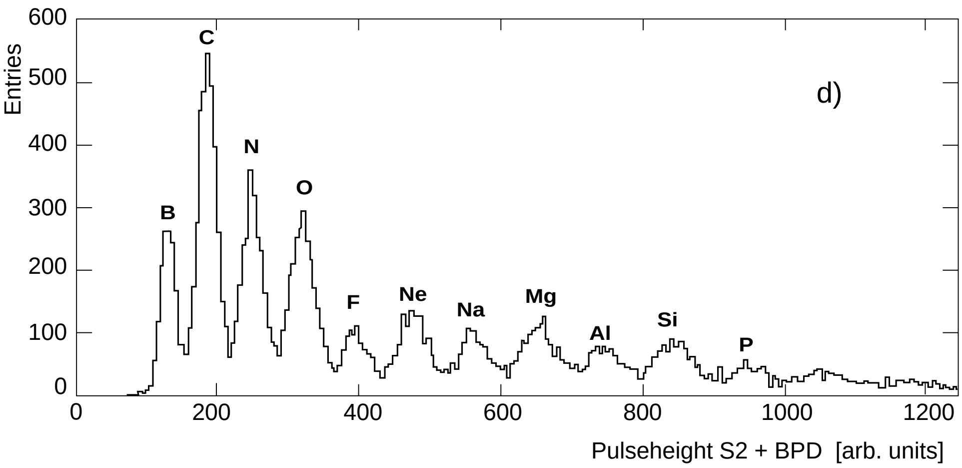

Figure 3.3: Pb-beam fragmentation spectrum from a 1 cm carbon target with the beam line set to select $Z/A = 1/2$. A clear Z-separation is achieved all the way from Boron to Phosphorus. Figure taken from [60].

For p, C and Si beams, interactions in the target are selected by anti-coincidence of the incoming beam particle with a small scintillation counter (S4) placed on the beam line between the two vertex magnets. For p+p interactions at 158 AGeV this counter selects a (trigger) cross section of 28.5 mb out of 31.6 mb of the total inelastic cross section. For Pb-ion beams, an interaction trigger is provided by anti-coincidence with a Helium Gas-Cerenkov counter (S3) directly behind the target. S3 counter is used to select minimum bias collisions by requiring a reduction of the Cerenkov signal by a factor of about 6. Since the Cerenkov signal is proportional to Z^2, this requirement ensures that the Pb projectile has interacted with a minimal constraint on the type of interaction. This set-up limits the triggers on non-target interactions to rare beam-gas collisions, the fraction of which proved to be small after cuts, even in peripheral Pb+Pb collisions.

3.2 Target

The targets, C (561 mg/cm^2), Si (1170 mg/cm^2) and Pb (224 mg/cm^2) for ion collisions and liquid hydrogen cylinder (20 cm length) for elementary interactions, are positioned about 80 cm upstream from Vertex TPC-1 (VTPC-1).

3.3 TPC tracking system

The main tracking devices of the NA49 experiment are four large volume Time Projection Chambers (drift chambers) (Fig. 3.1) which are able to detect 80% charged particles created in a central Pb+Pb collision at 158 AGeV (the acceptance losses are concentrated mainly in the backward rapidity region and around up-down regions of azimuthal angle). Two of TPCs, the Vertex TPCs (VTPC-1 and VTPC-2), are located in the magnetic field of two super-conducting dipole magnets (1.5 and 1.1 T, respectively at 158 AGeV; for lower energies the magnetic field is scaled down in proportion to the beam energy) and two other - Main TPCs (MTPC-L and MTPC-R) are positioned downstream with respect to the magnets on both sides of the beam. Due to the high magnetic field particles with opposite charges are cleanly separated in MTPSs. TPSs allow for particle tracking and precise measurement of specific energy loss (dE/dx) in the region of relativistic rise. NA49 TPCs allow for precise measurements of particle momenta p with a resolution of $\sigma(p)/p^2 \cong (0.3-7)\cdot 10^{-4}$ (GeV/c)$^{-1}$. The combined information on dE/dx and momentum allows for particle identification. A typical dE/dx resolution for central Pb+Pb collisions is 4.5%. About 50% of all particles produced in central Pb+Pb interaction are identified via dE/dx measurement. For purpose of this analysis dE/dx information is not used.

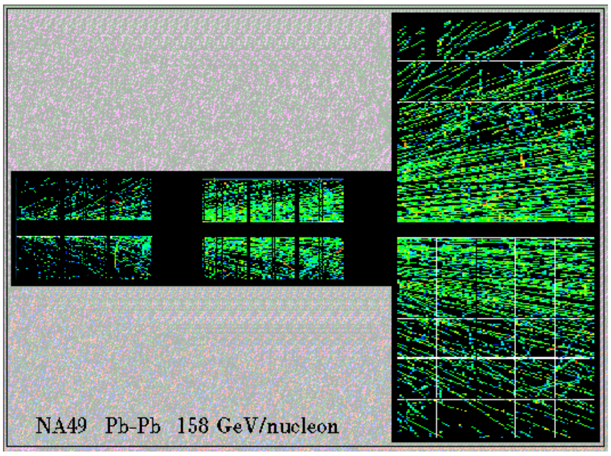

Figure 3.4: The typical Pb+Pb collision at 158 AGeV energy as seen by the detectors of the NA49 experiment. Figure taken from [60].

The typical Pb+Pb collision at 158 AGeV energy is presented in Fig. 3.4, where the tracks of produced charged particles are seen in all TPCs.

The NA49 track reconstruction software consists of several steps:

1. procedure of finding charge clusters in the TPC system and determining x, y and z position of each cluster (point on a track)
2. construction of track elements in each of TPCs separately
3. matching local track elements from TPCs into one global track
4. reconstruction of the main vertex position
5. determination of momentum by fitting the track through the magnetic field to the main vertex

6. reconstruction of secondary vertices and determination of momentum of the daughter particles

The results presented in this work were analyzed with a global tracking scheme [61], which combines track segments belonging to the same physical particle but detected in different TPCs.

3.4 TOF

Particle identification in the region of minimum ionization ($\beta\gamma \simeq 3$) is supplemented by four walls of Time of Flight (TOF) scintillator detectors placed behind MTPCs. Additional arrays of PesTOF counters, positioned in a plane between the two magnets, extend TOF determination into backward center-of-mass rapidity region. The combined information about the velocity of the particle (form TOF) and momentum (form TPCs) allow for particle identification close to mid-rapidity. A typical resolution of TOF is 60 ps. About 6% of all particles produced in central Pb+Pb interaction are identified by use of TOF scintillators (mid-rapidity particles mainly). For purpose of this analysis TOF information is not used.

3.5 Centrality of the collision

The centrality of the nuclear collision is selected (on-line for central Pb+Pb and off-line for minimum bias Pb+Pb interactions) by a trigger that uses information from a downstream Veto Calorimeter (VCAL), which measures the energy of the projectile spectator nucleons. The geometrical acceptance of the VCAL is adjusted in order to cover the projectile spectator region by a proper setting of the collimator (COLL).

The additional calorimeter which can determine the centrality of the collision is Ring Calorimeter, which measures the energy of hadronic showers created by charged pions. It is used to determine the hadronic component of the transverse energy of the collision. Information from Ring Calorimeter is not used for the purpose of this analysis.

The details of the NA49 detector set-up and performance of tracking software are described in [60].

Chapter 4

System size dependence of p_T fluctuations at 158 AGeV

4.1 Data sets used in analysis

The experimental material used for the analysis of the system size dependence of p_T fluctuations is composed by samples of p+p, C+C, Si+Si and Pb+Pb collisions at 158 AGeV. In the case of Pb+Pb interactions a minimum bias trigger has been used. The distribution of the energy measured in the VCAL for the minimum bias Pb+Pb events has been divided into six centrality bins (Table 4.1).

	year	No. of events	σ/σ_{tot} in each bin	$\langle N_W \rangle$	b range $[fm]$
p+p	2000	570 000	0.9	2	
C+C	1998	33 000	0.153	14	0 - 2.0
Si+Si	1998	63 000	0.122	37	0 - 2.6
Pb+Pb(6)	1996, 1999	117 000	0.57	42	10.2 -
Pb+Pb(5)	1996, 1999	59 000	0.10	88	9.1 - 10.2
Pb+Pb(4)	1996, 1999	68 000	0.10	134	7.4 - 9.1
Pb+Pb(3)	1996, 1999	68 000	0.11	204	5.3 - 7.4
Pb+Pb(2)	1996, 1999	45 000	0.075	281	3.4 - 5.3
Pb+Pb(1)	1996, 1999	180 000	0.05	352	0 - 3.4

Table 4.1: Data sets used in analysis. Listed for p+p, C+C, Si+Si and six centralities of Pb+Pb collisions at 158 AGeV are: year of data taking, number of events, σ/σ_{tot} - the fraction of the total inelastic cross section in that bin, $\langle N_W \rangle$ - the mean number of wounded nucleons, b - the impact parameter range.

Centrality bins are numbered from 1 (the most central collisions) to 6 (the most peripheral interactions). For each centrality bin the range of the impact parameter b, and the mean number of wounded nucleons $\langle N_W \rangle$ have been determined by use of the Glauber model of nuclear interactions and the VENUS event generator [62]. The fraction of the total inelastic cross section of A+A collisions (σ/σ_{tot}) corresponding to each data set has been calculated directly by use of the distribution of energy measured in VCAL. In order to determine the dependence of the energy deposited in the VCAL on the impact parameter minimum bias VENUS events have been processed through the GEANT detector simulation code, and the energy deposited in VCAL has been simulated. The correlation between b and $\langle N_W \rangle$ has been calculated from the Glauber model using the spectator-participant model of A+A interactions. Fig. 4.1 a) presents distribution of the energy

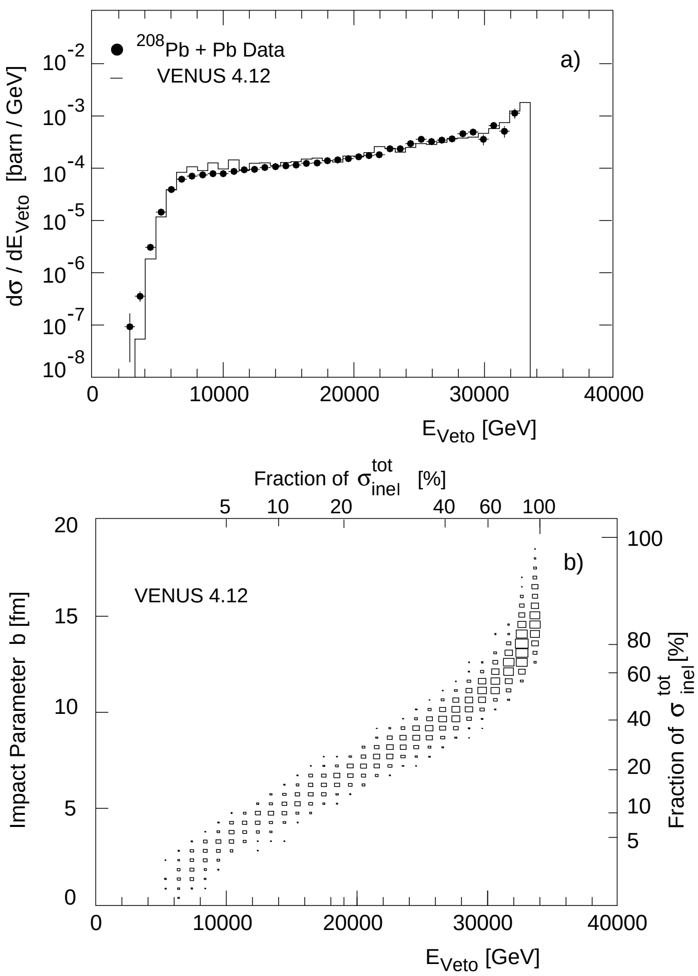

Figure 4.1: a) Energy spectrum measured in VCAL in minimum bias Pb+Pb interactions at 158 AGeV, b) impact parameter and fraction of the total inelastic cross section related to the energy in VCAL as derived from the VENUS model. Figure taken from [60].

measured in VCAL for real minimum bias Pb+Pb collisions and for VENUS Pb+Pb interactions. The left tail of the distribution corresponds to the most central interactions (1) and the right one to the most peripheral ones (6). In Fig. 4.1 b) b values, fractions of total inelastic cross sections and corresponding E_{Veto} ranges are shown. The values of σ/σ_{tot}, $\langle N_W \rangle$ and b presented in Table 4.1 are taken from [63] for minimum bias Pb+Pb collisions and from [64] for C+C and Si+Si interactions.

The most central Pb+Pb events correspond to 5% of the total geometric cross section. Since the minimum bias data provide only a small number of events in the most central Pb+Pb bin, additional central trigger runs have been used. In order to increase the statistics minimum bias Pb+Pb data have been taken in three data-taking periods and with opposite field polarities.

4.2 Event and particle selection criteria

4.2.1 Event cuts

The obvious aim of using the event selection criteria is to reduce a possible contamination due to non-target interactions. The primary vertex has been reconstructed by fitting the intersection point of the measured particle trajectories.

Only events with a proper quality and position of the reconstructed vertex are accepted in this analysis, e.g. the vertex coordinate z along the beam has to satisfy $|z - z_0| < \Delta z$, where z_0 is the nominal vertex position and Δz is a cut parameter. The values of z_0 and Δz are: -579.5 and 5.5 cm for p+p, -579.5 and 1.5 cm for C+C, -579.5 and 0.8 cm for Si+Si and -578.9 and 0.4 cm for Pb+Pb data. The values of the cut parameters of the x and y positions of the fitted vertex (Δx and Δy) are about 0.1 - 0.3 cm for p+p and Pb+Pb data and 0.5 - 1.0 cm for C+C and Si+Si samples. Additional cut on the number of tracks used to fit the primary vertex divided by the total number of tracks outgoing from the main vertex (ntf/nto) has been used. The value of this cut varies from 0.15 to 0.25 for all data sets. Fig. 4.2 shows the example of the fitted vertex position (x, y and z coordinates) and the distribution of the ntf/nto ratio for 5% central Pb+Pb interactions at 158 AGeV.

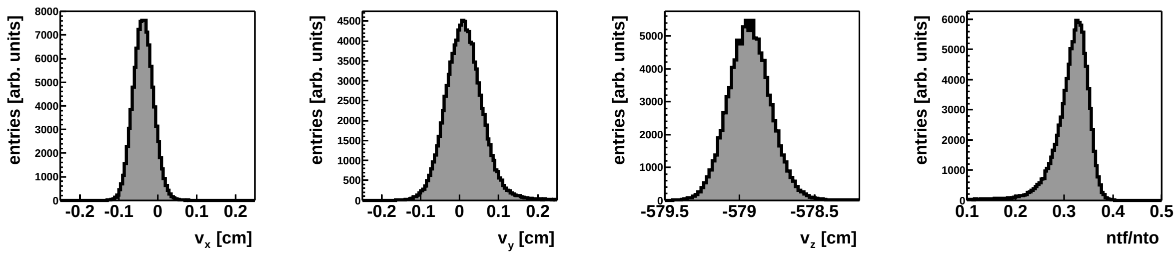

Figure 4.2: The distribution of x, y and z positions of the primary vertex and the distribution of the ntf/nto ratio for 5% central Pb+Pb collisions at 158 AGeV.

4.2.2 Track cuts

In order to reduce the possible contamination of particles from secondary interactions, weak decays and other sources of non-vertex tracks, several track cuts are applied.

1. The accepted track has to have a good fitting quality.
2. The accepted particles are required to contain points measured in at least one of the Vertex TPCs (the cut on the z position of the first point in the track).
3. A cut on the so-called track impact parameter, the distance between the reconstructed primary vertex and the track in the target plane ($|b_x| < 2$ cm and $|b_y| < 1$ cm) to reduce the contribution of non-vertex particles.
4. Particles are accepted only when the potential number of points (nmp), calculated on the basis of the geometry of the track, in the detector is higher than 30.
5. The ratio of the number of points on a track to the potential number of points (np/nmp) is required to be higher than 0.5 in order to avoid the counting of track segments instead of whole tracks.

In Fig. 4.3 b_x, b_y, np and np/nmp distributions are presented for 5% central Pb+Pb collisions at 158 AGeV. The two-modal shape of np distribution is a reflection of the fact that some tracks are registered in VTPCs only and some of them are detected both by VTPCs and MTPCs (their trajectories are longer and therefore the number of points is higher).

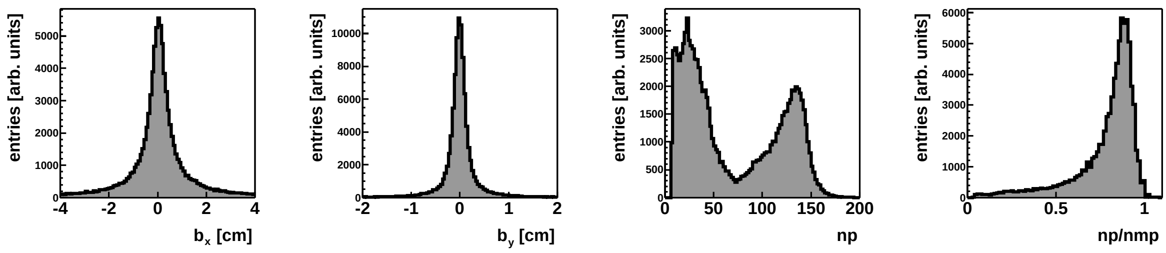

Figure 4.3: The distributions of b_x, b_y, np and np/nmp ratio for 5% central Pb+Pb collisions at 158 AGeV. Only tracks with $nmp > 30$ have been used to prepare np/nmp distribution.

4.2.3 The NA49 acceptance for the fluctuation analysis

The NA49 detector is able to register particles produced in a wide rapidity range covering almost the whole forward hemisphere. The aim of this work is to present quantitative results for Φ_{p_T} correlation measure within a well defined phase space region covered by the detector set-up. It allows to compare experimental results with theoretical models in a quantitative way. It would be very interesting to study p_T fluctuations in the mid-rapidity region (preliminary results have been already obtained). However, the geometry of the NA49 detector makes the acceptance in the azimuthal angle much worse for mid-rapidity particles. In addition, low momentum particles are registered in this rapidity region and their reconstruction efficiency differs from that for higher momentum particles. Therefore a direct comparison of results obtained in mid- and forward-rapidity regions becomes difficult and less reliable. Experimental corrections, easy to include in the case of single particle characteristics, depend significantly on the assumed nature of correlations in the case of a correlation measure, and they can be calculated only within a specific model of correlation. Moreover, from the experimental point of view, some not yet fully understood dependences of Φ_{p_T} value on event and track selection criteria have been observed for the data at mid-rapidity region and they have been intensively studied. This leads to the statement that up to now only qualitative understanding of results in mid-rapidity area has been achieved and the preliminary results cannot be directly compared to the well understood and quantitative forward-rapidity results.

Therefore, for the purpose of this work only very forward rapidity tracks ($4.0 < y_\pi < 5.5$, rapidity calculated assuming the pion mass for all particles) with $0.005 < p_T < 1.5$ GeV/c are used. The track-by-track particle identification, required in this analysis, is practically not possible in the experiment and therefore the pion mass has been set for all particles. The above y_π and p_T cuts imply that rapidities of the selected kaons and protons range from 2.7 to 5.0 and from 2.5 to 5.0, respectively. Note that the center-of-mass rapidity in the laboratory system is 2.91 at 158 AGeV.

As it has been already mentioned, the NA49 detector provides a large acceptance in the forward hemisphere. However, even in this kinematic region the geometrical acceptance is not complete. Three example plots of p_T versus azimuthal angle ϕ (see Fig. 3.1 for definition) for positively charged particles (the standard magnetic field polarity) are shown in Fig 4.4.

The solid lines represent the analytical parametrization of the acceptance limits given by the formula:

$$p_T(\phi) = \frac{1}{A + \phi^2/C} + B, \tag{4.1}$$

where A, B and C parameters depend on the rapidity interval and their values are estimated from the plots such as those shown in Fig. 4.4. The values of A, B and C

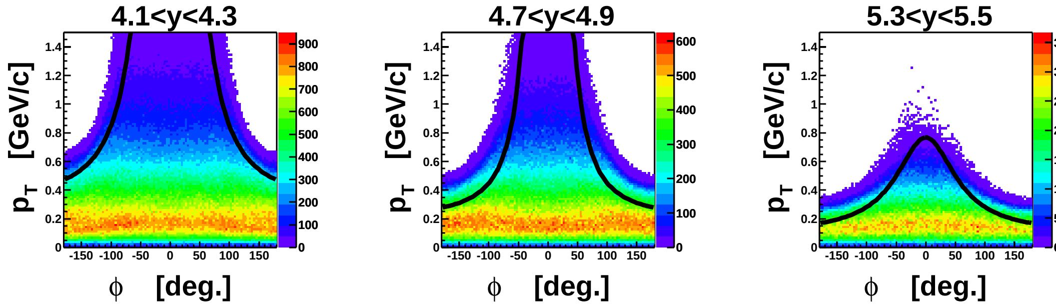

Figure 4.4: NA49 $\phi - p_T$ acceptance of positively charged particles (standard configuration of magnetic field) for three selected rapidity bins at 158 AGeV. The solid lines represent the analytical parametrization.

parameters for all rapidity bins are presented in Table 4.2.

y_π	$A[\frac{c}{GeV}]$	$B[\frac{GeV}{c}]$	$C[\frac{deg.^2 GeV}{c}]$
3.9 - 4.1	0	0.3	6500
4.1 - 4.3	0	0.3	5500
4.3 - 4.5	0	0.25	4500
4.5 - 4.7	0	0.25	3500
4.7 - 4.9	0	0.2	2500
4.9 - 5.1	0.5	0.2	2500
5.1 - 5.3	1.0	0.1	2500
5.3 - 5.5	1.5	0.1	2500

Table 4.2: The parametrization of the NA49 $y - p_T$ acceptance at 158 AGeV for positively charged particles (standard configuration of magnetic field). For negatively charged particles one has to change the definition of the azimuthal angle (see the text) and then use the same parametrization.

For the standard polarity of the magnetic field accepted positively charged particles are concentrated close to $\phi = 0^o$, whereas the accepted negatively charged particles are situated in the opposite direction ($\phi = 180^o$). In order to obtain the same p_T versus ϕ structure and to use the same analytical parametrization for negatively charged particles their azimuthal angle is calculated relative to the negatively oriented x axis (for all negatively charged particles with $\phi < 0^o$ their azimuthal angle is changed as follows $\phi = \phi + 360^o$ and finally for all negatively charged particles $\phi = \phi - 180^o$). Only particles within the analytical curves are used in this analysis. This well defined acceptance is essential for later comparison of the results with models and other experiments.

4.3 Error estimates and corrections

4.3.1 Statistical errors

The statistical errors of Φ_{p_T} values in this work, both for the system size and the energy dependence of Φ_{p_T} measure, are calculated using the so-called subsample procedure. The whole sample of events is divided into 30 subsamples. The value of Φ_{p_T} is evaluated for each subsample and the dispersion (D) of the results is then calculated. The statistical error of Φ_{p_T} is taken to be equal to $D/\sqrt{30}$.

4.3.2 Systematic errors

The event and track selection criteria used in the analysis reduce the possible systematic bias of the measured Φ_{p_T} values, however, there is always the remaining systematic uncertainty. In order to estimate the systematic error of Φ_{p_T} the value of a given cut parameter has been varied within a reasonable range and the partial (for this cut) systematic error has been estimated as a half of the difference between the highest and the lowest Φ_{p_T} value. The above procedure has been applied for all possible sources of systematic uncertainty (two event cuts and two track cuts) and as a final estimate of the total systematic error on Φ_{p_T} a maximal error resulting from such a study has been taken (cut parameters can be correlated thus one cannot simply add all contributions in order to estimate the total systematic error). As an additional check, results obtained from the analysis of data taken at two different magnetic field polarities as well as from different running periods have been compared and have been found to be consistent for all studied data sets.

Event cuts are used to reject a possible contamination of non-target interactions, however there is always a small fraction of remaining non-target events which can influence the Φ_{p_T} values. One of the event characteristics that can be used for a more reliable selection of the target interactions is the ratio of ntf/nto. Fig. 4.5 shows the Φ_{p_T} dependence on the ntf/nto cut for several data sets (p+p, Si+Si, the most central Pb+Pb and the most peripheral Pb+Pb collisions). The observed variation of Φ_{p_T} with ntf/nto is rather small and the partial systematic error due to this effect is not higher than 1.15 MeV/c for peripheral Pb+Pb collisions, 0.3 MeV/c for central Pb+Pb, 1.05 MeV/c for Si+Si data and 1.0 MeV/c for p+p interactions.

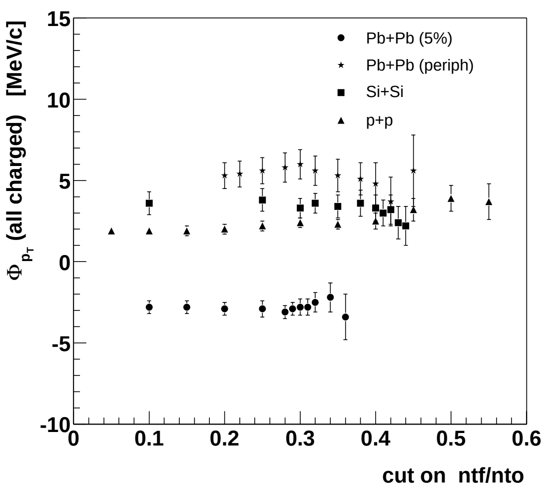

Figure 4.5: The dependence of Φ_{p_T} on one of the event cuts (ntf/nto ratio). Note: the values and their errors are correlated.

The dependence of Φ_{p_T} on an other event selection cut, Δz, is shown in Fig. 4.6 for p+p, Si+Si, the most central and the most peripheral Pb+Pb interactions. The observed variation of Φ_{p_T} with Δz is small even for the most peripheral Pb+Pb interactions where the expected contamination with non-target interactions and with interactions different than Pb+Pb nuclei is highest. The partial systematic error is lower than 0.95 MeV/c for peripheral Pb+Pb collisions, 0.45 MeV/c for central Pb+Pb, 0.55 MeV/c for Si+Si data and 0.5 MeV/c for p+p events.

The majority of tracks selected by the track selection criteria are primary vertex tracks and the remaining fraction (≈10%) originates mostly from weak decays and secondary

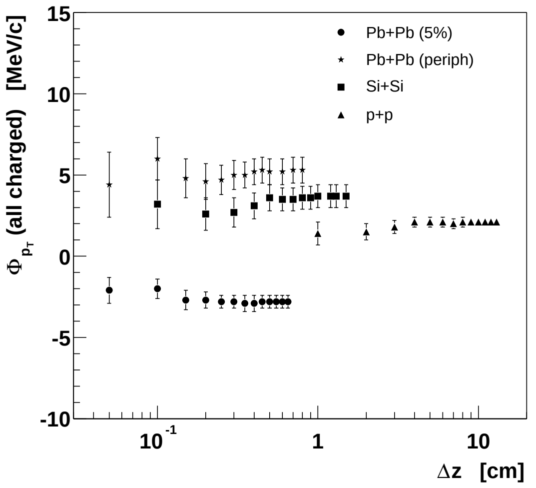

Figure 4.6: The dependence of Φ_{p_T} on the allowed distance Δz from the nominal position of the main vertex. Note: the values and their errors are correlated.

interactions with the material of the detector. In order to estimate the influence of this contamination on the measured value of Φ_{p_T}, the impact parameter cut has been varied within a reasonable range (Fig. 4.7). A small increase of Φ_{p_T} with increasing impact parameter cut is observed and may be due to the increased contribution of non-vertex tracks from weak decays and secondary interactions as suggested by VENUS [62] simulations. Fully simulated and reconstructed by the standard reconstruction chain VENUS events have been used for an independent estimate of the influence of the contribution of non-vertex tracks. It has been found that for central Pb+Pb collisions, where the bias is the largest, the value of Φ_{p_T} decreases by about 1 MeV when non-vertex tracks (about 12% of all accepted) are excluded from the analysis of the reconstructed VENUS events. The estimated partial systematic error due to the contamination of non-vertex tracks (resulting from 4.7) is lower than 1.6 MeV/c for central Pb+Pb collisions, 0.85 MeV/c for peripheral Pb+Pb, 0.75 MeV/c for Si+Si data and 0.35 MeV/c for p+p events.

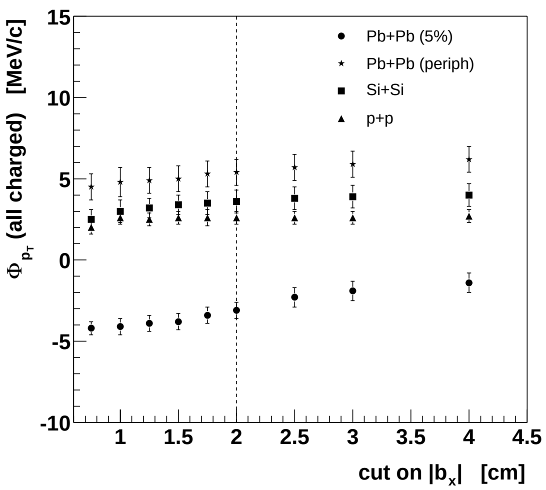

Figure 4.7: The dependence of Φ_{p_T} on upper cut in the impact parameter $|bx|$. For each point the cut on $|by|$ is equal half the cut on $|bx|$. Note: the values and their errors are correlated. The dashed line indicates the cut used in the analysis.

Another cut which can reduce the possible contamination with non-vertex tracks and select tracks with a better quality is np/nmp ratio. Fig. 4.8 shows the Φ_{p_T} dependence on the lower cut of np/nmp. The range of the variation of this cut parameter depends on data set. The reason is that p+p, C+C and Si+Si data have been reconstructed using a slightly different (than for Pb+Pb) reconstruction chain and, in principle, the shape of np/nmp is not the same in both cases. The estimated partial systematic error connected with the Φ_{p_T} dependence on the lower cut of np/nmp is smaller than 0.55 MeV/c for central Pb+Pb, 1.6 MeV/c for peripheral Pb+Pb, 1.15 MeV/c for Si+Si and 0.25 MeV/c for p+p collisions.

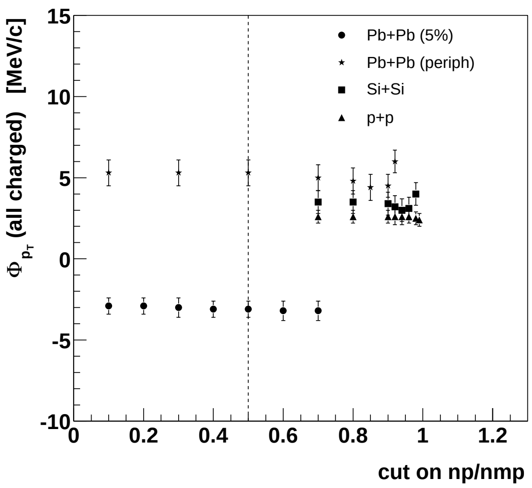

Figure 4.8: The dependence of Φ_{p_T} on lower cut on np/nmp ratio. Note: the values and their errors are correlated. The dashed line indicates the cut used in the analysis.

Table 4.3 summarizes the examples of the possible sources (components) of the systematic error resulting from the variation of the values of cut parameters. The examples are presented for p+p, Si+Si, the most central (1) Pb+Pb and the most peripheral (6) Pb+Pb interactions. The partial systematic errors have been calculated for all charged particles and for negatively and positively charged hadrons separately.

	Φ_{p_T} vs. Δz	Φ_{p_T} vs. ntf/nto	Φ_{p_T} vs. $\lvert bx\rvert$ and $\lvert by\rvert$	Φ_{p_T} vs. np/nmp
p+p (all)	0.35	1.00	0.35	0.10
p+p (-)	0.25	0.65	0.15	0.10
p+p (+)	0.50	0.65	0.05	0.25
Si+Si (all)	0.55	0.85	0.75	0.50
Si+Si (-)	0.50	1.00	0.50	0.35
Si+Si (+)	0.40	1.05	0.35	1.15
Pb+Pb(6) (all)	0.80	1.15	0.85	0.80
Pb+Pb(6) (-)	0.65	0.85	0.35	0.25
Pb+Pb(6) (+)	0.95	0.45	0.70	1.60
Pb+Pb(1) (all)	0.45	0.30	1.40	0.15
Pb+Pb(1) (-)	0.40	0.25	1.60	0.55
Pb+Pb(1) (+)	0.45	0.25	1.05	0.10

Table 4.3: The examples of the partial systematic errors of Φ_{p_T} values. All values in the table given in [MeV/c].

The above study leads to the conclusion that the typical total systematic error on Φ_{p_T} estimated as a maximal error resulting from all above considerations is not higher than 1.6 MeV/c for Pb+Pb collisions and 1.2 MeV/c for p+p, C+C and Si+Si data.

Losses of tracks due to the reconstruction inefficiency of the detector and track selection cuts can influence significantly the measured Φ_{p_T} values. In general the losses can reduce inter-particle correlations. In order to estimate this effect, the dependence of Φ_{p_T} on the percentage of randomly rejected particles has been calculated. This dependence for the most central (1), the most peripheral (6) Pb+Pb collisions and for p+p interactions is shown in Fig. 4.9. Within the considered forward rapidity region the tracking efficiency of the NA49 detector is higher than 95% [60], and therefore Fig. 4.9 implies that the bias due to tracking inefficiency is not higher than 0.5-1.0 MeV/c.

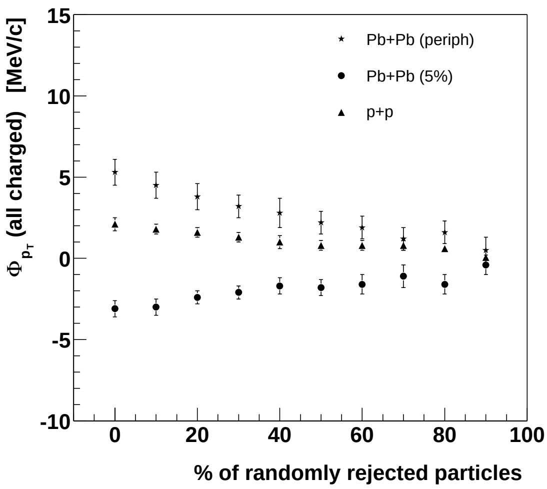

Figure 4.9: The dependence of Φ_{p_T} on the fraction of randomly rejected particles.

4.3.3 Two-track resolution corrections

It has already been shown in the previous analysis of the NA49 experiment [42] that the limited two-track resolution influences the measured values of Φ_{p_T}. In order to estimate such a contribution quantitatively several samples of mixed events (for p+p and different A+A collisions) have been produced.

Mixed events have been constructed on the basis of the original events, the multiplicities of mixed events have been the same as in the case of real events but each particle in a mixed event has been taken at random from a different real event. Such a mixing procedure washes out all possible inter-particle correlations and consequently the Φ_{p_T} value calculated for the sample of mixed events has been verified to be consistent with zero for all data sets. In the next step the sample of mixed events has been processed by the NA49 simulation software. The resulting simulated raw data have been reconstructed using standard reconstruction chain (as in the case of real data) and the Φ_{p_T} measure has been calculated. (The processing of prepared mixed events through the NA49 simulation software and through the reconstruction chain has been provided by one of my colleagues - Waldemar Retyk.) The obtained Φ_{p_T} values are negative as expected for the anti-correlation introduced by the losses due to the limited two-track resolution. The additive two-track resolution correction is calculated as the difference ($\Delta\Phi_{p_T}$) between the values of Φ_{p_T} after and before this procedure.

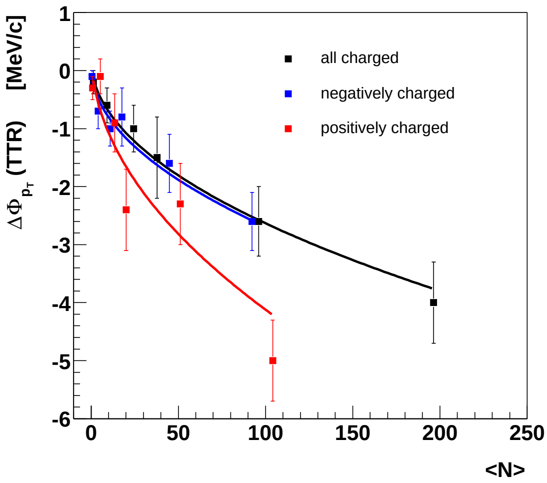

Figure 4.10: Additive correction $\Delta\Phi_{p_T}$ for limited two-track resolution effect versus multiplicity $\langle N\rangle$ of accepted particles. See the text for details.

In Fig. 4.10 the values of $\Delta\Phi_{p_T}$ versus mean multiplicity are presented for all charged particles and for negatively and positively charged particles, separately. Mixed events for p+p, C+C, Si+Si and three centralities of Pb+Pb collisions have been used to determine the two-track resolution corrections. The lines represent the analytical parametrization of this dependence given by the formula

$$\Delta\Phi_{p_T}(\langle N\rangle) = -a\sqrt{\langle N\rangle} + b$$

with a and b being parameters of a fit to the data points. The values of these parameters are given in Table 4.4 for all accepted charged particles and for negatively and positively charged, separately.

	a [MeV/c]	b [MeV/c]
all	0.28 ± 0.04	0.18 ± 0.20
negative	0.28 ± 0.04	0.07 ± 0.11
positive	0.45 ± 0.06	0.34 ± 0.21

Table 4.4: The values of a and b parameters of the fit of two-track resolution corrections versus mean multiplicity.

The absolute values of the two-track resolution corrections are higher for heavier colliding systems where the density of tracks is relatively high and become negligible for low-multiplicity interactions. The absolute values of $\Delta\Phi_{p_T}$ are also higher for positively charged particles than for negatively charged ones, which is mainly due to higher track density for positive particles caused by significantly larger number of protons than anti-protons. The $\Delta\Phi_{p_T}$ values are negative indicating that Φ_{p_T} measured with an ideal detector (with no two-track resolution problems) would be higher, therefore for a given multiplicity, Φ_{p_T} corrected for the limited two-track resolution effect equals 'raw' Φ_{p_T} minus the corresponding $\Delta\Phi_{p_T}$. The error of the corrected Φ_{p_T} is calculated by adding in squares the statistical error of the 'raw' Φ_{p_T} value and the statistical error of the correction. Finally all corrected Φ_{p_T} values are increased when compared to corresponding 'raw' Φ_{p_T} values.

4.4 Results

The results presented in this section refer to the so-called *accepted* particles, that means particles which are accepted both by the detector and by all kinematic cuts and track selection criteria. The results are obtained for charged particles produced in a broad range of transverse momenta ($0.005 < p_T < 1.5$ GeV/c). The rapidity of accepted particles is restricted to the interval 4.0 to 5.5 (rapidity calculated assuming pion mass for all particles) which corresponds to forward rapidities in the collision of equal mass nuclei (at 158 AGeV energy the center-of-mass rapidity equals about 2.9 for the fixed target geometry). As it has been already mentioned the azimuthal acceptance of the NA49 detector is relatively large for forward rapidity region.

Fig. 4.11 shows the distributions of mean (per event) transverse momentum $M(p_T)$ for p+p, Si+Si and the most central Pb+Pb collisions. Points correspond to data and the histograms to mixed events, in which no inter-particle correlations are present. Data are not corrected for any experimental effects (such as two-track resolution). Events with zero accepted particle multiplicity, that can appear especially for low multiplicity interactions (from p+p up to peripheral Pb+Pb), are not taken into account in figures. One has to keep in mind that in the case of calculating Φ_{p_T} such events will be normally included in the data sample. The small difference between $M(p_T)$ distributions for real and mixed events demonstrates that dynamical fluctuations are small in the investigated kinematic region (forward-rapidity). Moreover, no distinct class of events with unusual fluctuations is observed. The width of the $M(p_T)$ distribution strongly decreases with the colliding system size as expected from the increasing particle multiplicity.

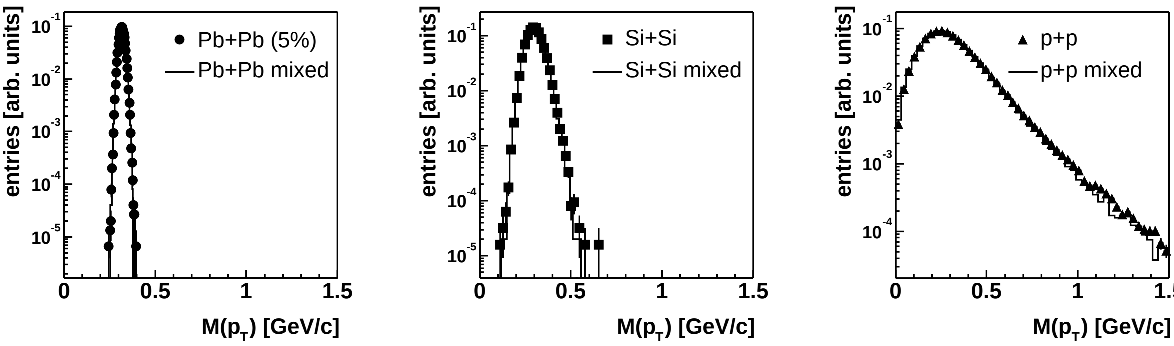

Figure 4.11: Distributions of mean transverse momentum for data (points) and mixed events (histograms). Data points are not corrected for acceptance and limited two-track resolution. Events with accepted particle multiplicity equal to zero are not used.

The fluctuation measure Φ_{p_T} seems to be more sensitive to small dynamical fluctuations. The measured values, corrected for two-track resolution, are plotted in Fig. 4.12 versus mean number of wounded nucleons for all accepted charged particles and also for positively and negatively charged particles, separately. Φ_{p_T} values are rather small (when compared for example to σ_{p_T}) for all investigated systems ($|\Phi_{p_T}| < 10$ MeV/c), but a significant centrality dependence is observed for all charge combinations. The Φ_{p_T} values increase by about 5 MeV from p+p collisions up to the maximum value which is observed for the most peripheral Pb+Pb collisions, and then Φ_{p_T} values decrease with increasing number of wounded nucleons. The statistical significance of this decrease can be estimated to be about 5.5, 4.6 and 4.5 σ for all charged, negatively charged and positively charged hadrons, respectively (this statistical significance

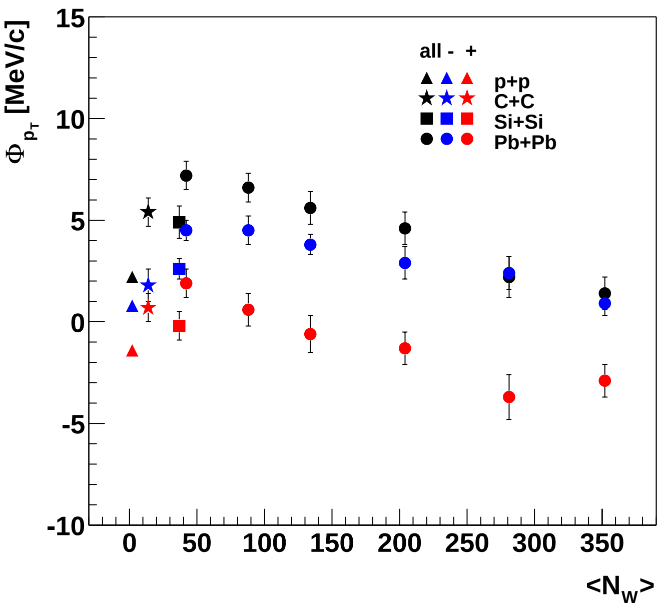

Figure 4.12: Φ_{p_T} versus mean number of wounded nucleons $\langle N_W \rangle$. Data points are corrected for limited two-track resolution. Errors are statistical only. Systematic errors are smaller than 1.6 MeV/c.

$= |\Phi_{p_T}(bin6) - \Phi_{p_T}(bin1)|/\sqrt{\sigma_{\Phi_{p_T}}(bin6)^2 + \sigma_{\Phi_{p_T}}(bin1)^2}$, where $\sigma_{\Phi_{p_T}}$ is a statistical error of Φ_{p_T} in a given centrality bin). The effect has been found to be stable with respect to the variation of the track selection cuts. The Φ_{p_T} value for Si+Si collisions seems to be systematically (for all charge combinations) lower than that for the most peripheral Pb+Pb ones although the number of wounded nucleons in both reactions is very close. This might suggest that $\langle N_W \rangle$ does not fully determine fluctuations in A+A collisions. The Φ_{p_T} measure calculated for positively charged particles is lower than that for the negatively charged ones. However, the measured difference of about 2-3 MeV/c is comparable with the systematic error. The Φ_{p_T} value for all charged particles seems to be higher than that for the negatively charged particles.

Table 4.5 presents the mean multiplicities of accepted particles, the dispersions $\sigma_N = \sqrt{\langle N^2 \rangle - \langle N \rangle^2}$ of the multiplicity distributions, the mean inclusive transverse momenta, the dispersions σ_{p_T} of inclusive transverse momentum distributions and Φ_{p_T} values for all data sets used in this analysis. The Φ_{p_T} values shown in this table have been calculated for all accepted charged particles and also for the negatively and the positively charged particles, separately. All values of Φ_{p_T} are corrected for the two-track resolution effect of the NA49 detector.

In order to study the dynamical fluctuations in a more differential way two-particle correlation plots have been prepared using cumulative x variable. As a fist step all p_T values have to be replaced by corresponding x values. An example of such a transformation for all charged particles at forward-rapidity region is presented in Fig. 4.13 for 5% the most central Pb+Pb interactions.

	$\langle N \rangle$	σ_N	$\overline{p_T}$ [MeV/c]	σ_{p_T} [MeV/c]	Φ_{p_T} [MeV/c]
p+p (all)	1.4	1.3	304	196	2.2 ± 0.3
p+p (-)	0.6	0.7	283	179	0.8 ± 0.1
p+p (+)	0.8	0.9	317	206	-1.4 ± 0.3
C+C (all)	10	4.3	300	210	5.4 ± 0.7
C+C (-)	4.5	2.4	279	190	1.8 ± 0.8
C+C (+)	5.5	2.7	317	224	0.7 ± 0.7
Si+Si (all)	27	7	301	217	4.9 ± 0.8
Si+Si (-)	12	4	277	195	2.6 ± 0.5
Si+Si (+)	15	4	320	231	-0.2 ± 0.7
Pb+Pb(6) (all)	39	18	299	220	7.2 ± 0.7
Pb+Pb(6) (-)	18	9	270	195	4.5 ± 0.5
Pb+Pb(6) (+)	21	10	325	237	1.9 ± 0.7
Pb+Pb(5) (all)	73	17	305	226	6.6 ± 0.7
Pb+Pb(5) (-)	34	9	273	199	4.5 ± 0.7
Pb+Pb(5) (+)	39	9	333	245	0.6 ± 0.8
Pb+Pb(4) (all)	104	19	309	230	5.6 ± 0.8
Pb+Pb(4) (-)	49	10	276	202	3.8 ± 0.5
Pb+Pb(4) (+)	55	11	337	249	-0.6 ± 0.9
Pb+Pb(3) (all)	148	21	312	233	4.6 ± 0.8
Pb+Pb(3) (-)	69	11	279	204	2.9 ± 0.8
Pb+Pb(3) (+)	79	12	342	252	-1.3 ± 0.8
Pb+Pb(2) (all)	193	21	315	234	2.2 ± 1.0
Pb+Pb(2) (-)	90	11	281	205	2.4 ± 0.8
Pb+Pb(2) (+)	103	13	344	254	-3.7 ± 1.1
Pb+Pb(1) (all)	230	19	317	236	1.4 ± 0.8
Pb+Pb(1) (-)	108	11	281	203	0.9 ± 0.6
Pb+Pb(1) (+)	122	12	349	257	-2.9 ± 0.8

Table 4.5: Measured inclusive and event-by-event parameters for accepted particles. $\langle N \rangle$, σ_N, $\overline{p_T}$ and σ_{p_T} values are not corrected for acceptance. Φ_{p_T} values are corrected for limited two-track resolution. The systematic errors of Φ_{p_T} are smaller than 1.6 MeV/c.

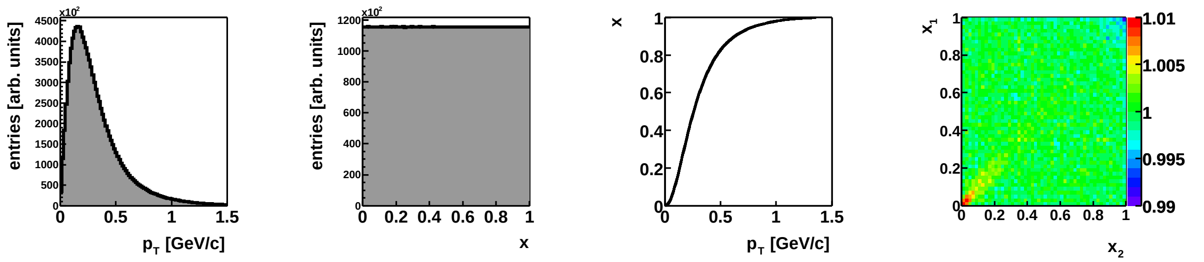

Figure 4.13: Example of $p_T - x$ transformation for all charged particles for 5% the most central Pb+Pb interactions. The last panel shows two-particle correlation plot (x_1, x_2).

Two-particle correlation plots of the cumulant transverse momentum variable x are presented in Fig. 4.14 for p+p, C+C, Si+Si and three centralities of Pb+Pb interactions at 158 AGeV. One can easily observe that the plots are not uniformly populated. A significant long range correlations on the level of about 40% (the color scale varies from 0.75 to 1.6) are observed for p+p data. This is rather unexpected when compared to the low Φ_{p_T} value. The color scale is the same for all plots (selected as the scale of the plot for p+p data) in order to show that these long range correlations observed for p+p data vanish when heavier colliding systems are studied. Instead, short range correlations become visible as an enhancement of the point density in the region close to the diagonal. Fig. 4.15 shows the same data but the color scales are different in order to make the details of these plots visible.

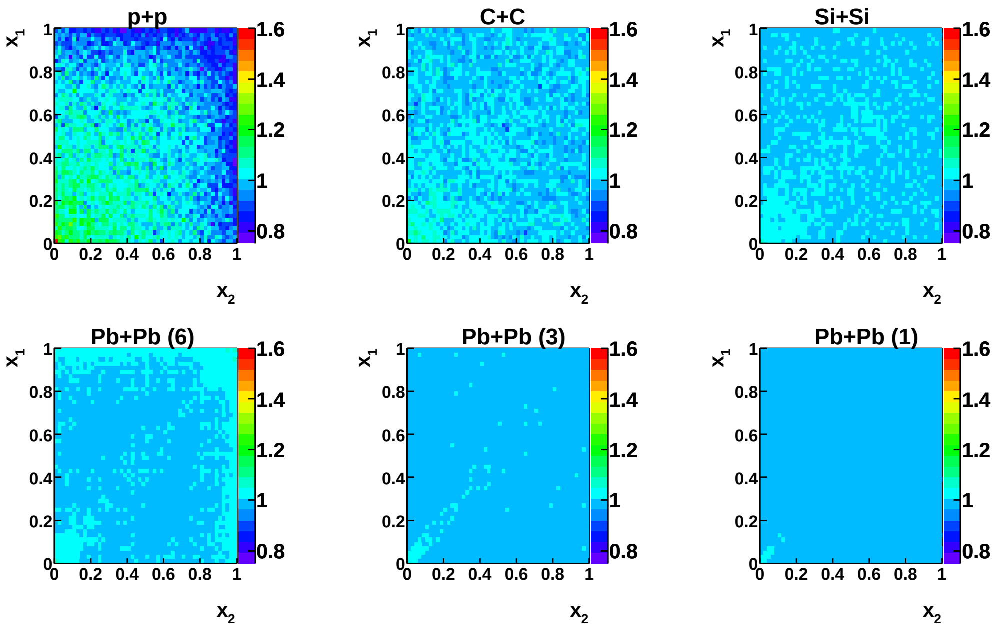

Figure 4.14: Two-particle correlation plots (x_1, x_2) for all charged particles. The data are plotted with the same color scale.

The short range correlations are most prominent for central Pb+Pb collisions and are consistent with the effect of Bose-Einstein statistics. For the most peripheral collisions the pattern seen in two-particle correlation plot is different from that for the remaining reactions. One observes an enhancement in the region close to $x_1 = 1$ and $x_2 = 1$. As the expected contamination with non-target interactions and with interactions different than Pb+Pb nuclei is highest for the most peripheral Pb+Pb collisions the two-particle correlation plot for peripheral data has been investigated using three different data sets, three different widths of the reconstructed vertex (Δz) and three different sets of $|b_x|$ and $|b_y|$ cuts. It has been found that this structure does not depend on event and track selection criteria used in the analysis and that it is indeed different from that for the remaining systems.

Fig. 4.16 shows two-particle correlation plots for central Pb+Pb collisions only but for several charge combinations, namely for all possible pairs, for pairs with opposite charges and for pairs with the same charge. As it has been already mentioned two-particle correlations for central Pb+Pb interactions are dominated by correlations at small scales (short range). A clear Bose-Einstein signal (the effect of Bose statistics) appears as an enhancement of the point density in the region close to the diagonal. This effect, which can be observed for the same-sign particles (++ and - -) is much better seen for low

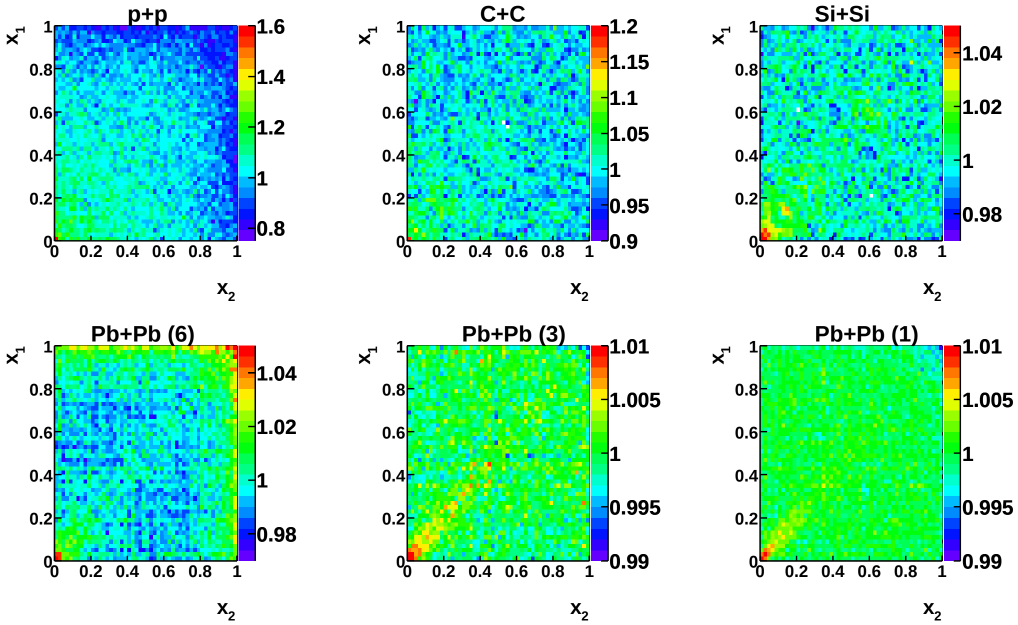

Figure 4.15: Two-particle correlation plots (x_1, x_2) for all charged particles. The data are plotted with different color scales.

momentum particles and decreases significantly for high momentum pairs. The Bose-Einstein signal is not observed when looking at correlations of particles with opposite charges (+- pairs) but an enhancement of the point density in the region of small x (peak at very low momenta) can be explained as an effect of Coulomb attraction of particles with different charges.

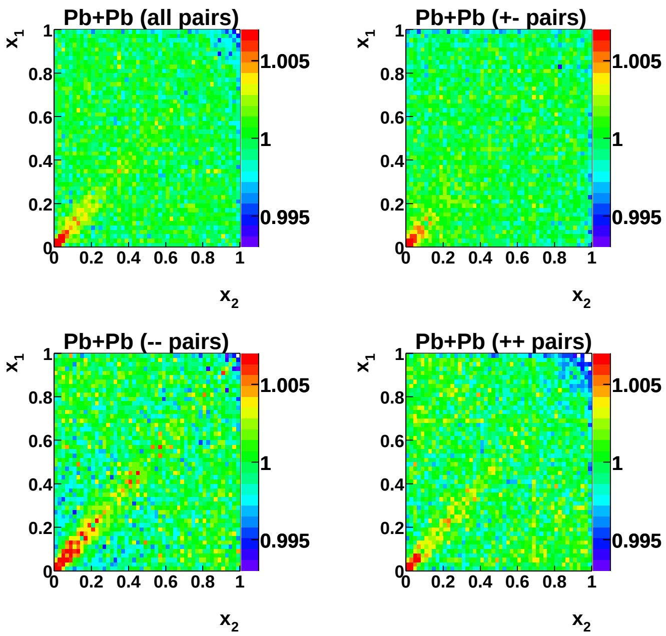

Figure 4.16: Two-particle correlation plots (x_1, x_2) for central (1) Pb+Pb interactions for different charge combinations. Note that the color scale is slightly different than than in Fig. 4.15.

4.5 Comparison with predictions of models

As it has been already mentioned Φ_{p_T} was calculated for a variety of theoretical models. In most of them the effects of detector acceptance were not taken into account and therefore their results cannot be directly compared to the data. Moreover, presently available models (such as VENUS, FRITIOF or RQMD) are usually too much complicated to properly extract and understand the effects which can influence transverse momentum fluctuations. It seems that it is much better to prepare simple "toy models" which can simulate different physical effects separately. In this section results of such simulations will be presented. Additionally predictions of one of the "more complicated" models - the HIJING model [65] will be shown. As the Φ measure is sensitive to the detector acceptance, its effects will be taken into account.

4.5.1 Model with the collective flow

Fig. 4.12 shows that the Φ_{p_T} measure is a non-monotonic function of centrality with the maximum at approximately $N_W = 40$. Such a behavior resembles the dependence of the magnitude of collective flow - directed (v_1) and elliptic (v_2) - on N_W [66] (the elliptic flow plays an important role only in the case of peripheral interactions and is negligible for p+p interactions). Therefore, a natural suggestion appears that the p_T fluctuations measured by Φ_{p_T} may be caused by the collective flow. As the most prominent effect is observed for the most peripheral Pb+Pb interactions this suggestion has been checked using a simple Monte Carlo analysis corresponding to peripheral Pb+Pb collisions. A generation of the events has been performed in the following way

1. Events have been generated with fixed multiplicity (after all below described steps the multiplicity had to be equal to the multiplicity of all accepted particles in peripheral Pb+Pb collisions).

2. For a given event φ_R (reaction plane azimuthal angle) has been randomly selected from a flat distribution ($0 < \varphi_R < 2\pi$).

3. Particles have been generated independently from each other and have followed the measured inclusive p_T distribution (p_T of a given particle has been taken from an exponential shape in m_T with $T = 299/2$ MeV (Table 4.5), pion mass has been assumed for all particles. Rapidity has been chosen from a Gaussian distribution (pion mass assumed) with y_{mid}=2.9 and the dispersion σ_y=1.7.

4. The azimuthal angle of a given particle (ϕ) has been generated with a distribution $\frac{dN}{d\phi} = 1{+}2{\cdot}v_2{\cdot}cos(2(\phi{-}\varphi_R))$. This formula causes that the natural uniform azimuthal angle distribution of the events is modified by the collective elliptic flow but the particles still remain independent from each other with respect to their transverse momenta. For such events the dynamical p_T fluctuations vanish if the azimuthal angle acceptance is complete (it has been checked in this analysis). However, the azimuthal angle acceptance of the NA49 detector is not flat, and consequently the azimuthal anisotropy can generate a finite value of Φ_{p_T}, even though the p_T values of particles are independent from each other.

5. As the last step the kinematic cuts ($4.0 < y_\pi < 5.5$, $0.005 < p_T < 1.5$ GeV/c) have been applied and the acceptance of the NA49 detector (Table 4.2) has been taken into account. Finally the Φ_{p_T} value has been calculated.

Table 4.6 presents Φ_{p_T} measure calculated for several values of v_2 used in the model. It can be observed that the abnormally large value of $v_2 = 0.45$ leads to Φ_{p_T} as large as 16 MeV/c, but a realistic magnitude of v_2, which depends on p_T (according to [66] taken as $0.05 \cdot p_T$(GeV/c)), results in value of Φ_{p_T} which is consistent with zero ($\Phi_{p_T} = 0.0 \pm 0.6$ MeV/c). Thus, one can conclude that the effect of the azimuthal anisotropy caused by the collective flow combined with the incomplete azimuthal acceptance of the detector is not responsible for the observed dynamical p_T fluctuations (high Φ_{p_T} value for peripheral Pb+Pb interactions).

v_2	Φ_{p_T} [MeV/c]
0.45	16.1 ± 0.5
0.3	7.2 ± 0.4
0.2	3.4 ± 0.5
0.1	0.0 ± 0.5
$0.3 \cdot \frac{p_T}{1GeV/c}$	2.9 ± 0.5
$0.05 \cdot \frac{p_T}{1GeV/c}$	0.0 ± 0.6

Table 4.6: The Φ_{p_T} values calculated for Monte Carlo model corresponding to peripheral Pb+Pb interactions. The model incorporates the collective flow (several v_2 values are used). All p_T values given in GeV/c.

4.5.2 The HIJING model and the model with $M(p_T) - N$ dependence

Fig. 4.17 shows the dependence of Φ_{p_T} on the mean number of wounded nucleons directly compared to predictions of the HIJING [65] model. For all kinds of collisions the output from the HIJING generator has been prepared by Robert Korus. In the model default parameters have been used. Separate plots present results for all charged particles, and for negatively charged and positively charged particles, separately. In the study of the HIJING results the same kinematic cuts are applied as in the case of real data. The black lines correspond to the results of the HIJING simulations where the effect of the limited NA49 acceptance (p_T versus azimuthal angle) is taken into account, whereas the gray lines refer to the HIJING predictions for full azimuthal acceptance. The difference between these two lines demonstrates how the limited acceptance of the NA49 detector influences measured Φ_{p_T} values.

In contrast to the data, Φ_{p_T} calculated within the HIJING model shows no centrality dependence; this can be understood as due to the fact that in the HIJING model A+A collision is an essentially independent superposition of N+N interactions. The fact that Φ_{p_T} does not change when going from elementary (p+p) interactions through different centralities of Pb+Pb collisions up to the most central Pb+Pb events at 158 AGeV has been also observed within the FRITIOF model in the previous study of the author of this work ([67]), however in this analysis the effect of limited acceptance of the NA49 detector has been then not taken into account. The very similar values of Φ_{p_T} for p+p and central Pb+Pb interactions (160 AGeV) have been also reported in [51] both for the FRITIOF model and for the UrQMD model without re-scattering. In the UrQMD model the Φ_{p_T} value for central Pb+Pb interactions is strongly decreased when re-scattering effects (large amount of mainly meson-baryon and meson-meson secondary collisions) are incorporated. In Fig. 4.17 the effects of short range correlations (Bose-Einstein and Coulomb) have not

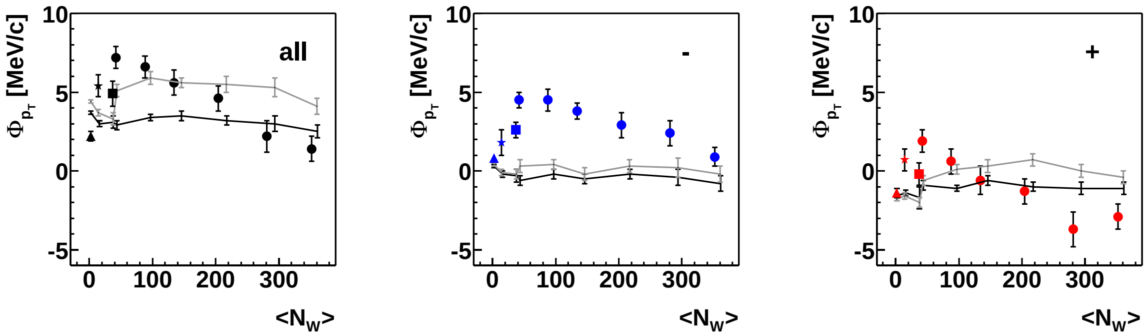

Figure 4.17: Φ_{p_T} versus mean number of wounded nucleons calculated using the HIJING model with geometrical acceptance cuts included (black lines) and without geometrical acceptance restrictions (gray lines). Results are compared to data (points) corrected for limited two-track resolution (the markers are the same as in Fig. 4.12). The panels represent: all charged, negatively charged and positively charged particles. Data points contain both short and long range correlations. The effects of short range correlations are not incorporated in the HIJING model.

been incorporated in the HIJING model. However it has been estimated in the previous analysis of the NA49 experiment [42] that the combined effect of short range correlations produces Φ_{p_T} values on the level of 5 MeV/c for central Pb+Pb collisions. The magnitude of this effect strongly depends on multiplicity and becomes negligible for p+p interactions. For the HIJING model Φ_{p_T} values for positively charged particles are, as in the case of real data, lower than for negatively charged and for all charged particles. The fact that Φ_{p_T} values for positively charged particles are always lower than for negatively charged ones has been found (using HIJING simulations) to be related to the limited acceptance and treating protons as pions (assuming pion mass for all produced particles).

When Φ_{p_T} has been first introduced [34] it has been believed that its value should be non-zero for elementary interactions. This non-vanishing value has been suggested to be connected mainly with strong $M(p_T)$ versus N dependence which was observed for elementary interactions. On the other hand Φ_{p_T} should vanish for heavier colliding systems as a result of equilibration. The results presented in the previous section do not confirm this expectation. Φ_{p_T} is indeed close to zero for central Pb+Pb collisions, but the maximum value is observed not for p+p data, but for colliding systems with $N_W \simeq 40$ (for peripheral Pb+Pb interactions). Although the Φ_{p_T} measure is small for p+p collisions, a significant structure appears in the two-particle correlation plot. The first candidate for its origin is (already mentioned) the dependence of $M(p_T)$ on N, observed for elementary interactions [34]. In Fig. 4.18 the comparison of $\langle M(p_T)\rangle$ versus N for the HIJING model and for real p+p data is presented. In the HIJING model both the limited acceptance of the NA49 detector and all kinematic cuts are included. The HIJING model shows a good agreement with the data.

The next step is to check whether the two-particle correlation plots for data and for the HIJING model are similar. In Fig. 4.19 the two-particle correlation plots for p+p data (a) are compared to the results of the HIJING model (b) and to data obtained from a simple random generator, which reproduces the dependence of $M(p_T)$ on N observed in the data (c). The multiplicity distribution of all accepted particles generated by the random generator (c) is the same as in the case of data. Particles are generated independently from each other, with a Gaussian shaped rapidity distribution and exponential shaped m_T distribution where the inverse slope parameter T of a given event depends on the

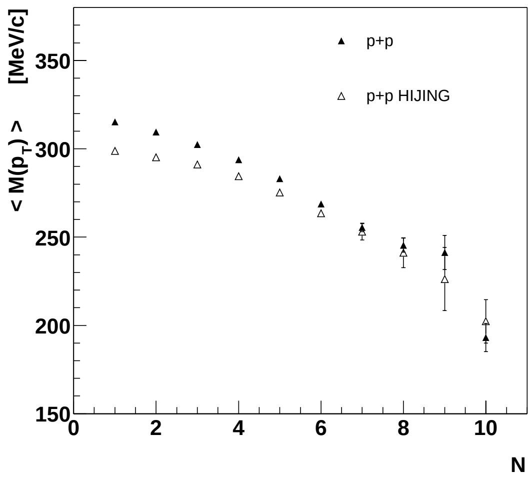

Figure 4.18: Mean transverse momentum versus multiplicity of all accepted particles. The closed symbols represent p+p data at 158 AGeV (data are not corrected for limited two-track resolution effect) and the open symbols corresponds to p+p events simulated using the HIJING model (the effect of the limited NA49 acceptance included). Events with accepted particle multiplicity equal zero are not used.

multiplicity of this event as observed in the data (Fig. 4.18). All kinematic cuts and the NA49 geometric acceptance are included in the random model. Both models (b) and (c) qualitatively reproduce the structure of the two-particle correlation plot which is observed in the data, however, the HIJING model (b) shows additionally a small enhancement of the point density in the region of high x.

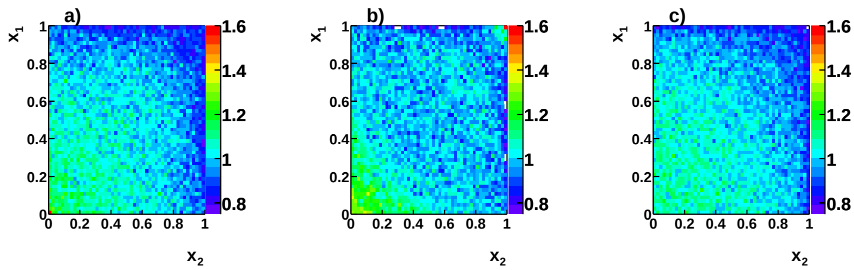

Figure 4.19: Two-particle correlation plot (x_1, x_2) for all charged particles for p+p data (a) compared to: simulated p+p HIJING events with limited NA49 acceptance included (b), simple random generator model, which reproduces $M(p_T)$ versus N correlation for p+p data (c).

The value of Φ_{p_T} calculated for all charged particles by use of the model (c) equals 1.2 $\pm$ 0.2 $\pm$ 1.8 MeV/c and within errors is consistent with Φ_{p_T} for p+p data (2.2 $\pm$ 0.3 $\pm$ 1.2 MeV/c). Nevertheless the small difference (on the level of 1 MeV/c) might indicate that, in agreement with the analysis presented in [55], one cannot exclude that there can be an additional source of correlations present in the data. Due to the relatively high statistical and systematic errors the effect cannot be estimated quantitatively. The correlations caused by resonances and by charge conservation are expected to be smaller for negatively charged particles only than for all charged particles and therefore the same analysis has been carried out for negatively charged particles. The experimental value of Φ_{p_T} calculated for negatively charged particles only for p+p interactions is 0.8 $\pm$ 0.1 $\pm$ 1.2 MeV/c while the model (c) applied for negatively charged particles results in Φ_{p_T} equal 0.6 $\pm$ 0.2 $\pm$ 0.3 MeV/c. Fig. 4.20 shows two-particle correlation plots for negatively charged particles only for p+p data (a) compared to results from the model where the dependence of $M(p_T)$ on N was reproduced for negatively charged particles only (b). It can be seen that both plots are very similar. Thus, one concludes that the results on negative particles from p+p interactions are consistent with the conjecture [68] that the particles are emitted independently but their y and p_T distributions depend on event multiplicity.

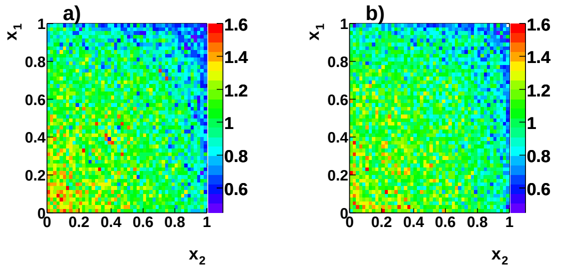

Figure 4.20: Two-particle correlation plot (x_1, x_2) for negatively charged particles for p+p data (a) compared to simple random generator model, which reproduces $M(p_T)$ versus N correlation for negatively charged particles for p+p data (b).

The HIJING model has also been used to obtain a two-particle correlation plot for C+C collisions (Fig. 4.21 b), which appears to be similar to that observed for real events (Fig. 4.15). The structure which can be observed for p+p collisions vanishes for heavier systems due to the dilution effect resulting from the higher number of uncorrelated particles (resulting from different N+N interactions). One has to keep in mind that the Φ_{p_T} measure by its definition is not sensitive to this dilution effect.

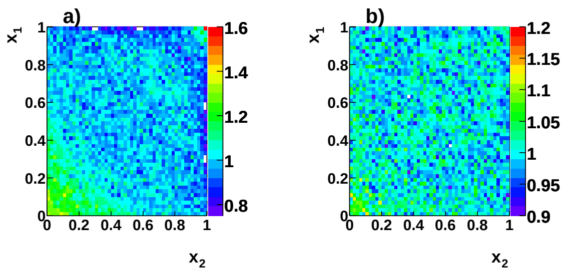

Figure 4.21: Two-particle correlation plot (x_1, x_2) simulated by the HIJING model for all charged particles for p+p events (a) and for C+C events (b). Limited NA49 acceptance is taken into account.

4.5.3 Model with fluctuations of the inverse slope parameter

Results for p+p and the most central Pb+Pb interactions are also compared to a simple temperature fluctuation model - the concept is proposed and described in [56]. This model assumes that the only source of fluctuations is event-by-event fluctuation of the inverse slope parameter (T) of the transverse mass spectra. The inverse slope parameter has been varied from event to event with a Gaussian shaped distribution of width σ_T. Particles have been generated independently from each other. The model has assumed a Gaussian shaped rapidity distribution for generated particles (pion mass set for all particles) and an exponential shape of the transverse mass distribution with the mean inverse slope parameter $\langle T \rangle = 152$ MeV for p+p data and 190 MeV for central Pb+Pb collisions adjusted to agree with the experimental results. All kinematic cuts (y, p_T)

applied for the real data have been also used in this model and the effect of the finite detector acceptance has been properly taken into account. The mean multiplicity of all accepted particles is the same as in the case of data (about 1.4 for p+p and about 240 for the most central Pb+Pb interactions). The Φ_{p_T} measure has been calculated for several sets of σ_T. Tables 4.7 and 4.8 show the results of calculations for simulations of p+p and the most central Pb+Pb interactions.

$\sigma_T [MeV/c]$	σ_T/T	Φ_{p_T} [MeV/c]
4	2.6%	0.1 ± 0.2
8	5.3%	0.7 ± 0.3
16	10.5%	3.1 ± 0.2
20	13.1%	5.2 ± 0.2
24	15.8%	7.0 ± 0.3
32	21.0%	12.2 ± 0.3
40	26.3%	17.8 ± 0.3

Table 4.7: The Φ_{p_T} values calculated for Monte Carlo model with fluctuations of the inverse slope parameter (T). The mean value of T has been set to be equal 152 MeV/c. Generated events correspond to p+p data (the mean multiplicity of all accepted particles is 1.4).

σ_T [MeV/c]	σ_T/T	Φ_{p_T} [MeV/c]
5	2.6%	19.6 ± 0.7
10	5.3%	73.1 ± 0.9
20	10.5%	223.7 ± 1.0
25	13.1%	310.6 ± 1.7
30	15.8%	398.7 ± 2.5
40	21.0%	594.2 ± 2.0
50	26.3%	782.0 ± 4.5

Table 4.8: The Φ_{p_T} values calculated for Monte Carlo model with fluctuations of the inverse slope parameter (T). The mean value of T has been set to be equal 190 MeV/c. Generated events correspond to the most central Pb+Pb data (the mean multiplicity of all accepted particles is about 240).

The fluctuations of the inverse slope parameter lead to so-called saddle shaped structure in the two-particle correlation plots. Fig. 4.22 and Fig. 4.23 present example (x_1, x_2) plots for different levels of the inverse slope parameter fluctuations for the model of p+p and Pb+Pb collisions, respectively. The results of simulations are always compared to the data (a). A saddle shaped structure is not visible neither in p+p nor in central Pb+Pb data. Moreover, Φ_{p_T} values increase drastically with increasing σ_T/T (better seen for Pb+Pb simulations); consequently the fluctuations of T should be very small in order to reproduce Φ_{p_T} value for the most central Pb+Pb collisions. The differences between panels a) and b), c) and d) show that fluctuations of the inverse slope parameter are not the (main) source of correlations in p+p and central Pb+Pb data at top SPS energy.

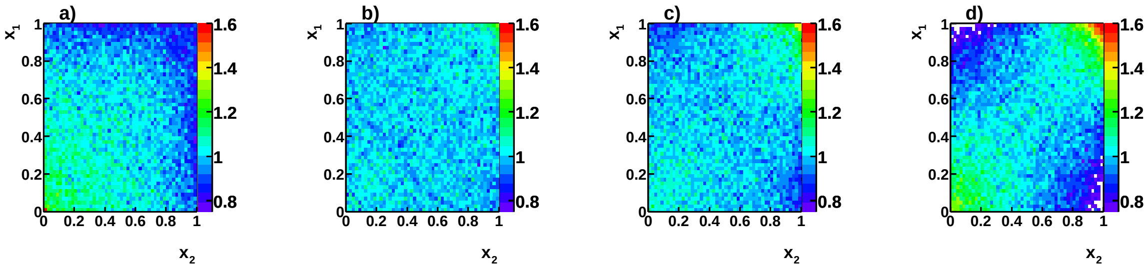

Figure 4.22: Two-particle correlation plots (x_1, x_2) for all charged particles for p+p collisions (a) at 158 AGeV compared to the inverse slope parameter fluctuation model. The mean value of the inverse slope parameter has been set to be 152 MeV. The dispersions of the Gaussian shaped inverse slope parameter distributions are: $\sigma_T = 16$ MeV (b), $\sigma_T = 24$ MeV (c), $\sigma_T = 40$ MeV (d).

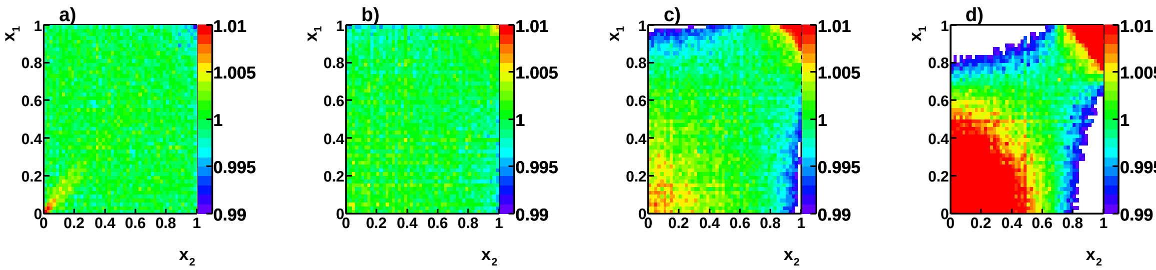

Figure 4.23: Two-particle correlation plots (x_1, x_2) for all charged particles for the 5% most central Pb+Pb collisions (a) at 158 AGeV compared to the inverse slope parameter fluctuation model. The mean value of the inverse slope parameter has been set to be 190 MeV. The dispersions of the Gaussian shaped inverse slope parameter distributions are: $\sigma_T = 5$ MeV (b), $\sigma_T = 10$ MeV (c), $\sigma_T = 20$ MeV (d).

In Fig. 4.24 the predicted dependence of Φ_{p_T} on T fluctuations (the shape of the curve was taken from [56]) is plotted and compared to Φ_{p_T} measured for the 5% most central Pb+Pb interactions. The experimental Φ_{p_T} value ($1.4 \pm 0.8 \pm 1.6$ MeV/c) contains both short and long range correlations. The solid line in Fig. 4.24 corresponds to the T fluctuation model presented in [56] which does not include short range correlations. The dashed line is a combination of this model with a contribution of short range correlations (additive component) estimated experimentally [42] as 5 MeV/c, in agreement with theoretical arguments [35, 36]. One can see that the observed value of Φ_{p_T} is already below the contribution of the Bose-Einstein correlations and that the inclusion of slope fluctuations makes the difference even larger. Thus, one concludes, in agreement with the previous results of the NA49 experiment [42] and with the above study of two-particle correlation plots, that the data leave no space for significant T fluctuations. Even if the fluctuations of the inverse slope parameter exist in the data they have been probably canceled by other (negative) correlations.

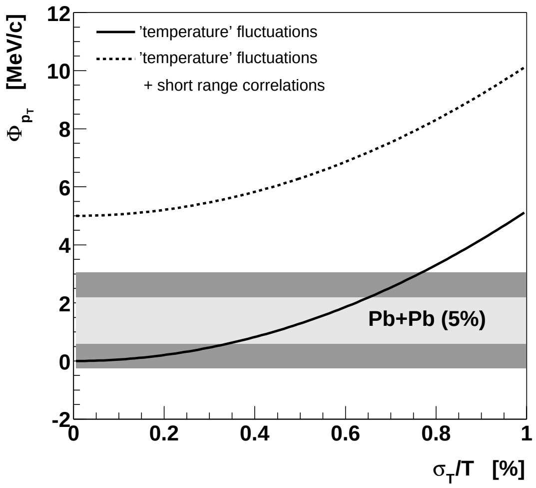

Figure 4.24: Predicted dependence of Φ_{p_T} on T fluctuations [56] compared to the measured Φ_{p_T} for the 5% most central Pb+Pb collisions. The uncertainty of the measured Φ_{p_T} value is represented by the bands for statistical (gray) and systematic (dark gray) errors.

Chapter 5

Energy dependence of p_T fluctuations for central Pb+Pb collisions

5.1 Data sets used in analysis

The experimental material used for the analysis of the energy dependence of p_T fluctuations consist of samples of Pb+Pb collisions at 20, 30, 40, 80 and 158 AGeV energy. The fraction of the total inelastic cross section of A+A collisions (σ/σ_{tot}) was set to 7.2% (central trigger runs have been used). In Table 5.1 data sets used in analysis are described.

	year	No. of events	$\sqrt{s_{NN}}$ [GeV]	y_{mid}
Pb+Pb at 20 AGeV	2002	229 000	6.27	1.88
Pb+Pb at 30 AGeV	2002	297 000	7.62	2.08
Pb+Pb at 40 AGeV	1999	165 000	8.73	2.22
Pb+Pb at 80 AGeV	2000	228 000	12.3	2.56
Pb+Pb at 158 AGeV	1996	166 000	17.3	2.91

Table 5.1: Data sets used in analysis. Listed for 7.2% central Pb+Pb collisions are: year of data taking, number of events, $\sqrt{s_{NN}}$ - center-of-mass energy for N+N pair, y_{mid} - center-of-mass rapidity (rapidity of the center-of-mass in the laboratory frame).

5.2 Event and particle selection criteria

5.2.1 Event cuts

As in the case of the analysis of the system size dependence of p_T fluctuations several event selection cuts are applied to reduce a contamination with non-target interactions. Only events with a proper quality and position of the reconstructed vertex are accepted in the analysis. The vertex coordinate z along the beam has to satisfy $|z - z_0| < \Delta z$, where z_0 is the nominal vertex position and Δz is a cut parameter. The values of z_0 and Δz are: -581.05 and 0.25 cm for 20 AGeV, -581.3 and 0.3 cm for 30 AGeV, -581.1 and 0.3 cm for 40 AGeV, -581.2 and 0.3 cm for 80 AGeV and -578.9 and 0.3 cm for 158 AGeV. The values of the cut parameters of the x and y positions of the fitted vertex (Δx and Δy) varies from 0.1 cm (for 158 AGeV) to 0.25 cm (for low energies). The cut on the ratio of the number of tracks used to fit the primary vertex divided by the total number of tracks outgoing from the main vertex (ntf/nto) is set to be higher than 0.25 for all energies.

5.2.2 Track cuts

For the analysis of the energy dependence of p_T fluctuations the same list of the particle selection cuts is used as in the case of the system size dependence. Namely, the accepted tracks have to have a good fitting quality, measured points at at least one of the Vertex TPCs, the distance between the main vertex and the track in the target plane should be small ($|b_x| < 2$ cm and $|b_y| < 1$ cm), the potential number of points (nmp) should be higher than 30 and finally the ratio of number of points to the potential number of points (np/nmp) is required to be higher than 0.5. The above list of cuts significantly reduces the possible contamination of particles from weak decays, secondary interactions and other sources.

5.2.3 The NA49 acceptance for the energy dependence of p_T fluctuations

For the purpose of studying the energy dependence of p_T fluctuations again only very forward-rapidity tracks with $0.005 < p_T < 1.5$ GeV/c are used. For all energies rapidity region is selected as $1.1 < y^*_\pi < 2.6$. For a given particle y^*_π is the rapidity calculated in the center-of-mass reference system; the rapidities are calculated assuming the pion mass for all particles. Forward-rapidity region $4.0 < y_\pi < 5.5$ used in the previous chapter for 158 AGeV analysis corresponds to $1.09 < y^*_\pi < 2.59$.

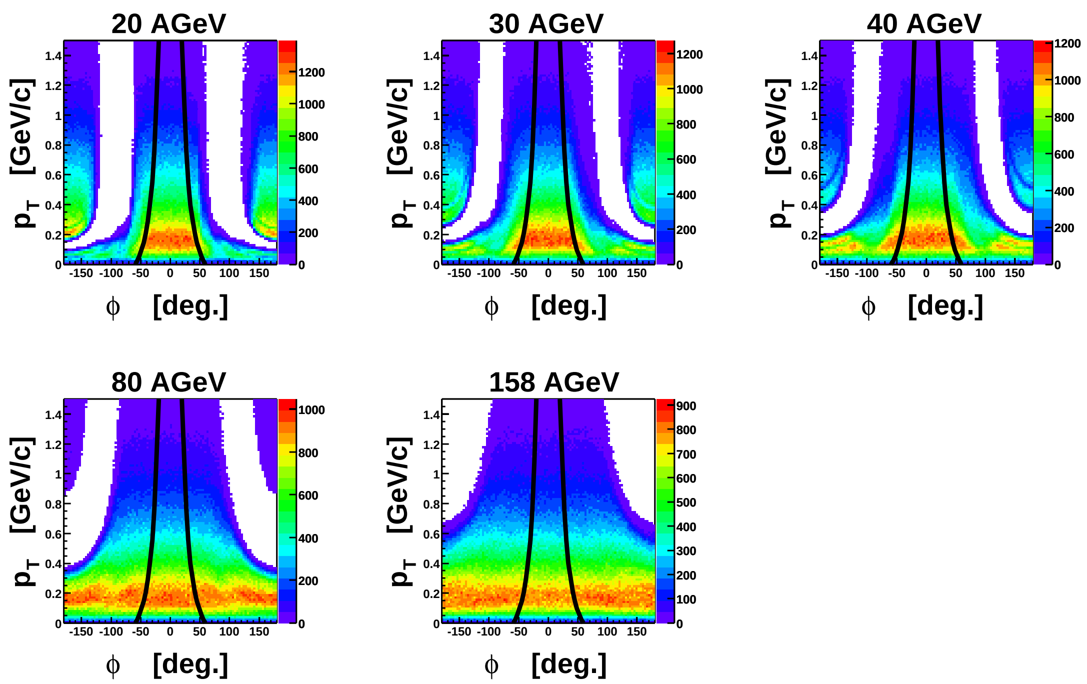

Figure 5.1: NA49 $\phi - p_T$ acceptance of all charged particles for $1.2 < y^*_\pi < 1.4$. The solid lines represent the analytical parametrization of the common acceptance.

Fig. 5.1 and Fig. 5.2 present examples of $\phi - p_T$ acceptance for $1.2 < y^*_\pi < 1.4$ and $2.0 < y^*_\pi < 2.2$ rapidity bins, respectively. All charged particles are used in the plots but the azimuthal angle of negatively charged particles (standard configuration of magnetic field) has been redefined - as described in the previous chapter. One can easily observe that the regions of a good detector acceptance are different for different energies.

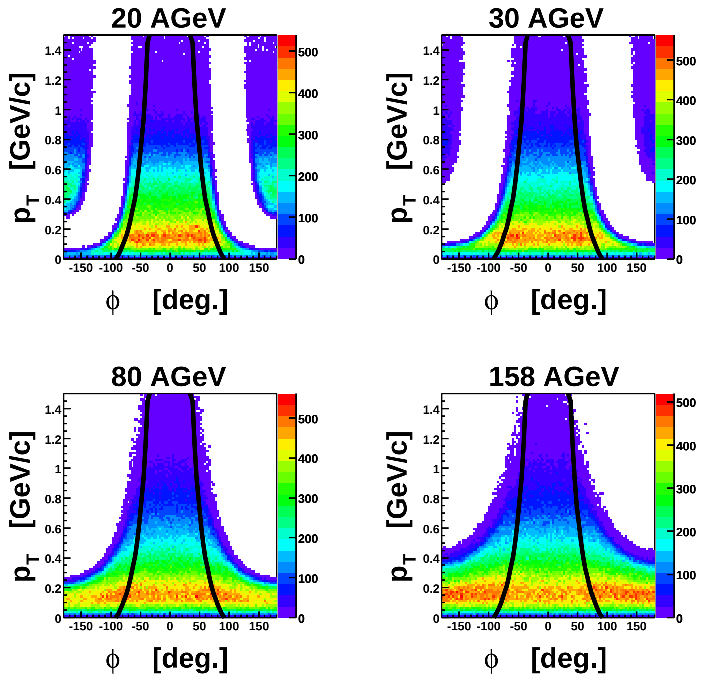

Figure 5.2: NA49 $\phi - p_T$ acceptance of all charged particles for $2.0 < y^*_\pi < 2.2$. The solid lines represent the analytical parametrization of the common acceptance.

Therefore in order to quantitatively compare Φ_{p_T} measures for all five energies the regions of the common acceptance have to be defined.

The solid lines in Fig. 5.1 and Fig. 5.2 correspond to the analytical parametrization of the common acceptance limits for all five energies given by the formula:

$$p_T(\phi) = \frac{1}{\phi^2/A} - B, \tag{5.1}$$

The parameters A and B depend on the rapidity range as shown in Table 5.2. The same curves can be used both for the negatively charged particles and for positively charged particles but in the case of the negatively charged ones (assuming standard configuration of magnetic field) their azimuthal angle has to be redefined as described in the previous chapter (section 4.2). The situation is opposite in the case of the opposite configuration of the magnetic field, namely one has to change the azimuthal angle definition for positively charged particles. Only particles within the analytical curves are used in the analysis.

All kinematic restrictions (rapidity mainly) and all track selection cuts together with the requirement to use the same (and - therefore - limited) $\phi - p_T$ acceptance lead to the fact that *for all five energies only about 5.0 - 5.2 % of all charged particles produced in central Pb+Pb interaction are used in the analysis.*

y^*_π	1.0-1.2	1.2-1.4	1.4-1.6	1.6-1.8	1.8-2.0	2.0-2.2	2.2-2.4	2.4-2.6
$A[\frac{deg.^2 GeV}{c}]$	600	700	1000	2600	3000	2500	1800	1000
$B[\frac{GeV}{c}]$	0.2	0.2	0.2	0.5	0.4	0.3	0.3	0.1

Table 5.2: The parametrization of the NA49 $y - p_T$ acceptance common for all five energies for positively charged particles (standard configuration of magnetic field). For negatively charged particles one has to change the definition of the azimuthal angle (see text) and then use the same parametrization.

5.3 Error estimates and corrections

5.3.1 Statistical errors

The method of calculating the statistical error of Φ_{p_T} (so-called subsample method) is described in the previous chapter (section 4.2).

5.3.2 Systematic errors

As in the case of the system size dependence of transverse momentum fluctuations the values of event and track cut parameters have been varied (within a reasonable range) in order to estimate the systematic errors of Φ_{p_T}. For a given cut parameter the partial systematic error has been taken as a half of the difference between the highest and the lowest Φ_{p_T} value. Two event cuts and two track cuts have been considered and as a final estimate of the total systematic error on Φ_{p_T} a maximal error resulting from such a study has been taken (the same procedure has been applied in the previous chapter).

The systematic error of Φ_{p_T} which comes from the small remaining contamination of non-target interactions can be estimated by use of Φ_{p_T} dependence on two vertex cut parameters - ntf/nto and Δz. Fig. 5.3 shows the dependence of Φ_{p_T} on ntf/nto ratio for 20, 30, 40, 80 and 158 AGeV data. The observed variation of Φ_{p_T} with this cut is rather small and the partial systematic error due to this effect varies from 0.45 MeV/c for 158 AGeV up to a slightly higher value of 2.4 MeV/c for 30 AGeV (see the next table). In Fig. 5.4 the dependence of Φ_{p_T} on the allowed distance Δz from the nominal position of the main vertex is presented for all five energies. The observed variation of Φ_{p_T} with this cut is quite small for all investigated data sets. The highest partial systematic error has been found to be 0.7 MeV/c for 80 AGeV interactions.

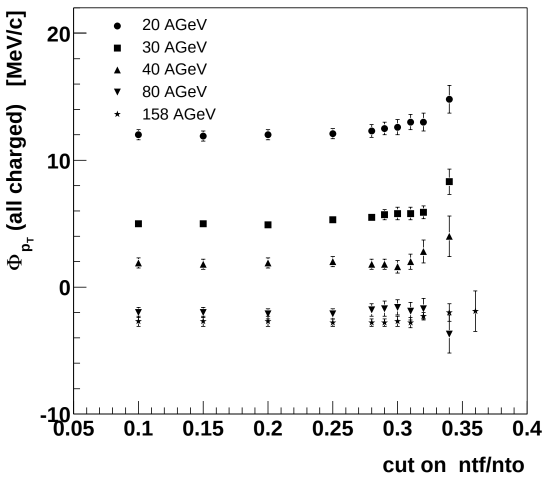

Figure 5.3: The dependence of Φ_{p_T} on one of the event cuts (ntf/nto ratio). Note: the values and their errors are correlated.

The influence of the remaining fraction of tracks from weak decays, secondary interactions and other sources of non-vertex tracks can be determined by use of the dependence of Φ_{p_T} on track cuts parameters - $|b_x|$ and $|b_y|$ and np/nmp ratio. Fig. 5.5 and Fig. 5.6 present how the value of Φ_{p_T} changes with the impact parameter cut and np/nmp ratio, respectively. It can be easily seen that Φ_{p_T} is quite stable with both cut parameters.

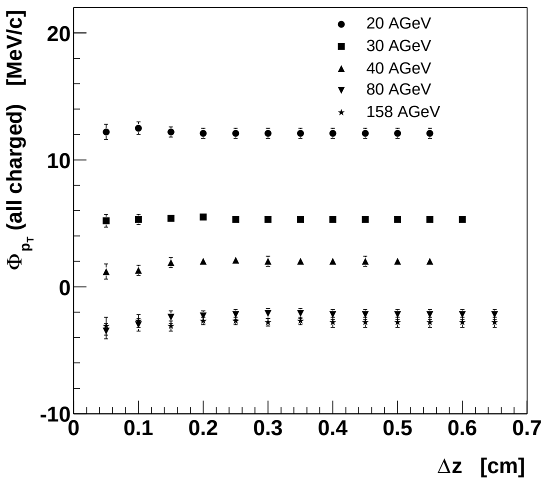

Figure 5.4: The dependence of Φ_{p_T} on the allowed distance Δz from the nominal position of the main vertex. Note: the values and their errors are correlated.

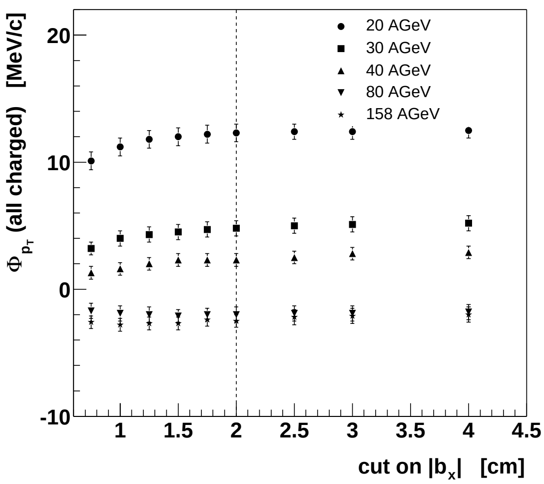

Figure 5.5: The dependence of Φ_{p_T} on upper cut in the impact parameter $|bx|$. For each point the cut on $|by|$ is equal half the cut on $|bx|$. Note: the values and their errors are correlated. The dashed line indicates the cut used in the analysis.

A small increase of Φ_{p_T} with increasing impact parameter cut may be due to the increasing contamination on non-vertex tracks for higher $|b_x|$ and $|b_y|$ values (see the previous chapter). The partial systematic error from Φ_{p_T} versus impact parameter cut varies from 0.4 MeV/c for 80 AGeV to 1.1 MeV/c for 40 AGeV, whereas the partial systematic error from Φ_{p_T} versus np/nmp ratio varies from 0.6 MeV/c for 20 AGeV to 1.1 MeV/c for 30 AGeV.

Table 5.3 presents the possible components of the systematic error resulting from the variation of the values of cut parameters. The examples are presented for 20, 30, 40, 80 and 158 AGeV for 7.2% central Pb+Pb collisions. The partial systematic errors have been calculated for all charged particles and for negatively and positively charged hadrons, separately.

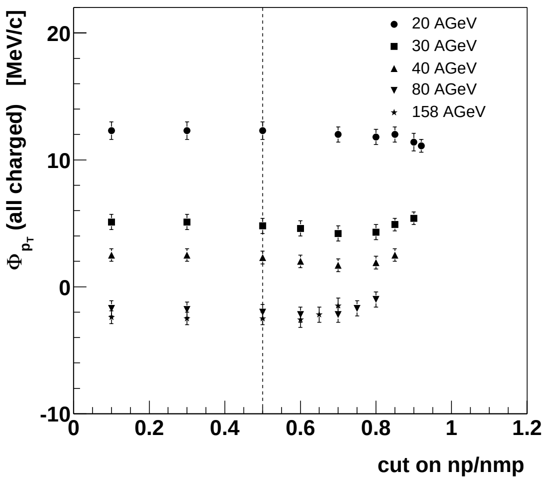

Figure 5.6: The dependence of Φ_{p_T} on lower cut on np/nmp ratio. Note: the values and their errors are correlated. The dashed line indicates the cut used in the analysis.

	Φ_{p_T} vs. Δz	Φ_{p_T} vs. ntf/nto	Φ_{p_T} vs. $\|bx\|$ and $\|by\|$	Φ_{p_T} vs. np/nmp
20 AGeV (all)	0.20	1.45	1.20	0.60
20 AGeV (-)	0.10	0.40	0.40	0.30
20 AGeV (+)	0.25	1.65	1.55	0.60
30 AGeV (all)	0.15	1.70	1.00	0.60
30 AGeV (-)	0.20	0.30	0.25	0.65
30 AGeV (+)	0.25	2.40	1.05	1.10
40 AGeV (all)	0.45	1.20	0.80	0.40
40 AGeV (-)	0.35	0.60	0.05	0.30
40 AGeV (+)	0.45	1.00	1.10	0.75
80 AGeV (all)	0.70	1.05	0.15	0.60
80 AGeV (-)	0.40	0.15	0.40	0.20
80 AGeV (+)	0.60	0.60	0.20	0.75
158 AGeV (all)	0.20	0.45	0.40	0.50
158 AGeV (-)	0.25	0.35	0.95	0.30
158 AGeV (+)	0.55	0.45	0.30	0.75

Table 5.3: The partial systematic errors of Φ_{p_T} values for 7.2% most central Pb+Pb interactions. All values in the table are given in [MeV/c].

From the above analysis one concludes that the typical systematic error on Φ_{p_T} determined as a maximal error from the above calculations is not higher than 1.7 MeV/c for 20 AGeV, 2.4 MeV/c for 30 AGeV and 1.1 MeV/c for 40, 80 and 158 AGeV data.

The observed values of Φ_{p_T} can be reduced significantly due to the losses of tracks resulting from the reconstruction inefficiency of the detector and track selection cuts. The dependence of Φ_{p_T} on the fraction of randomly rejected particles has been calculated (Fig. 5.7) in order to estimate this effect quantitatively. Within forward-rapidity region at all five energies the tracking efficiency of the detector is higher than 95% and therefore Fig. 5.7 shows that the bias due to tracking inefficiency and track selection cuts is lower than 0.5 - 1.0 MeV/c.

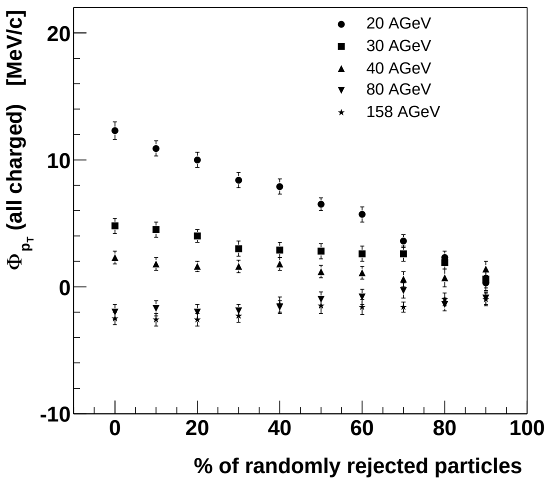

Figure 5.7: The dependence of Φ_{p_T} on the fraction of randomly rejected particles.

5.3.3 Two-track resolution corrections

In order to estimate how the limited two-track resolution influences the measured values of Φ_{p_T} five samples (30 000 events in each) of mixed events have been prepared (for 20, 30, 40, 80 and 158 AGeV). Mixed events have been constructed on the basis of the original events, multiplicities of mixed events have been the same as for real events but each particle in a given mixed event has been taken at random from a different real event. The inclusive spectra such as transverse momentum or rapidity distributions have been the same both for data and mixed events. Such a mixing procedure leads to vanishing of all possible correlations so the Φ_{p_T} value calculated for the sample of mixed events has been found to be consistent with zero. It has been checked for all data sets and all possible charge configurations. In the next step the prepared mixed events have been processed by the NA49 simulation software and reconstructed as in the case of the real data (see also the previous chapter). The additive two-track resolution correction is determined as the difference ($\Delta\Phi_{p_T}$) between the values of Φ_{p_T} after simulation and reconstruction and before this procedure (mixed events). In contrary to the system size dependence of $\Delta\Phi_{p_T}$ for the energy scan mixed events have been prepared for all five energies and therefore any interpolations of $\Delta\Phi_{p_T}$ and any analytical parametrization of $\Delta\Phi_{p_T}$ versus multiplicity are not necessary. The values of $\Delta\Phi_{p_T}$ for all energies and all possible charge combinations are given in Table 5.4.

	20 AGeV	30 AGeV	40 AGeV	80 AGeV	158 AGeV
$\Delta\Phi_{p_T}$ [MeV/c] (all)	-0.7 ± 0.4	-0.3 ± 0.3	-0.9 ± 0.5	-1.7 ± 0.4	-3.4 ± 0.6
$\Delta\Phi_{p_T}$ [MeV/c] (-)	-0.2 ± 0.2	0.4 ± 0.2	-0.8 ± 0.4	-1.5 ± 0.2	-1.7 ± 0.5
$\Delta\Phi_{p_T}$ [MeV/c] (+)	-0.4 ± 0.4	-0.6 ± 0.3	-0.6 ± 0.5	-1.9 ± 0.5	-4.2 ± 0.7

Table 5.4: The values of two-track resolution corrections $\Delta\Phi_{p_T}$ for all accepted charged particles and for negatively and positively charged, separately.

The absolute values of the two-track resolution corrections are higher for higher energies where the multiplicities of produced particles are higher and consequently the densities of tracks are relatively high. The two-track resolution corrections become much smaller for low-multiplicity interactions (20 and 30 AGeV data). The absolute values of $\Delta\Phi_{p_T}$ are typically higher for positively charged particles than those for negatively charged ones, which is mainly due to higher track density for positive particles caused by larger number of protons than anti-protons. In most cases the values of $\Delta\Phi_{p_T}$ are negative thus indicating that the corrected values of Φ_{p_T} will be higher when compared with 'raw' Φ_{p_T} values. As in the case of the system size dependence the Φ_{p_T} corrected for the limited two-track resolution effect equals 'raw' Φ_{p_T} minus the corresponding $\Delta\Phi_{p_T}$. The error of the corrected Φ_{p_T} is calculated by adding in squares the statistical error of the 'raw' Φ_{p_T} value and the statistical error of the correction.

5.4 Results

The results shown in this section refer to the so-called *accepted* particles, that means particles which are accepted both by the detector and by all kinematic cuts and track selection criteria. The results are obtained for charged particles produced in a broad range of transverse momenta ($0.005 < p_T < 1.5$ GeV/c). The rapidity of accepted particles is restricted to the interval 1.1 to 2.6 in the center-of-mass reference system, which corresponds to forward-rapidities (the same rapidity region is selected for all five energies; rapidity is calculated assuming pion mass for all particles).

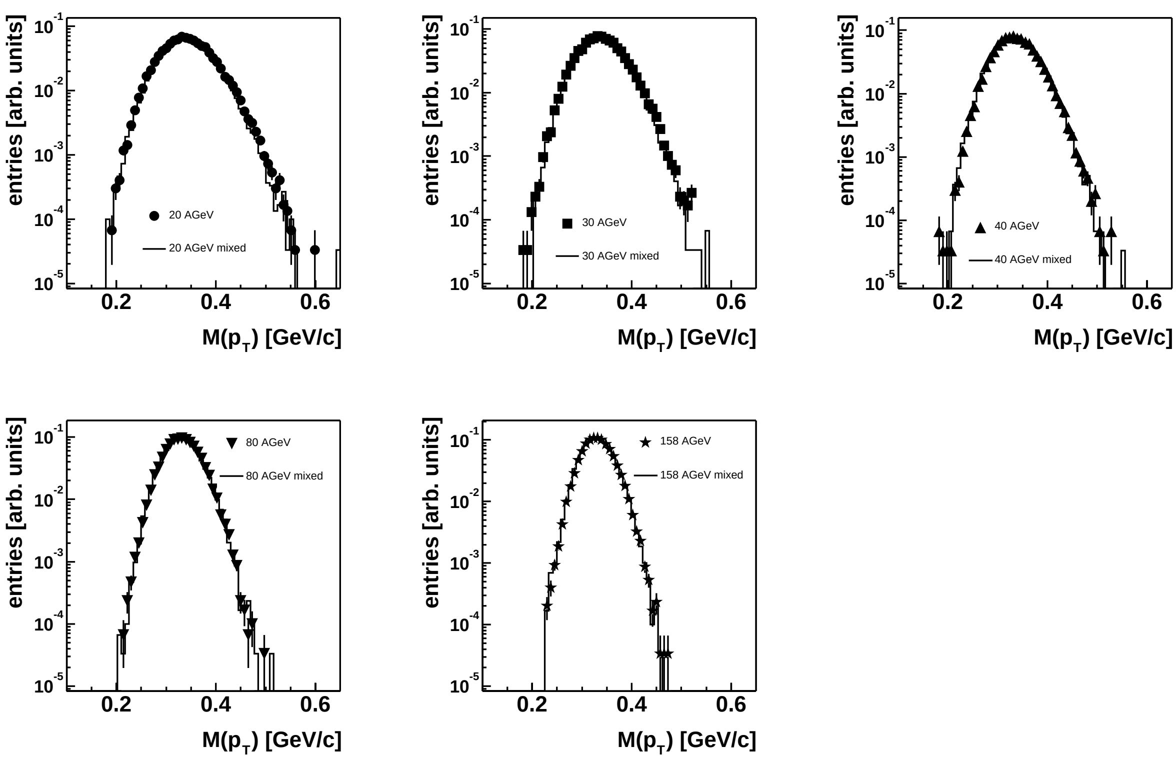

Figure 5.8: Distributions of mean transverse momentum for data (points) and mixed events (histograms). Data points are not corrected for acceptance and limited two-track resolution. Events with accepted particle multiplicity equal to zero are not used.

Fig. 5.8 shows the distribution of mean (per event) transverse momentum $M(p_T)$ for central 20, 30, 40, 80 and 158 AGeV Pb+Pb interactions. Points correspond to the data and the histograms to mixed events, where there are no inter-particle correlations. Data are not corrected for any experimental effects (such as two-track resolution). Events with zero accepted particle multiplicity (there can be a few of them especially for low energies) are not taken into account in figures but one has to remember that in the case of calculating

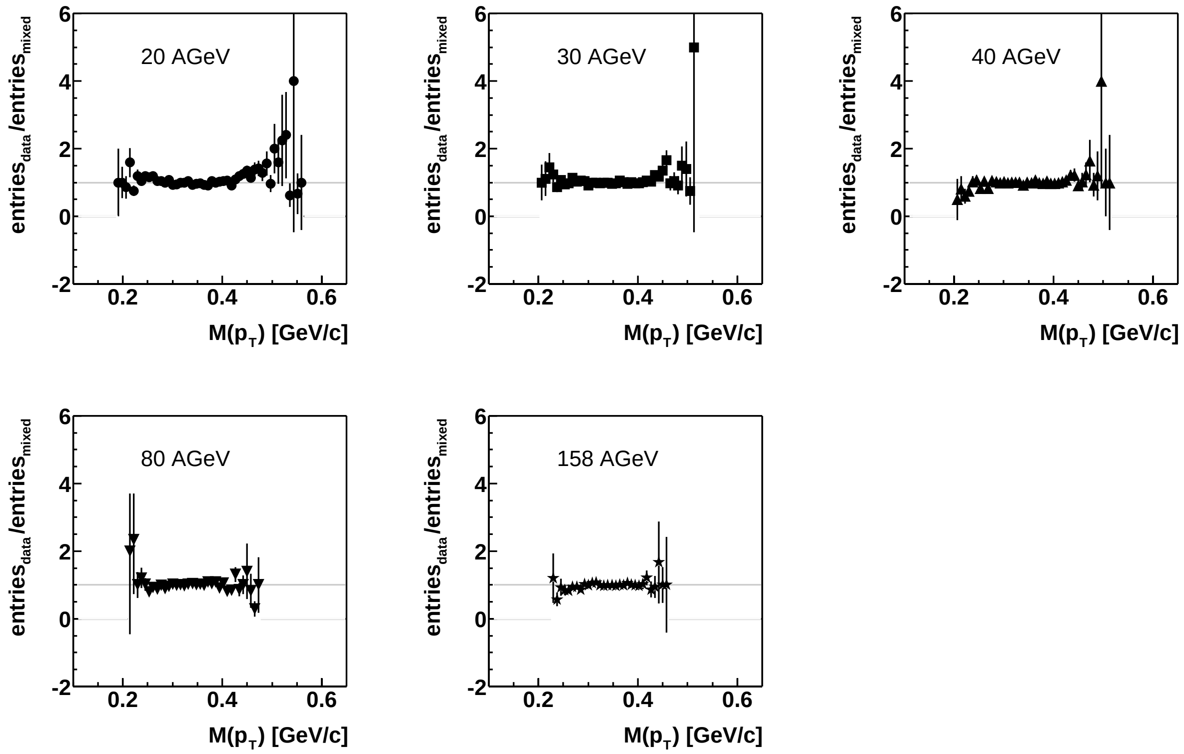

Figure 5.9: Distributions of mean transverse momentum for data divided by distribution for mixed events (see the previous figure).

Φ_{p_T} such events will be normally included in the data sample. All charged particles are used to prepare these plots. The difference between $M(p_T)$ distributions for real and mixed events can be observed for low energies (20 and 30 AGeV) - the distributions for data are a bit wider than for mixed events; it might indicate the presence of dynamical fluctuations in transverse momentum but as it will be shown later (Φ_{p_T} measure) the possible signal appears for positively charged particles only. The difference between the histograms for data and mixed events is better seen in Fig. 5.9 where the ratio od these two histograms is presented for all five energies. For higher energies $M(p_T)$ distributions for data and mixed events become very similar. The width of the $M(p_T)$ distribution decreases with increasing the energy of the colliding system as expected from the increasing particle multiplicity.

The fluctuation measure Φ_{p_T}, which is more sensitive to small dynamical fluctuations, is shown in Fig. 5.10. The measured values are corrected for limited two-track resolution. In Fig. 5.10 the Φ_{p_T} values are presented for all charged particles and for the negatively and positively charged, separately. A significant decrease with increasing energy can be observed for positively charged particles whereas for negatively charged ones Φ_{p_T} is independent of energy (Φ_{p_T} values are nearly in agreement with those for the case of an independent particle production). This fact seems to be quite surprising, especially that a non-monotonic structure of the systems size dependence of Φ_{p_T} fluctuations could be observed for all three charge combinations. As the Φ_{p_T} value for all charged particles can be a non-trivial combination of Φ_{p_T} for negatively and positively charged particles a main emphasis should be placed on understanding qualitatively the difference between positively and negatively charged particles.

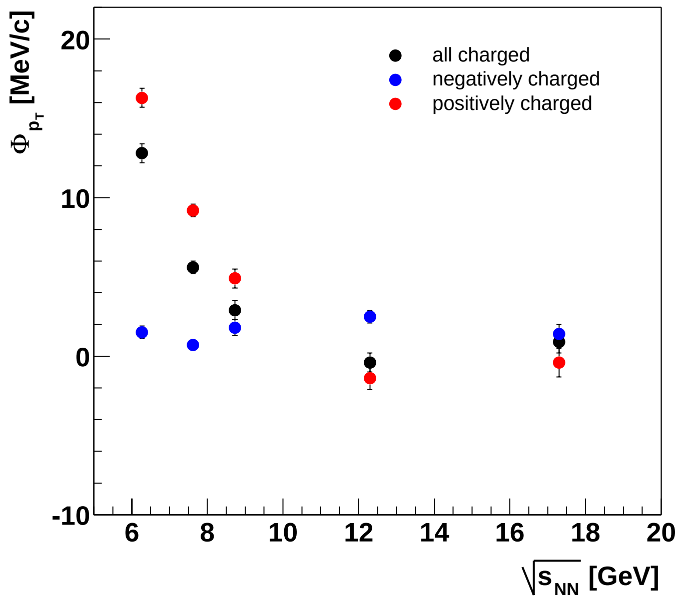

Figure 5.10: Φ_{p_T} versus energy for 7.2% most central Pb+Pb interactions. Data points are corrected for limited two-track resolution. Errors are statistical only. Systematic errors are smaller than 2.4 MeV/c.

	$\langle N \rangle$	σ_N	$\overline{p_T}$ [MeV/c]	σ_{p_T} [MeV/c]	Φ_{p_T} [MeV/c]
20 *A*GeV (all)	31	6	342	256	12.8 ± 0.6
20 *A*GeV (-)	10	3	223	166	1.5 ± 0.4
20 *A*GeV (+)	21	5	396	271	16.3 ± 0.6
30 *A*GeV (all)	39	6	339	259	5.6 ± 0.4
30 *A*GeV (-)	14	4	239	180	0.7 ± 0.3
30 *A*GeV (+)	25	5	395	278	9.2 ± 0.4
40 *A*GeV (all)	45	7	335	259	2.9 ± 0.6
40 *A*GeV (-)	17	4	242	183	1.8 ± 0.5
40 *A*GeV (+)	28	5	391	282	4.9 ± 0.6
80 *A*GeV (all)	61	9	331	256	-0.4 ± 0.6
80 *A*GeV (-)	26	5	270	205	2.5 ± 0.4
80 *A*GeV (+)	35	6	378	280	-1.4 ± 0.7
158 *A*GeV (all)	77	10	331	255	0.9 ± 0.7
158 *A*GeV (-)	34	6	282	214	1.4 ± 0.6
158 *A*GeV (+)	43	7	370	277	-0.4 ± 0.9

Table 5.5: Measured inclusive and event-by-event parameters for accepted particles. $\langle N \rangle$, σ_N, $\overline{p_T}$ and σ_{p_T} values are not corrected for acceptance. Φ_{p_T} values are corrected for limited two-track resolution. The systematic errors of Φ_{p_T} are smaller than 2.4 MeV/c.

Table 5.5 presents the mean multiplicities of accepted particles, the dispersions $\sigma_N = \sqrt{\langle N^2 \rangle - \langle N \rangle^2}$ of the multiplicity distributions, the mean inclusive transverse momenta, the dispersions σ_{p_T} of inclusive transverse momentum distributions and Φ_{p_T} values for all data sets used in this analysis. The Φ_{p_T} values shown in this table have been calculated for all accepted charged particles and also for the negatively and the positively charged particles, separately. All values of Φ_{p_T} are corrected for the two-track resolution effect of the NA49 detector.

Two-particle correlation plots (for all charged particles) of the cumulant transverse momentum variable x are presented in Fig. 5.11 for 20, 30, 40, 80 and 158 AGeV central Pb+Pb collisions. It can be seen that the plots are not uniformly populated. The color scale is the same for all plots (selected as the scale of 20 AGeV data) in order to show how the correlation pattern changes when the energy is changed. Fig. 5.12 shows the same data but the color scales are different in order to make the details of these plots visible. For all five energies short range correlations are visible as an enhancement of the point density in the region close to the diagonal. Additionally one observes an enhancement in the region close to $x_1 = 1$ and $x_2 = 1$ for 20 and 30 AGeV data. (One should remember about the observation of wider $M(p_T)$ distributions and about increased Φ_{p_T} values also at lower energies.) Beyond Bose-Einstein contribution and an enhancement in the region close to $x_1 = 1$ and $x_2 = 1$ one can observe - in the background of the plot - long range correlations similar to these for p+p interactions at 158 AGeV, however the scale is different. These long range correlations seem to be slightly reduced for higher energies.

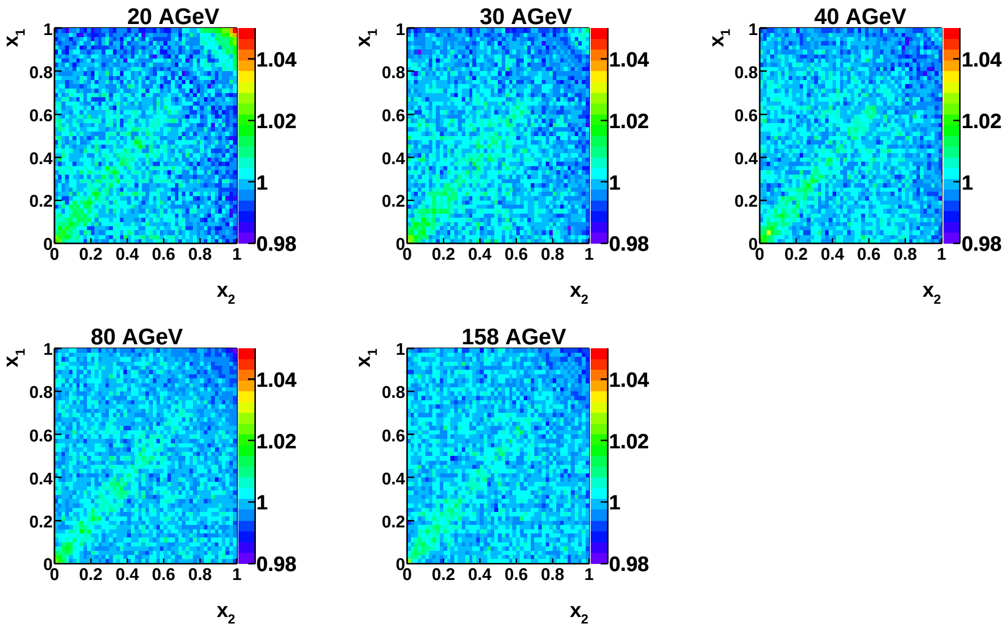

Figure 5.11: Two-particle correlation plots (x_1, x_2) for all charged particles for central Pb+Pb collisions at 20 - 158 AGeV. The data are plotted with the same color scale.

It can be observed that Φ_{p_T} values for 20 AGeV Pb+Pb collisions are different for positively and negatively charged particles. A natural suggestion is then to check how the two-particle correlations plot look like for these two charge combinations. Fig. 5.13 shows that, in agreement with the intuitive predictions, an enhancement in the region close to $x_1 = 1$ and $x_2 = 1$ can be observed for positively charged particles only, whereas the negatively charged ones follow the structure observed for higher energies.

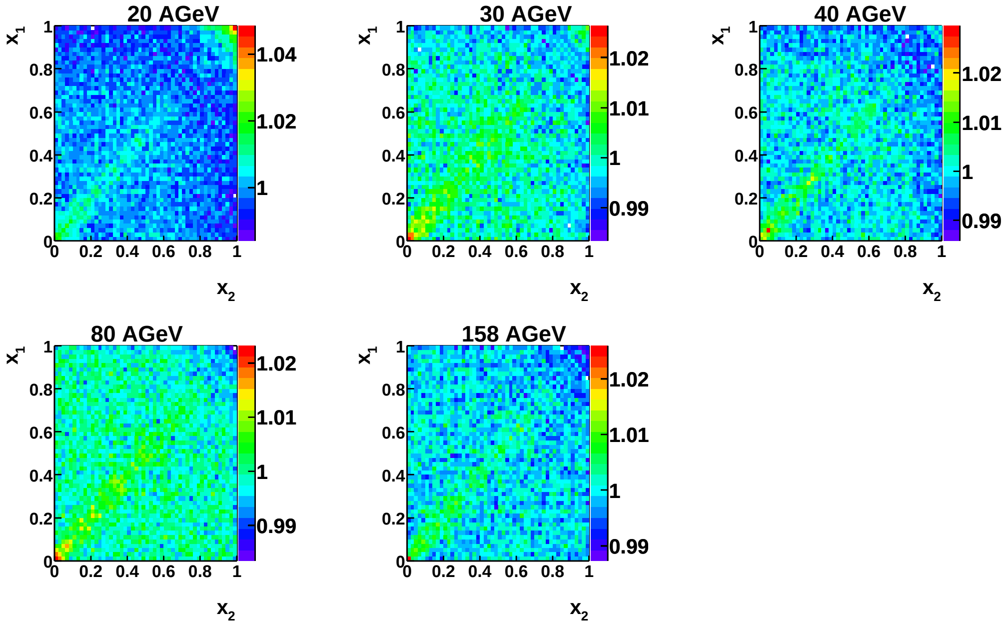

Figure 5.12: Two-particle correlation plots (x_1, x_2) for all charged particles for central Pb+Pb collisions at 20 - 158 AGeV. The data are plotted with different color scales.

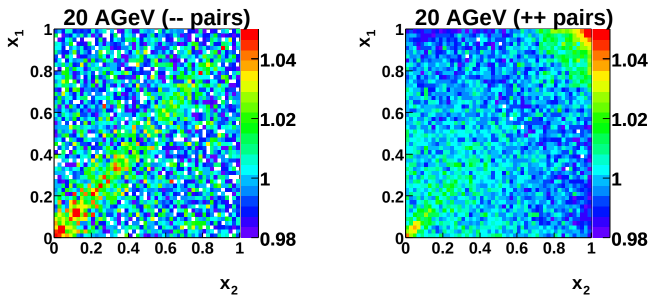

Figure 5.13: Two-particle correlation plots (x_1, x_2) for negatively and positively charged particle pairs for central Pb+Pb collisions at 20 AGeV.

5.5 Comparison with predictions of models

5.5.1 The UrQMD model

The Φ_{p_T} values can be compared to predictions of the UrQMD model [69, 70] - version 1.3. UrQMD is a transport model allowing for the formation, decay and re-scattering of resonances and strings. By its construction, in the UrQMD model no fluctuations due to possible phase transition are incorporated. However, resonance decays and effects of correlated particle production due to energy (momentum) and quantum number conservation laws are included. In the model default parameters have been used (meson-meson and meson-baryon scattering effects included). The time during which all particles are tracked (so-called *tim* parameter) has been set as 80 fm/c (after kinetic freeze-out). For each energy (20, 30, 40, 80 and 158 AGeV) from the sample of minimum bias Pb+Pb events the most central 7.2% interactions have been selected, accordingly to the centrality of real data recorded by the NA49 experiment. Such selection corresponds to the impact parameter range $0 < b < 4.35$ (linear weighting of b has been used in the model).

The Φ_{p_T} values for data have been calculated using all charged particles that come from the main vertex. Practically it means that pions, protons, kaons and their anti-particles are used in the analysis (particles from the decays of Λ, ϕ, Ξ and Ω are rejected by use of a list of track cuts). It can be quite natural that also in the UrQMD model only charged pions, protons and kaons should be considered in calculations. In the study of the UrQMD events the same kinematic cuts have been applied as in the case of data (very forward-rapidities only). In order to be in an agreement with data the pion mass has been assumed for all particles. The p_T - azimuthal angle acceptance is common for all energies and selected to be the same as for the real data. All these kinematic and acceptance restrictions - similarly as in the case of data - lead to the fact that only 5-6% of all charged particles produced in central Pb+Pb collision are used to study transverse momentum fluctuations.

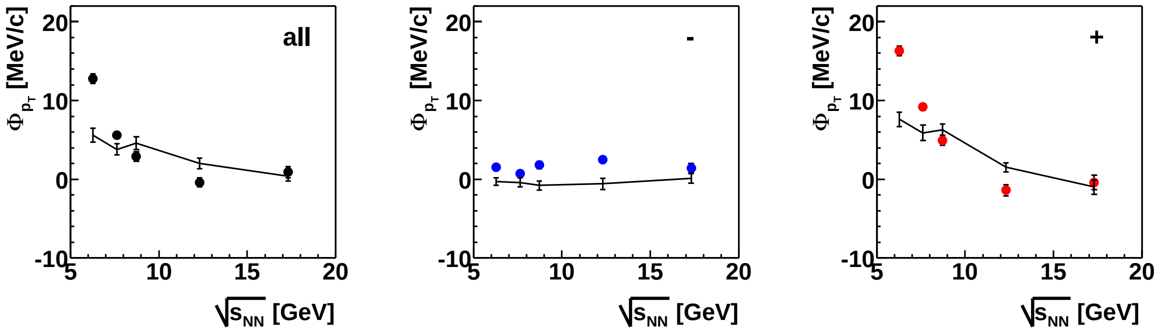

Figure 5.14: Φ_{p_T} versus energy calculated by use of the UrQMD model (black lines) with the acceptance restrictions the same as for data. Pion mass has been assumed for all produced particles. Results are compared to data (points) corrected for limited two-track resolution. The panels represent: all charged, negatively charged, positively charged particles, respectively.

In Fig. 5.14 the Φ_{p_T} values versus energy are compared for data and for the UrQMD model. Separate plots represent results for all charged particles, and for negatively charged and positively charged particles, separately. Similarly to data the UrQMD model shows the energy dependence of transverse momentum fluctuations for all charged particles and for positively charged ones whereas there is no energy dependence for negatively charged particles. Therefore, as it has been already mentioned, the most important problem is to understand qualitatively the difference between positively and negatively charged particles. It should be stressed that - although the same kinematic and acceptance cuts are used for the data and for the UrQMD model - the Φ_{p_T} values should not be directly compared in these two cases. One of the reasons is that models generally do not incorporate effects of short range correlations (specially Bose-Einstein). Moreover, it has been shown by the CERES experiment that the measured values of mean p_T fluctuations calculated by use of the UrQMD model with default parameters can be under-estimated [50] and that switching off secondary scattering (specially meson-baryon re-scattering) results in the values of p_T fluctuations similar to these observed in the data. It has been also checked that this under-estimation (when re-scattering processes are included in the UrQMD model) can be even stronger for lower energies. This effect observed by the CERES experiment might help to qualitatively explain the under-estimation of Φ_{p_T} values in Fig. 5.14.

In Fig. 5.15 two-particle correlation plots for UrQMD 20 AGeV interactions are presented for all possible particle pairs (left) and for negatively (middle) and positively (right) charged particles, separately. As it has been already mentioned the UrQMD model does not exhibit Bose-Einstein effects (an enhancement close to the diagonal) and the main difference between data and model is that an enhancement in the region close to $x_1 = 1$ and $x_2 = 1$ observed in the data is practically not seen in the model. A rudimentary enhancement for positively charged particles probably might be observed if one changes the scale of the plot (Fig. 5.16) but the statistics of the UrQMD data, used in this analysis, is much smaller than in the case of real events. Nevertheless, even with a better statistics, it can be rather naive to expect a very similar two-particle correlation plot for data and model, especially when one remembers that the Φ_{p_T} value at 20 AGeV for data is slightly higher than that for the UrQMD model. Anyhow, both data and the model at 20 AGeV have one common feature - long range correlations similar to those for p+p collisions.

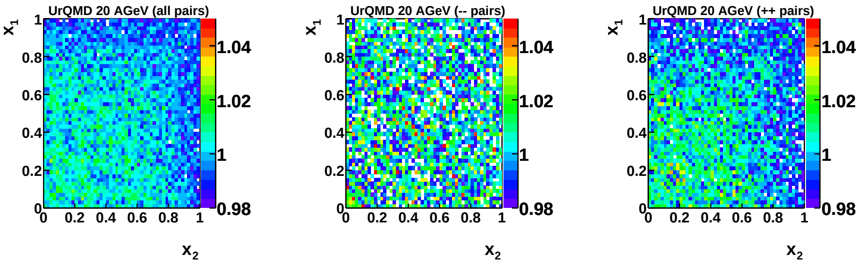

Figure 5.15: Two-particle correlation plots (x_1, x_2) for 20 AGeV Pb+Pb interactions obtained from the UrQMD model for different charge combinations. The same acceptance is used as for data.

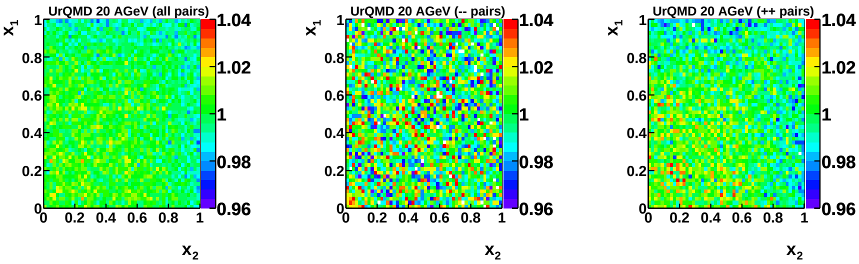

Figure 5.16: Two-particle correlation plots (x_1, x_2) for 20 AGeV Pb+Pb interactions obtained from the UrQMD model for different charge combinations. The same acceptance is used as for data.

Although the track-by-track identification is not possible for the data it can be quite interesting to check, by use of the UrQMD model, what is the content of the *accepted* particles in the studied forward-rapidity region. The sample of negatively charged particles is composed mainly by negative pions (94.4% of all negative for 20 AGeV and 89.4% of all negative for 158 AGeV) and negatively charged kaons (5.6% for 20 AGeV and 9.2% for 158 AGeV), whereas the number of produced anti-protons can be treated as negligible (below 0.1% for 20 AGeV and 1.6% for 158 AGeV). The sample of positively charged particles is less homogeneous: it contains positive pions (42.8% for 20 AGeV and 69% for 158 AGeV), positive kaons (8.5% for 20 AGeV and 10.4% for 158 AGeV) and protons (48.7% for 20 AGeV and 20.6% for 158 AGeV). Protons observed in the final state probably originate mainly from projectile and target nuclei (re-scattered participants). In the studied region the total multiplicity of protons remains constant for all energies (11.1 - 13.2), in contrary to multiplicities of newly produced particles such as π^+ or K^+. However, the fraction of protons in a sample of positively charged particles is significantly higher for lower energies.

Keeping in mind that re-scattered participants may be strongly correlated in transverse momentum (due to the momentum conservation law) one can expect that the increased Φ_{p_T} values for lower energies might be connected with the presence of correlated protons in a sample. The qualitative verification of this hypothesis is presented in Fig. 5.17 where the Φ_{p_T} values are calculated separately for different types of particles. The right panel of Fig. 5.17 shows that the curve for protons qualitatively reproduces the curve for positively charged particles thus confirming that protons indeed might be responsible for increased Φ_{p_T} values for lower energies.

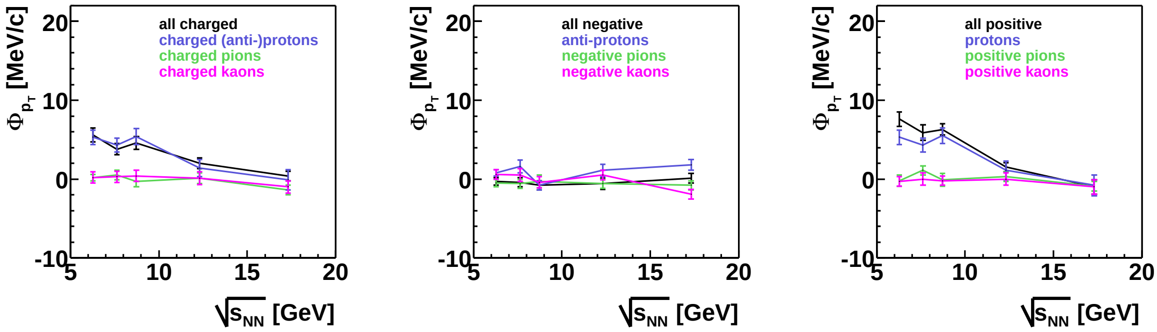

Figure 5.17: Φ_{p_T} versus energy calculated by use of the UrQMD model, separately for different types of produced particles. The kinematic cuts and acceptance restrictions for the UrQMD model are the same as for data. Pion mass has been assumed for all produced particles.

The effect of the limited $p_T - \phi$ acceptance (common acceptance) might modify the correlations present in the systems therefore before making any solid conclusions one has to make sure that Φ_{p_T} behavior versus energy remains qualitatively not changed for complete azimuthal angle acceptance. Fig. 5.18 presents Φ_{p_T} values for forward-rapidity region (also for "4π" acceptance) where no $p_T - \phi$ acceptance restrictions were used. In the case of so-called "4π" acceptance the only one remaining cut is a limitation for p_T of produced particles (0.005 - 1.5 GeV/c). The Φ_{p_T} dependence on energy both for charged particles and for (anti-)protons only is comparable with that in Fig. 5.17 thus indicating that the limited $p_T - \phi$ acceptance does not influence the observed effect significantly. In the forward-rapidity region (with $0.005 < p_T < 1.5$ GeV/c) the total multiplicity of final state protons is similar for all five energies and varies between 42.4 and 47.6.

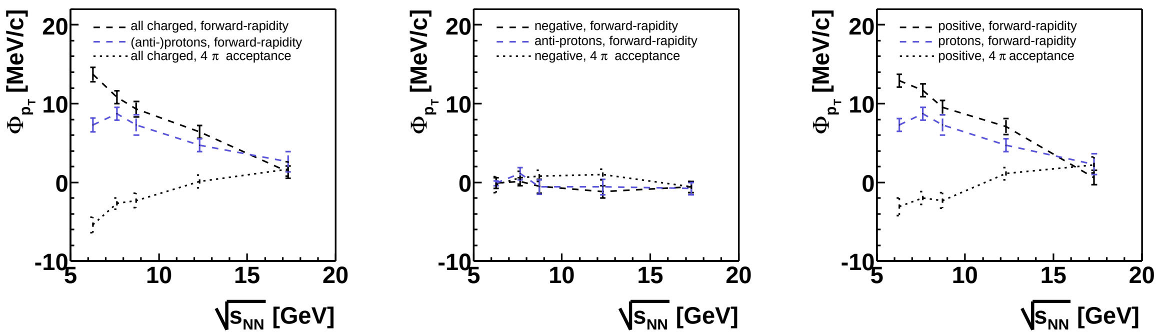

Figure 5.18: Φ_{p_T} versus energy calculated by use of the UrQMD model without $p_T - \phi$ acceptance restrictions. Pion mass has been assumed for all produced particles. The dashed lines correspond to forward-rapidity region ($1.1 < y^*_\pi < 2.6$), the dotted lines to "4π" acceptance. The panels represent: all charged, negatively charged and positively charged particles. Forward-rapidity (anti-)protons only are represented by dashed violet line.

If the re-scattered participating protons (strongly correlated in transverse momentum due to the momentum conservation law) are indeed responsible for the observed effect (increased Φ_{p_T} values for lower energies), the observed correlation should be stronger for the detector with complete ("4π") acceptance because the number of correlated pairs would be significantly higher. Moreover, also participating neutrons should be strongly correlated in transverse momentum thus increasing the total correlation in the system. The results of the UrQMD calculations confirming this hypothesis are presented in Fig. 5.19 where Φ_{p_T} is calculated for "4π" acceptance ($0.005 < p_T < 1.5$ GeV/c) for protons only (left) and for protons and neutrons (middle). The total multiplicity of protons is similar for all five energies and varies between 167.1 and 169.9 whereas the total multiplicity of neutrons and protons equals 358.9 - 366.1 (the estimated number of wounded nucleons for 7.2% most central Pb+Pb interactions equals approximately 349). The very strong correlation observed for protons (Φ_{p_T} on the level of 130 MeV/c) is two times enlarged when neutrons are included. On the other hand Φ_{p_T} values for different combinations of newly produced particles such as pions or anti-protons remain small even for a "4π" acceptance (Fig. 5.19 - right) although the total multiplicity of all pions is much higher than the multiplicity of protons + neutrons and strongly depends on energy. It seems to finally confirm the hypothesis that the increased Φ_{p_T} values for positively charged forward-rapidity particles at lower energies can be connected with the increased fraction of correlated participants in the sample. It should be however stressed, that the other sources of correlations are not excluded neither in the UrQMD model nor in the data and in principle in real collisions there might be additional, qualitatively new, onsets of fluctuations that are not incorporated in all the considered models.

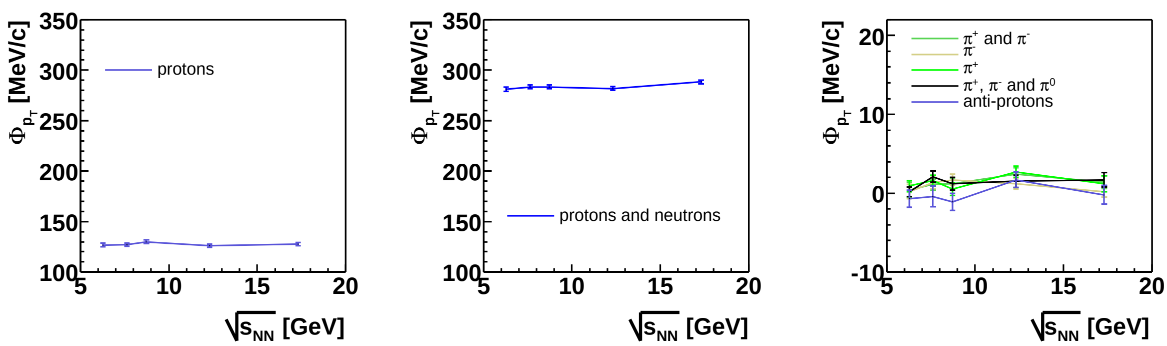

Figure 5.19: Φ_{p_T} versus energy calculated by use of the UrQMD model for "4π" acceptance ($0.005 < p_T < 1.5$ GeV/c) for protons only (left), protons and neutrons (middle) and for different combinations of newly produced particles (right).

Chapter 6

Comparison of results with other experiments and discussion

There are a lot of fluctuation measures used in the literature e.g. $\sigma_{p_T,dyn}$, $\Delta\sigma_{p_T}$, Σ_{p_T}, F_{p_T}, Σ_{p_T} (%) and Φ_{p_T} however under reasonable assumptions all of them are related [71]. All fluctuation quantities measure the difference in the width of $M(p_T)$ distribution from a "random expectation". The random expectation can be represented by mixed events or eventually by Gamma distribution that can be determined by use of parameters (moments) of inclusive p_T and multiplicity distributions. Apart from the fact that all fluctuation measures are related, their multiplicity dependence can be different. Even within the same measure different experiments can apply different quality and kinematic cuts what makes a direct and coherent comparison of the measured values impossible. In the future it would be very important to invent a method of standardizing the results between experiments with different acceptance and thus making their results comparable. In the following, the results on p_T fluctuations obtained by different experiments are summarized.

NA22

The value of $\Phi_{p_T} = 10.9 \pm 1.5$ MeV/c for charged hadrons has been reported by the NA22 experiment in π^+p and K^+p interactions [72] at 250 GeV in a rapidity acceptance similar to that used in this paper. The value obtained by the NA22 experiment is higher than the result presented in this paper for p+p interactions at 158 AGeV ($\Phi_{p_T} = 2.2 \pm 0.3 \pm 1.2$ MeV/c). This can be caused by the differences in the azimuthal acceptance, energy and types of interacting hadrons. Additionally, the NA22 experiment has observed a dependence of Φ_{p_T} on the rapidity region showing that Φ_{p_T} is significantly higher for mid-rapidity region and its value is very small in the projectile fragmentation region (forward-rapidity). This is consistent with low Φ_{p_T} value for the forward hemisphere presented in this thesis. Φ_{p_T} value determined by the NA22 experiment in the mid-rapidity region is above 25 MeV/c and significantly depends on the lower p_T cut.

CERES

The CERES experiment at the SPS has obtained $\Phi_{p_T} \approx 5$ MeV/c for charged hadrons in semi-central Pb+Au collisions at 158 AGeV [50]. This measurement has been performed close to mid-rapidity (pseudo-rapidity [1] $2.2 < \eta < 2.7$) in the p_T range $0.1 < p_T < 1.5$ GeV/c and with full azimuthal angle acceptance. A somewhat lower value, $\Phi_{p_T} \approx 1.5$ MeV/c is found in this work for the similar Pb+Pb reaction at forward-rapidities. The recent CERES results, obtained for minimum bias Pb+Au interactions at 158 AGeV (all charged particles, $2.2 < \eta < 2.7$, $0.15 < p_T < 1.5$ GeV/c and 2π azimuthal acceptance) show significant centrality dependence of transverse momentum fluctuations - a very similar to that reported in this thesis [73]. In Fig. 6.1 the comparison of Φ_{p_T} values for the CERES and for the NA49 experiment is presented. Both experiments show consistent structure, however due to differences in azimuthal acceptance, p_T and rapidity ranges the absolute values of Φ_{p_T} are different for CERES and NA49.

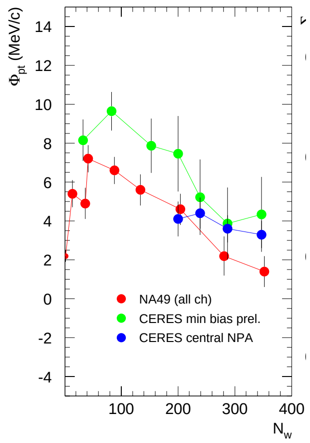

Figure 6.1: Comparison of the system size dependence of transverse momentum fluctuations at top SPS energy (CERES and NA49 results). Figure taken from [73].

The more recent CERES results [74] present the F_{p_T} dependence on the number of participants (F_{p_T} [49] measures the percent difference of the standard deviations of $M(p_T)$ for the data and mixed events). In Fig. 6.2 the non-monotonic behavior can be observed with a maximum for semi-central Pb+Au collisions at 158 AGeV. Non-statistical p_T fluctuations may be caused by momentum space correlations arising from resonance decays. Therefore the CERES experiment has compared their results to the cascade models RQMD and UrQMD. The non-monotonic behavior of F_{p_T} as a function of centrality can be qualitatively reproduced by the RQMD model with re-scattering (the model also correctly describes mean inclusive p_T dependence on centrality) but UrQMD model with re-scattering fails to reproduce the data. Both the RQMD and the UrQMD models without re-scattering are consistent with the baseline (dotted line in the left panel of Fig. 6.2) representing the extrapolation from N+N interactions (superposition of N+N).

The most recent CERES results show that the significant centrality dependence can be observed also for lower energies [75]. The structure of the dependence of p_T fluctuations on the number of participants has been found to be very similar for 40, 80 and 158 AGeV (minimum bias 40 AGeV, minimum bias 158 AGeV and semi-central 80 AGeV Pb+Au data have been used; see the figure in [75]). Moreover, the magnitude of the fluctuations does not depend on beam energy.

Before focusing on the centrality dependence of p_T fluctuations (see above) the CERES experiment has been studying the energy dependence of transverse momentum fluctuations by use of central Pb+Au collisions only at 40, 80 and 158 AGeV (mid-rapidity

[1] pseudo-rapidity is defined as $\eta = -ln(tg\frac{\Theta}{2})$, where Θ is an angle between the beam direction and the direction of a given particle; Θ varies between zero and π

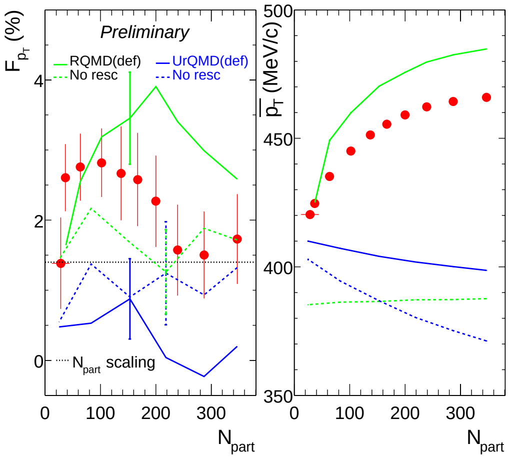

Figure 6.2: Transverse momentum fluctuations (left) and inclusive mean transverse momentum (right) as a function of centrality measured by the CERES experiment. Fluctuations are corrected for short range momentum correlations. Data are compared to predictions of models. Figure taken from [74].

region). The $M(p_T)$ distributions for all three energies have been found to be slightly wider than the corresponding distributions for mixed events, indicating small but finite dynamical fluctuations [50]. For 6.5% most central Pb+Au events Φ_{p_T} values (calculated without the removal of short range correlations) vary between 2.4 and 5.0 MeV/c with a typical error of about 2 MeV/c. It indicates that the possible significant non-monotonic behavior of p_T fluctuations with collision energy (the probable effect of approaching the phase boundary) or unusually large fluctuations that might indicate the hadronization at the critical end-point of the QCD phase diagram have not been observed by the CERES experiment. Moreover, the CERES results show that mean p_T fluctuations (when using Σ_{p_T} (%) fluctuation quantity [50] that measures the strength of non-statistical fluctuations in percent of mean inclusive p_T - measure different than F_{p_T}) are small and only weakly dependent on energy (very similar for SPS and RHIC energies) [74]. These fluctuations do not show any non-monotonic behavior with energy and their magnitude is far below the level predicted at the critical end-point [19, 45, 74]. Therefore, the study of the energy dependence of p_T fluctuations at central A+A collisions the CERES experiment suggests that the critical point may not be located in the μ_B regime below 450 MeV [50]. Note that, as suggested in [45] the observation of a large magnitude of fluctuations cannot be itself a signature of the critical point but should be combined with the non-monotonic behavior of fluctuation observables.

STAR

The results from the STAR experiment at RHIC [48] show significant event-by-event dynamical fluctuations in transverse momentum for Au+Au collisions at $\sqrt{s_{NN}} = 130$ GeV energy. For 15% most central events and for the mid-rapidity region ($|\eta| < 1.0$, $0.15 < p_T < 2.0$ GeV/c and complete - 2π acceptance in azimuthal angle) it has been observed that the distribution of $M(p_T)$ is about 14% wider ($F_{p_T} = 14$ %) than the uncorrelated reference represented by the corresponding Gamma distribution [76]. These significant non-statistical fluctuations have been also observed in the two-particle correlation plot as a saddle-shaped structure symmetric about the diagonal [77, 48]. The Φ_{p_T} value measured for all charged particles has been calculated as 52.6 ± 0.3 MeV/c [76] but its large value can be connected with significant contribution of correlated particles originating from (mini-)jet fragmentation.

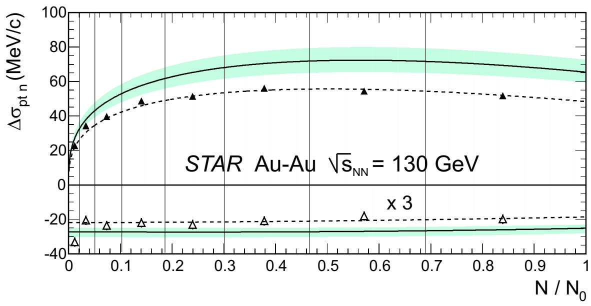

Figure 6.3: Centrality dependence of p_T fluctuations ($\Delta\sigma_{p_T}$ measure [47] on the vertical axis) measured by the STAR experiment in minimum bias Au+Au collisions at $\sqrt{s_{NN}}$ = 130 GeV. Figure taken from [76]. See [76] for details.

A non-monotonic but smooth centrality dependence of p_T fluctuations ($\Delta\sigma_{p_T}$ measure [47]) has been also observed by the STAR experiment for minimum bias Au+Au collisions at $\sqrt{s_{NN}}$ = 130 GeV (Fig. 6.3). A maximum can be observed for semi-central Au+Au interactions [76]. The effects of elliptic flow on the $\Delta\sigma_{p_T}$ measure can be safely ignored in this analysis [78].

Recent STAR results [79] measured in a very similar kinematic region ($|\eta| < 1.0$, $0.1 < p_T < 2.0$ GeV/c and 2π azimuthal acceptance) but for 5% most central Au+Au interactions at $\sqrt{s_{NN}}$ = 20, 130 and 200 GeV demonstrate the presence of the dynamical p_T fluctuations at all three energies. $M(p_T)$ histograms for real events are wider than the corresponding distributions for mixed events and this difference seems to slightly increase with increasing energy.

PHENIX

Event-by-event p_T fluctuations have been also measured by another RHIC experiment PHENIX in Au+Au collisions at $\sqrt{s_{NN}}$ = 130 and 200 GeV. The F_{p_T} measure [49], determining the percent difference of the standard deviations of $M(p_T)$ for the data and mixed events, has been used in the analysis. Dynamical fluctuations have been found to be very small - on the level of few percent (this can be due to the rather limited acceptance of the PHENIX detector). Due to large errors no significant system size dependence has been observed at $\sqrt{s_{NN}}$ = 130 GeV [49], however recent results at $\sqrt{s_{NN}}$ = 200 GeV (with better azimuthal acceptance and higher statistics) demonstrate strong non-monotonic centrality dependence of p_T fluctuations with a maximum for semi-central Au+Au collisions [80, 81].

Fig. 6.4 presents PHENIX p_T fluctuations for all charged particles near mid-rapidity region ($|\eta| < 0.35$, $0.2 < p_T < 2.0$ GeV/c and azimuthal acceptance about 180 degrees). By use of Monte Carlo simulations it has been checked that the effect of elliptic flow is small and does not explain the observed behavior. The reported correlations have been found to be consistent with correlations due to jets at large p_T (lines in figure). This consistency is even better when additionally jet suppression (jet quenching) is assumed for more central events (dashed line). Due to large errors at $\sqrt{s_{NN}}$ = 130 GeV it is not possible to obtain the reliable difference between F_{p_T} values for 130 GeV and 200 GeV interactions (the possible energy dependence of p_T fluctuations).

Fig. 6.5 shows that the trend of the non-monotonic behavior of the system size dependence of p_T fluctuations qualitatively agrees for NA49, CERES and PHENIX experiment.

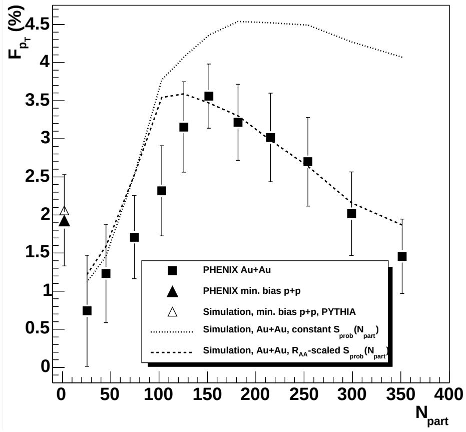

Figure 6.4: Centrality dependence of p_T fluctuations (F_{p_T} versus number of participants) measured by the PHENIX experiment in Au+Au and p+p collisions at $\sqrt{s_{NN}} = 200$ GeV. Lines correspond to Monte Carlo simulations with additional hard-scattering processes (jets). See [81] for details. Figure taken from [82].

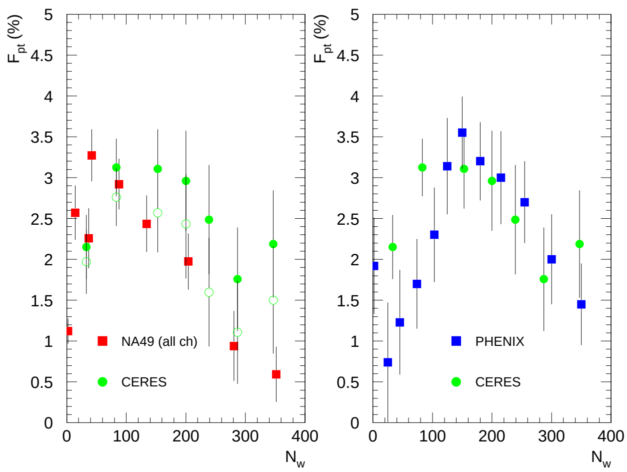

Figure 6.5: Comparison of the system size dependence of transverse momentum fluctuations between SPS and RHIC. Figure taken from [73].

Summary of the system size dependence of event-by-event fluctuations

The system size dependence of mean p_T fluctuations has been studied by several experiments at different energies, namely by the NA49 and CERES experiments at $\sqrt{s_{NN}} = 17.3$ GeV, by the CERES experiment at $\sqrt{s_{NN}} = 7.7$ GeV and partially at $\sqrt{s_{NN}} = 10.7$ GeV, by the STAR experiment at $\sqrt{s_{NN}} = 130$ GeV and by the PHENIX experiment at $\sqrt{s_{NN}} = 200$ GeV. Several fluctuation measures have been used and different kinematic and acceptance regions have been investigated but the final results give qualitatively clear and consistent picture: significant system size dependence of p_T fluctuations is observed both at SPS and RHIC energies. This dependence cannot be explained by known and/or trivial effects such as elliptic flow. The contribution from short range correlations is also too small to reproduce the data. Both CERES and PHENIX experiments observe the larger contribution to dynamical p_T fluctuations at higher p_T; this can indicate that hard scattering processes (jets) might be a source of correlations at high p_T (jets inherently add particles correlated in p_T). The PHENIX experiment employs a phenomenological PYTHIA-based model that estimates the relative contribution due to jet production as a function of centrality (jet production in A+A collisions is suppressed for more central events). The following procedure is used - the PYTHIA jet events are embedded to a simulation of soft processes with reproduced inclusive p_T and N distributions as a function of centrality. There are two possible embedding ways - with PYTHIA event embedding rate constant for all centralities and with the rate scaled by the *nuclear modification factor* R_{AA} for each centrality bin (nuclear modification factor compares the transverse momentum spectra in A+A and N+N collisions thus measuring the deviation of A+A from an incoherent superposition of N+N interactions). The later one much better describes the data (when a correlated $q\bar{q}$ pair - jet - is produced both quark and anti-quark hadronize into particles but the presence of high density matter in central collisions can affect for example hadrons coming from one of the quarks that can lead to melting the correlation - the schematic illustration of jet suppression is presented in Fig. 6.6). Fig. 6.7 shows the system size dependence of transverse momentum fluctuations at SPS and RHIC energies compared to the predictions of this model (the cross section for the jet production is significantly reduced at SPS energies, however non-zero contribution can still be present). The model seems to explain the anomaly observed in the system size dependence of p_T fluctuations.

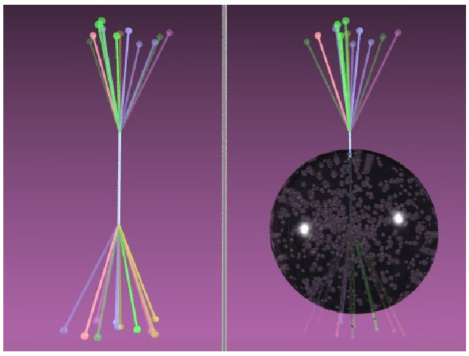

Figure 6.6: The schematic illustration of jet suppression in the presence of high density matter. Figure taken from [83].

There are also different models explaining the non-monotonic centrality dependence of mean p_T fluctuations. One of them is a thermalization model (onset of thermal equilibrium) reasonably explaining RHIC (STAR and PHENIX) results [71, 84]. The string percolation model [85] gives a good description of the PHENIX and NA49 data. It has been already mentioned that cascade models (RQMD) with re-scattering reasonably describe the CERES results [74].

The system size dependence of event-by-event fluctuations has not been studied for mean transverse momentum only but also for other fluctuation measures. The recent NA49 results present non-monotonic behavior of the system size dependence of multiplicity fluctuations (Fig. 6.8). The system size dependence of mean p_T fluctuations and multiplicity (negatively charged particles only) are very similar and as the $M(p_T)$ definition is connected with multiplicity it would not be surprising that these two quantities may fluctuate in a correlated way. However, it is quite obvious that a single theoretical approach explaining all these effects for all fluctuation measures would be very helpful in understanding the recent promising results.

There might be also a different explanation of the observed non-monotonic behavior of the system size dependence of both transverse momentum and multiplicity fluctuations. An increase of the dynamical fluctuations in transverse momentum and multiplicity has been predicted to occur in A+A collisions which freeze out near a second-order critical

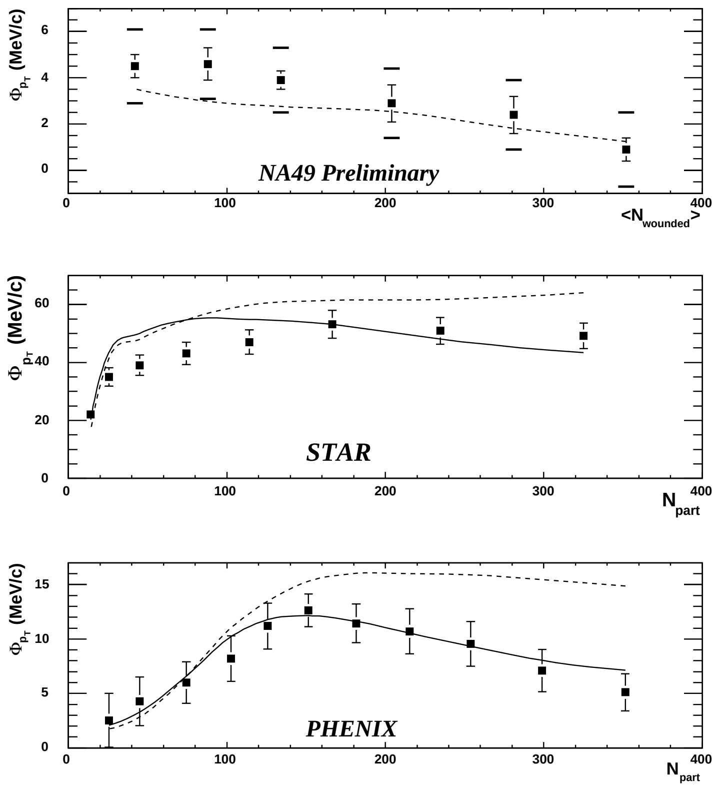

Figure 6.7: Comparison of the system size dependence of transverse momentum fluctuations for Pb+Pb collisions at $\sqrt{s_{NN}} = 17$ GeV (top) - negatively charged particles only, for Au+Au collisions at $\sqrt{s_{NN}} = 130$ GeV (middle) and for Au+Au collisions at $\sqrt{s_{NN}} = 200$ GeV (bottom). The lines correspond to the calculations of the model that estimates the relative contribution due to jet production as a function of centrality for a fixed PYTHIA event embedding rate (dashed lines) and for an R_{AA}-scaled embedding rate (solid lines). See [83] for details. Figure taken from [83]. Note that at present the NA49 results are accepted as final.

end-point of the QCD phase diagram [19]. In this work it is argued that the central Pb+Pb interactions at 158 AGeV probably do not hadronize near the critical end-point. However, it has been already mentioned in Introduction that for a given energy the freeze-out temperature is higher for lower centralities (or for lighter ions) and therefore from the point of view of the phase diagram a reduction of the centrality can result in increasing of the freeze-out temperature. One can expect an increase of fluctuations if it makes the freeze-out point to approach the critical point. Additional argument for the fluctuations at the critical end-point is the simultaneous detection of a maximum both at transverse momentum and multiplicity (similar N_w). On the basis of calculations in [19] and of the numbers shown in Table 4.5 it can be estimated that such critical fluctuations alone should give the Φ_{p_T} value on the level of 20 MeV/c. However, one has to remember that in this theoretical estimate the effect of the limited experimental acceptance of the detector has not been taken into account. It is expected that the limited acceptance of the detector would reduce the signal to $\Phi_{p_T} \simeq 10$ MeV/c [86]. This value is close to the maximum value of Φ_{p_T} found in this analysis - for peripheral Pb+Pb interactions ($\Phi_{p_T} = 7.2 \pm 0.7 \pm 1.6$ MeV/c). This theoretical estimate, however, is subject to many uncertainties, (among them how close the freeze-out is to the critical point).

One has to remember that the non-monotonic behavior of p_T fluctuations is observed by several experiments at different energies (not only at 158 AGeV) and the maximum is placed at different positions. Among different theories and calculations there is no

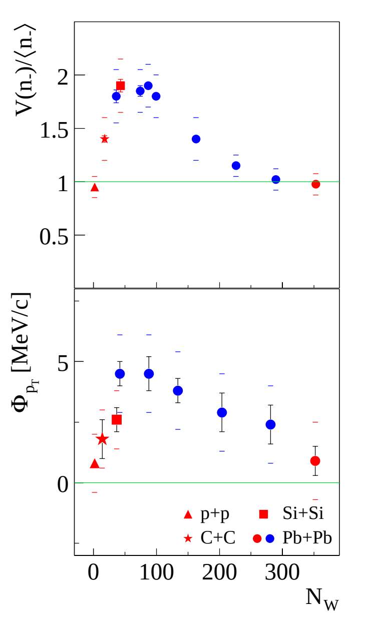

Figure 6.8: The system size dependence of the ratio of variance to mean for the multiplicity distributions of negatively charged particles (top) and the system size dependence of transverse momentum fluctuations of negatively charged particles (bottom). All data measured by the NA49 experiment. Figure taken from [14].

agreement concerning the location of the critical end-point in the (T, μ_B) plane. Consequently, before making any reliable conclusions concerning either discovering or ruling out the presence of the critical point in this domain one should have a more detailed theory predictions for the location of the critical region.

Fig. 6.8 shows that both p_T and multiplicity fluctuations display a very similar system size dependence. Recently it has been shown [87] that the event-by-event fluctuations of mean transverse momentum and multiplicity measured by the NA49 experiment are correlated indeed. Namely, the non-monotonic behavior of p_T fluctuations as a function of the system size can be fully explained by the non-monotonic dependence of multiplicity fluctuations. In [87] it is assumed that the correlation between the mean transverse momentum of the event and the multiplicity is present both in p+p and in A+A interactions. Moreover, the correlation strength is assumed to be independent on the collision centrality. This approach suggests that the Φ_{p_T} measure can be expressed in terms of multiplicity fluctuations by the formula [87]

$$\Phi_{p_T} = \sqrt{2}\frac{(\delta T)^2}{T}\frac{V(n_{-})}{\langle n_{-}\rangle} \tag{6.1}$$

where δT measures the correlation strength between temperature (corresponding to mean p_T in thermal model) and multiplicity (the detailed definition of δT can be found in [87]) and $\frac{V(n_-)}{\langle n_-\rangle}$ is a ratio of variance to mean for the multiplicity distribution of negatively charged particles. A centrality independent δT can be determined for example for p+p interactions (the NA49 data in this thesis) and for forward-rapidity negatively charged particles $\sqrt{2}\frac{(\delta T)^2}{T} \approx 2.48$ MeV. This numerical coefficient applied to the formula 6.1 with experimental values of $\frac{V(n_-)}{\langle n_-\rangle}$ (also from the NA49 experiment with the same acceptance restrictions) gives Φ_{p_T} values comparable to those measured by the NA49 experiment (open circles and triangles in Fig. 6.9). It shows that the p_T fluctuations can be indeed determined by multiplicity fluctuations only. The analytical formula, however, is not free of several approximations and therefore, additionally, a Monte Carlo simulation has been performed (the full circles in Fig. 6.9; see [87] for the details). Both the analytical formula and a Monte Carlo simulation show a good agreement with the data confirming the strong correlation between mean p_T and multiplicity fluctuations of forward-rapidity negatively charged particles registered in the NA49 experiment.

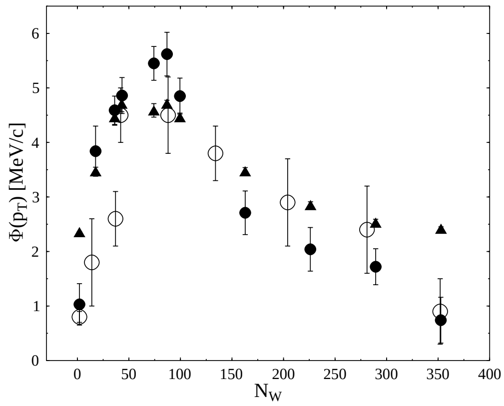

Figure 6.9: Φ_{p_T} as a function of number of wounded nucleons measured for negatively charged particles by the NA49 experiment (open circles) compared to the simulation from [87] (full circles) and to the prediction of the analytical formula (6.1) (triangles). Figure taken from [87].

By its definition the Φ_{p_T} measure includes the particle multiplicity and therefore the fact that the mean transverse momentum and multiplicity fluctuations are strongly correlated seems to be not very surprising. Moreover, one has to point out that the fluctuation measures used by other experiments should also be influenced by multiplicity fluctuations. Nevertheless, even if the multiplicity fluctuations fully explain the fluctuations observed for transverse momentum a mechanism responsible for multiplicity fluctuations still remains unexplained.

Summary of the energy dependence of event-by-event fluctuations

The main motivation to study the energy dependence of p_T fluctuations has been the prediction of possible anomalies connected with the onset of deconfinement phase transition (approaching the phase boundary), particularly it has been expected that the dynamical fluctuations would be increased for lower SPS energies. The latest results concerning $\langle K^+\rangle/\langle\pi^+\rangle$ production [15, 17, 14] have made the low SPS energy region truly attractive. Additionally, the preliminary results on the energy dependence of event-by-event K/π fluctuations shows increased fluctuations at lower energies (Fig. 6.10).

The energy dependence of p_T fluctuations has been studied by the CERES experiment in central Au+Pb collisions at 40, 80 and 158 AGeV but no significant differences between these three energies has been observed. The event-by-event p_T fluctuations measured by the STAR experiment for central Au+Au collisions seem to indicate a slight increase with energy (from $\sqrt{s_{NN}}$ = 20 to 200 GeV) but in opinion of the author of this thesis it might be connected with the increased contribution from jet production. Moreover, the CERES experiment argues that the energy dependence of p_T fluctuations between SPS and RHIC energies is very weak and the magnitude of p_T fluctuations is far below the value predicted at the QCD critical point. The NA49 experiment does not observe any energy dependence of p_T fluctuations measured for negatively charged particles in central Pb+Pb collisions at full SPS energy range (20 - 158 AGeV). Transverse momentum fluctuations for positively charged particles are significantly increased for lower energies which might

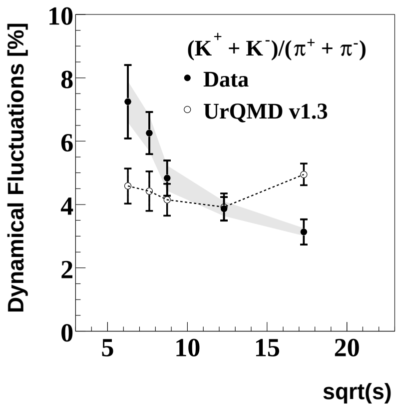

Figure 6.10: The energy dependence of event-by-event fluctuations of K/π ratio measured by the NA49 experiment. Figure taken from [44]. See [44] for details.

be connected with increased content of protons (re-scattered participants correlated by momentum conservation law) in a sample of positively charged particles.

A direct comparison of dynamical p_T fluctuation, based on the method of determining the magnitude of residual temperature fluctuations [55] has been presented in [83]. For the most central interactions the estimated temperature fluctuations are on the level of 1.8%, 1.7%, 1.3% and 0.6% for PHENIX ($\sqrt{s_{NN}}$ = 200 GeV), STAR ($\sqrt{s_{NN}}$ = 130 GeV), CERES ($\sqrt{s_{NN}}$ = 17 GeV) and NA49 ($\sqrt{s_{NN}}$ = 17 GeV) experiments, respectively. It shows that there is no significant energy dependence of temperature fluctuations between SPS and RHIC energies.

Summarizing, due to different acceptance and kinematic cuts in several experiments one can not directly compare the values of fluctuation measures; however it seems that no *significant* energy dependence of event-by-event transverse momentum fluctuations has been observed. No clear signal of any anomalies or enlarged p_T fluctuations at regions close to the expected phase transition has been reported.

The NA49 experiment has been also analyzing event-by-event fluctuations of the net charge in central Pb+Pb interactions at 20, 30, 40, 80 and 158 AGeV, but only a very weak dependence on the energy has been observed. Similarly to p_T fluctuations no anomalies or enlarged fluctuations due to the phase transition has been measured. For all five energies the results are inconsistent with expected suppressed fluctuations in a QGP and show that the measured fluctuations are consistent with fluctuations due to global charge conservation [88]. This is also in agreement with the PHENIX results at $\sqrt{s_{NN}}$ = 130 GeV [83].

Chapter 7

Summary, conclusions and future plans

In this thesis transverse momentum event-by-event fluctuations have been analyzed for p+p, C+C, Si+Si and Pb+Pb collisions at 158 AGeV and for central Pb+Pb interactions at 20, 30, 40, 80 and 158AGeV. Due to the NA49 detector features the analysis has been limited to the forward-rapidity region. Three different characteristics have been studied: the fluctuations of average transverse momentum ($M(p_T)$) of the event, the Φ_{p_T} fluctuation measure and transverse momentum two-particle correlations.

The first observation for the system size dependence of transverse momentum fluctuations is that event-by-event fluctuations are rather small, namely all measured Φ_{p_T} values are below 10 MeV/c and are much smaller than the dispersion of the inclusive p_T distribution. However, the correlations observed in p+p collisions are not simply more and more diluted when going to heavier colliding systems as one could expect if the created matter approaches a higher level of equilibrium with increasing system size. Instead, a significant system size dependence of the Φ_{p_T} measure is seen with a maximum for peripheral Pb+Pb interactions. The NA49 experiment is the first SPS experiment that observed such non-monotonic behavior. A very similar dependence has been shown by other experiments both at SPS and at RHIC energies. None of the models considered in this thesis explain this anomaly and therefore solid theoretical predictions and new ideas are needed to make these interesting results useful and understandable.

The two-particle correlation plot for p+p data shows a prominent structure which has been found to be connected with the dependence of $M(p_T)$ on multiplicity. This structure disappears when going to heavier colliding systems. Instead, short range correlations become visible as an enhancement of the point density in the region close to the diagonal. This effect is strongest for the most central Pb+Pb interactions. No structure characteristic of event-by-event temperature fluctuations is observed for data. The HIJING model, which has been used for a comparison of the system size dependence of transverse momentum fluctuations qualitatively reproduces the structure of two-particle correlation plots for p+p and C+C data. However, in contrast to the data, it shows no centrality dependence of Φ_{p_T}.

The energy dependence of transverse momentum fluctuations that has been studied for central Pb+Pb collisions at 20, 30, 40, 80 and 158 AGeV does not show any possible anomalies connected with the fact that the system is approaching the phase boundary (from hadron gas scenario to QGP) for a sample of negatively charged particles (pions mainly). The Φ_{p_T} values for negatively charge particles are very close to zero (independent particles production). Transverse momentum fluctuations are significantly increased for lower energies when a sample of positively charged particles is considered. However, as it has been checked by use of the UrQMD model, this anomaly might be explained by the increased fraction of protons (re-scattered participants strongly correlated in p_T) in a sample of positively charged particles at lower energies. None of the SPS and RHIC experiments observed significant energy dependence of transverse momentum fluctuations.

Finally, it should be stressed that although the recent experimental results indicate that event-by-event physics is still accessible for smaller acceptance experiments the most of currently available event-by-event measurements have been performed in a limited acceptance - the multiplicity of observed particles being below 20% of the total multiplicity. Consequently, the sensitivity of these measurements to, in particular, long range correlations is reduced. It is desirable to perform future event-by-event measurements in an extended acceptance. The planned experiments at LHC accelerators, with significantly increased multiplicities, may provide new opportunities for event-by-event analysis.

Looking for the critical point by use of the fluctuation analysis

It has been suggested theoretically that enlarged multiplicity and transverse momentum fluctuations should appear for systems that hadronize near the second-order critical end-point of the first-order phase transition. The results presented in this thesis show significant non-monotonic behavior of mean p_T fluctuations. Also multiplicity fluctuations, studied by the NA49 experiment, are very promising. However, one has to keep in mind that the non-monotonic behavior of p_T fluctuations has been observed by several experiments at different energies and - consequently - for different positions of freeze-out points. From the one hand there are large theoretical uncertainties in the determination of the position of the critical point in the (T, μ_B) plane, from the other hand it has been suggested that the critical "point" can be rather the critical "region" of ΔT and $\Delta\mu_B$ parameters [89]. Therefore one cannot exclude that the observed p_T and multiplicity fluctuations might be a signature of the critical point. Additionally, the recently observed enlarged K/π fluctuations at lower energies might be connected with the onset of deconfinement or possibly with the critical point, or both.

Looking for the critical point of strongly interaction matter is one of the main motivations of the possible LIGHT ION PROGRAM at CERN SPS that might start after 2009 year. In order to discover or rule out the critical point the (T, μ_B) plane has to be carefully scanned. As it has been already discussed in this thesis - the change of the center-of-mass energy of the system leads to the change of the position of the freeze-out point (see Fig. 1.7). Also changing the system size can effect the position of freeze-out point. It has been observed by the NA49 experiment (using p+p, C+C, Si+Si and Pb+Pb interactions at 158 AGeV) that the temperatures of both the chemical and thermal freeze-out decrease linearly with increasing N_W (figure in [90]). The results of a light ion program at CERN SPS (energy scan of collisions with lighter than Pb ions) together with the existing data would allow to cover a broad range at the (T, μ_B) plane (Fig. 7.1). Accordingly to the current theoretical predictions the second-order critical end-point of the first-order phase transition can be located inside this region. Fluctuation analysis may become the most important tool in discovering the critical point, namely search for the critical point can be interpreted as a search for the fluctuation peak in the (T, μ_B) plane. The possible light ion program at CERN SPS and a search for the critical point can be also supplemented by programs at RHIC accelerator which is going to decrease the center-of-mass energy down to the top SPS value.

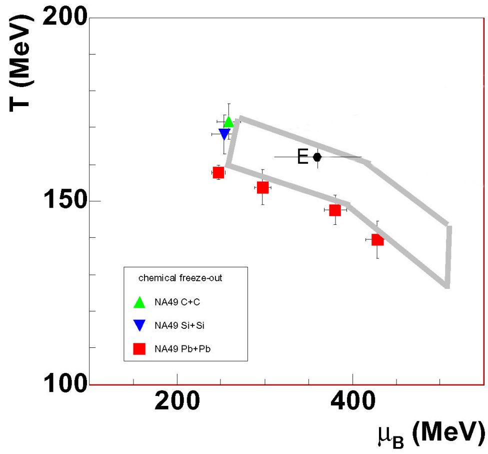

Figure 7.1: Phase diagram of strongly interacting matter. The marked area corresponds to the phase diagram domain possibly covered by chemical freeze-out points in the future SPS study. Figure taken from [90].

Bibliography

[1] D. H. Perkins, *"Introduction to High Energy Physics"*, Addison-Wesley Publishing Company (1982).

[2] J. C. Collins and M. J. Perry, *"Superdense matter: neutrons or asymptotically free quarks?"*, Phys. Rev. Lett. **34**, 1353 (1975); E. V. Shuryak, *"Quantum chromodynamics and the theory of superdense matter"*, Phys. Rept. **61**, 71 (1980); E. V. Shuryak, *"Theory and phenomenology of the QCD vacuum"*, Phys. Rept. **115**, 151 (1984).

[3] I. K. Yoo, Ph.D. thesis *"Bose-Einstein correlations of charged kaons and pions in central Pb+Pb collisions at 158 AGeV"*, Fachbereich Physik der Universität, Marburg (2001).

[4] The NA49 web page - http://na49info.cern.ch/Public/

[5] K. G. Wilson, *"Confinement of quarks"*, Phys. Rev. **D10**, 2445 (1974).

[6] F. Karsh, *"Lattice Results on QCD Thermodynamics"*, Nucl. Phys. **A698**, 199 (2002).

[7] K. Kanaya, *"Recent lattice results relevant for heavy ion collisions"*, Nucl. Phys. **A715**, 233 (2003).

[8] H. Reeves, *"Big Bang Nucleosynthesis and the Quark - Hadron Phase Transition"*, Phys. Rept. **201**, 335 (1991).

[9] H. Grigorian, B. Hermann and F. Weber, *"Quark-Hadron Phase Transition in Neutron Stars"*, Phys. Part. Nucl. **30**, 156 (1999).

[10] Z. Fodor and S. D. Katz, *"Lattice determination of the critical point of QCD at finite T and μ"*, JHEP **0203**, 014 (2002).

[11] Z. Fodor and S. D. Katz, *"Critical point of QCD at finite T and μ, lattice results for physical quark masses"*, JHEP **0404**, 050 (2004).

[12] R. Hagedorn, *"Multiplicities, p_t distrubutions and the expected hadron - quark-gluon phase transition"*, Riv. Nuovo Cim. **6N10**, 1 (1984).

[13] F. Antinori et al. (WA97 Collab.), *"Transverse mass spectra of strange and multistrange particles in Pb+Pb collisions at 158 AGeV/c"*, Eur. Phys. J. **C14**, 633 (2000).

[14] M. Gaździcki et al. (NA49 Coll.), *"Report from NA49"*, J. Phys. **G30**, S701 (2004).

[15] M. van Leeuwen et al. (NA49 Coll.), *"Recent results on spectra and yields from NA49"*, Nucl. Phys. **A715**, 161 (2003) and references therein.

[16] F. Becattini, M. Gaździcki and J. Sollfrank, *"On chemical equilibrium in nuclear collisions"*, Eur. Phys. J. **C5**, 143 (1998).

[17] V. Friese et al. (NA49 Coll.), *"Strangeness from 20 AGeV to 158 AGeV"*, J. Phys. **G30**, S119 (2003) and references therein.

[18] F. Becattini, M. Gaździcki, A. Keranen, J. Manninen and R. Stock, *"Chemical equilibrium study in nucleus+nucleus collisions at relativistic energies"*, Phys. Rev. **C69**, 024905 (2004).

[19] M. Stephanov, K. Rajagopal, and E. V. Shuryak, *"Event-by-event fluctuations in heavy ion collisions and the QCD critical point"*, Phys. Rev. **D60**, 114028 (1999).

[20] J. D. Bjorken, *"Highly relativistic nucleus-nucleus collisions: the central rapidity region"*, Phys. Rev. **D27**, 140 (1983).

[21] T. Alber at al. (NA49 Collab.), *"Transverse energy production in Pb+Pb collisions at 158 GeV per nucleon"*, Phys. Rev. Lett. **75**, 3814 (1995).

[22] P. Steinberg, *"Global observables at RHIC"*, Nucl. Phys. **A698**, 314 (2002).

[23] T. Ullrich, *"Experimental summary on global observables, hadron spectra and ratios."*, Nucl. Phys. **A715**, 399 (2003).

[24] J. Rafelski and B. Muller, *" Strangeness production in the quark-gluon plasma"*, Phys. Rev. Lett. **48**, 1066 (1982), Erratum-ibid. **56**, 2334 (1986); J. Rafelski, *"Formation and observables of the quark-gluon plasma"*, Phys. Rept. **88**, 331 (1982); J. Rafelski, *"Strange anti-baryons from quark-gluon plasma"*, Phys. Lett. **B262**, 333 (1991);

[25] C. Bormann et al. (NA49 Coll.), *"Kaon, lambda and anti-lambda production in Pb+Pb collisions at 158-GeV per nucleon"*, J. Phys. **G23**, 1817 (1997) and references therein.

[26] A. Andrighetto et al. (WA85 and WA94 Collab.), *"Enhancement of strange and multi-strange hyperons and anti-hyperons in S+S and S+W interactions at 200 GeV/c"*, J. Phys. **G25**, 209 (1999).

[27] T. Matsui and H. Satz, *"J/psi suppression by quark-gluon plasma formation"*, Phys. Lett **B178**, 416 (1986).

[28] M. C. Abreu et al. (NA50 Coll.), *"Anomalous J/psi suppression in Pb-Pb interactions at 158 GeV/c per nucleon"*, Phys. Lett. **B410**, 337 (1997).

[29] M. C. Abreu et at. (NA50 Coll.), *"Observation of a threshold effect in the anomalous J/psi suppression"*, Phys. Lett. **B450**, 456 (1999).

[30] D. Adamova et al. (CERES Collab.), *"New results from CERES"*, Nucl. Phys. **A698**, 253 (2002)

[31] M. Gaździcki and M. I. Gorenstein, *"On the early stage of nucleus-nucleus collisions"*, Acta Phys. Polon. **B30**, 2705 (1999).

[32] C. Blume (for the NA49 Coll.), *"Review of results from the NA49 Collaboration"*, nucl-ex/0411039 (2003) and references therein.

[33] V. Friese (for the NA49 Coll.), *"Energy dependence of strangeness production"*, nucl-ex/0412013(2004) and references therein.

[34] M. Gaździcki and St. Mrówczyński, *"A method to study 'equilibration' in nucleus-nucleus collisions"*, Z. Phys. **C54**, 127 (1992).

[35] St. Mrówczyński, *"Transverse momentum and energy correlations in the equilibrium system from high-energy nuclear collisions"*, Phys. Lett. **B439**, 6 (1998).

[36] St. Mrówczyński, *"Generalizing Φ measure of event-by-event fluctuations in high-energy heavy ion collisions"*, Phys. Lett. **B465**, 8 (1999).

[37] M. Gaździcki, *"A method to study chemical equilibration in nucleus-nucleus collisions"*, Eur. Phys. J. **C8**, 131 (1999).

[38] St. Mrówczyński, *"Chemical fluctuations in high-energy nuclear collisions"*, Phys. Lett. **B459**, 13 (1999).

[39] N. G. Antoniou et al., *"Critical events and intermittency in nuclear collisions"*, Phys. Lett. **B432**, 8 (1998).

[40] K. Haglin and D. Seibert, *"Scaled factorial moments and split bin correlation functions: a thermodynamic model comparison"*, Phys. Lett. **B273**, 211 (1991).

[41] M. Gaździcki, M. I. Gorenstein and St. Mrówczyński, *"Fluctuations and Deconfinement Phase Transition in Nucleus-Nucleus Collisions"*, Phys. Lett. **B585**, 115 (2004).

[42] H. Appelshäuser (NA49 Collab.), *"Event-by-event fluctuations of average transverse momentum in central Pb+Pb collisions at 158 Gev per nucleon"*, Phys. Lett. **B459**, 679 (1999).

[43] S. V. Afanasiev et al. (NA49 Collab.), *"Event-by-event fluctuations of the kaon to pion ratio in central Pb+Pb collisions at 158 GeV per nucleon"*, Phys. Rev. Lett. **86**, 1965 (2001).

[44] C. Roland et al. (NA49 Collab.), *"Event-by-event fluctuations of particle ratios in central Pb+Pb collisions at 20 to 158 AGeV"*, J. Phys. **G30**, S1381 (2004).

[45] M. Stephanov, *"QCD phase diagram and the critical point"*, Prog. Theor. Phys. Suppl. **153**, 139 (2004).

[46] S. A. Voloshin, V. Koch and H. G. Ritter, *"Event-by-event fluctuations in collective quantities"*, Phys. Rev. **C60**, 024901 (1999).

[47] T. Trainor, *"Event-by-event analysis and the central limit theorem"*, hep-ph/0001148 (2000).

[48] R. L. Ray (for the STAR Collab.), *"Correlations, fluctuations, and flow measurements from the STAR experiment"*, Nucl. Phys. **A715**, 45 (2003).

[49] K. Adox et al. (PHENIX Collab.), *"Event-by-event fluctuations in mean p_T and mean e_T in $\sqrt{s_{NN}}$ = 130 GeV Au+Au collisions"*, Phys. Rev. **C66**, 024901 (2002).

[50] D. Adamova et al. (CERES Collab.), *"Event-by-event fluctuations of the mean transverse momentum in 40, 80, and 158 AGeV/c Pb-Au collisions"*, Nucl. Phys. **A727**, 97 (2003).

[51] M. Bleicher et al., *"Can momentum correlations proof kinetic equilibration in heavy ion collisions at 160 AGeV"*, Phys. Lett. **B435**, 9 (1998).

[52] A. Capella, E. G. Ferreiro and A. B. Kaidalov, *"Event by event fluctuations in heavy ion collisions and the quark gluon string model"*, Eur. Phys. J. **C11**, 163 (1999).

[53] F. Liu, A. Tai, M. Gaździcki and R. Stock, *"On transverse momentum event by event fluctuations in string hadronic models"*, Eur. Phys. J. **C8**, 649 (1999).

[54] O. V. Utyuzh, G. Wilk and Z. Wlodarczyk, *"Limitations of the Φ measure of fluctuations in event-by-event analysis"*, Phys. Rev. **C64**, 027901 (2001).

[55] R. Korus and St. Mrówczyński, *"p_T-fluctuations in high-energy p-p and A-A collisions"*, Phys. Rev. **C64**, 054906 (2001).

[56] R. Korus, St. Mrówczyński, M. Rybczyński and Z. Wlodarczyk, *"Transverse momentum fluctuations due to temperature variation in high-energy nuclear collisions"*, Phys. Rev. **C64**, 054908 (2001).

[57] J. G. Reid (for the NA49 Collab.), *"Event-by-event physics in NA49"*, Nucl. Phys. **A661**, 407 (1999).

[58] M. Belkacem et al. *"Moments of event observable distributions and many body correlations"*, nucl-th/9903017 (1999).

[59] A. Bialas and M. Gaździcki, *"A new variable to study intermittency"*, Phys. Lett. **B252**, 483 (1990).

[60] S. Afanasiev et al. (NA49 Collab.), *"The NA49 large acceptance hadron detector"*, Nucl. Instrum. Meth. **A430**, 210 (1999).

[61] L. S. Barnby et al. (NA49 Collab.), *"Reconstruction over a large rapidity interval of lambda, anti-lambda and K0(S) in the NA49 experiment"*, J. Phys. **G25**, 469 (1999).

[62] K. Werner, *"Strings, pomerons and the Venus model of hadronic interactions at ultrarelativistic energies"*, Phys. Rept. **232**, 87 (1993).

[63] G. Cooper, Ph.D. thesis *"Baryon Stopping and Hadronic Spectra in Pb-Pb Collisions at 158 GeV/nucleon"*, Department of Physics, University of California, Berkeley, LBNL-45467 (2000).

[64] C. Hoehne, Ph.D. thesis *"System-Size Dependence of Strangeness Production in Heavy-Ion Collisions at 158 AGeV"*, Fachbereich Physik der Universität, Marburg (2003).

[65] M. Gyulassy and X.-N. Wang, *"HIJING 1.0: A Monte Carlo program for parton and particle production in high-energy hadronic and nuclear collisions"*, Comput. Phys. Commun. **83**, 307 (1994).

[66] C. Alt et al. (NA49 Collab.), *"Directed and elliptic flow of charged pions and protons in Pb+Pb collisions at 40 and 158 AGeV"*, Phys. Rev. **C68**, 034903 (2003).

[67] K. Perl, M.S. thesis *"Measurement of the correlation function Φ_{p_T} in Pb+Pb interactions at 158 AGeV"* (in Polish), Faculty of Physics, Warsaw University, Warsaw (2000).

[68] A.I. Golokhvastov, *" Independent π^- meson production in pp interactions"* (in Russian), Yad. Fiz. **67**, 2252 (2004).

[69] S. A. Bass et al., *"Microscopic Models for Ultrarelativistic Heavy Ion Collisions"*, Prog. Part. Nucl. Phys. **41**, 225 (1998).

[70] M. Bleicher et al., *"Relativistic Hadron-Hadron Collisions and the Ultra-Relativistic Quantum Molecular Dynamics Model (UrQMD)"*, J. Phys. **G25**, 1859 (1999).

[71] S. Gavin *"Traces of Thermalization from p_t Fluctuations in Nuclear Collisions"*, Phys. Rev. Lett. **92**, 162301 (2004).

[72] M. R. Ataian et al. (NA22 Collab.), *"Transverse momentum fluctuations in π^+p and K^+p collisions at 250 GeV/c"*, Phys. Rev. Lett. **89**, 121802 (2002).

[73] H. Appelshäuser, *"Event-by-event fluctuations: An experimental overview"*, talk on Workshop on Event-by-Event Fluctuations at GSI - Darmstadt (December 2003) and private communication.

[74] H. Sako and H. Appelshäuser (for the CERES Collab.), *"Event-by-event Fluctuations at 40, 80 and 158 AGeV/c in Pb+Au Collisions"*, J. Phys. **G30**, S1371 (2004).

[75] H. Appelshäuser and H. Sako (for the CERES Collab.), *"Event-by-event fluctuations at SPS"*, nucl-ex/0409022 (2004).

[76] J. Adams et al. (STAR Collab.), *"Event-by-event $\langle p_t \rangle$ fluctuations in Au-Au collisions at $\sqrt{s_{NN}}$ = 130 GeV"*, nucl-ex/0308033 (2003).

[77] T. Trainor, *"First results from STAR event-by-event analysis at RHIC"*, Acta Phys. Hung. New Ser. Heavy Ion Phys. **15**, 183 (2002).

[78] J. G. Reid, Ph.D. thesis *"Event-by-event analysis methods and applications to relativistic heavy ion collisions"*, University of Washington, nucl-ex/0302001 (2002).

[79] G. D. Westfall (for the STAR Collab.), *"Correlations and Fluctuations in STAR"*, J. Phys. **G30**, S1389 (2004).

[80] J. Nystrand (for the PHENIX Collab.), *"Charge Fluctuations at Mid-Rapidity in Au+Au Collisions in the PHENIX Experiment at RHIC"*, Nucl. Phys. **A715**, 603 (2003).

[81] S. S. Adler et al. (PHENIX Collab.), *"Measurement of Non-Random Event-by-Event Fluctuations of Average Transverse Momentum in $\sqrt{s_{NN}}$ = 200 GeV Au+Au and p+p Collisions"*, Phys. Rev. Lett. **93**, 092301 (2004).

[82] M. J. Tannenbaum (for the PHENIX Collab.), *"Event-by-event average p_T fluctuations in $\sqrt{s_{NN}}$ = 200 GeV Au+Au and p+p collisions in PHENIX: measurements and jet contribution simulations"*, J. Phys. **G30**, S1367 (2004).

[83] J. T. Mitchell, *"An Overview of Fluctuation and Correlation Results in Relativistic Heavy Ion Collisions"*, J. Phys. **G30**, S819 (2004), and slides at the conference (Quark Matter 2004).

[84] S. Gavin, *"Traces of Thermalization at RHIC"*, J. Phys. **G30**, S1385 (2004).

[85] E. G. Ferreiro, F. del Moral and C. Pajares, *"Transverse momentum fluctuations and percolation of strings"*, Phys. Rev. **C69**, 034901 (2004).

[86] M. A. Stephanov, *"Thermal fluctuations in the interacting pion gas"*, Phys. Rev. **D65**, 096008 (2002) and private communication.

[87] St. Mrówczyński, M. Rybczyński and Z. Wlodarczyk, *"Transverse momentum versus multiplicity fluctuations in high-energy nuclear collisions"*, Phys. Rev. **C70**, 054906 (2004).

[88] C. Alt et al. (NA49 Collab.), *"Electric charge fluctuations in central Pb+Pb collisions at 20, 30, 40, 80 and 158 AGeV"*, Phys. Rev. **C70**, 064903 (2004).

[89] Y. Hatta and T. Ikeda, *" Universality, the QCD critical/tricritical point and the quark number susceptibility"*, Phys. Rev. **D67**, 014028 (2003).

[90] M. Gaździcki, *"Search for the critical point - possible programs at SPS and RHIC"* - talk presented on International Workshop XXXIII on Gross Properties of Nuclei and Nuclear Excitations, Hirschegg, Kleinwalsertal, Austria (January 2005), and private communication.